THE MAGNETOHYDROSTATIC EQUILIBRIUM OF QUIESCENT SOLAR PROMINENCES

Christopher Ridgway

A Thesis Submitted for the Degree of PhD
at the
University of St Andrews

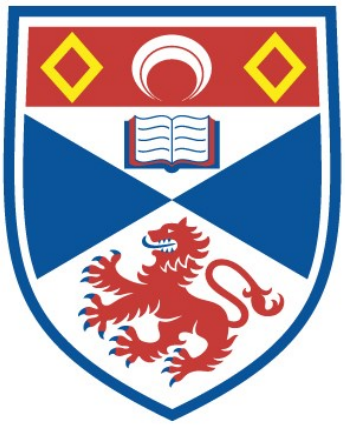

1992

THE MAGNETOHYDROSTATIC EQUILIBRIUM OF QUIESCENT SOLAR PROMINENCES

C. RIDGWAY

Submitted for the Degree of Doctor of Philosophy at the University of St. Andrews.

Th

B59

COPYRIGHT

POSTGRADUATE CAREER

I was admitted to the Faculty of Science of the University of St. Andrews under Ordinance General No. 12 on 1/10/88 and as a candidate for the degree of Ph.D. on 1/10/89.

Signed

Date 20/9/91

DECLARATION

I Christopher Ridgway hereby certify that this thesis has been composed by myself, that it is a record of my own work, and that it has not been accepted in partial or complete fulfilment of any other degree or professional qualification.

Signed ...

Date 20/9/91

CERTIFICATE

I hereby certify that the candidate has fulfilled the conditions of the Resolution and Regulations appropriate to the Degree of Ph.D.

Signed .... Date 23.9.91

ACKNOWLEDGEMENTS

I would like to thank all the members of the Solar Theory Group at the University of St Andrews whose guidance and support have made this thesis possible. Unfortunately, they are too numerous to list here but particular thanks are owed to my supervisor Eric Priest and to Tahar Amari, both of whose expertise and enthusiasm have added enormously to my interest and knowledge of solar prominences. I am also grateful to the Science and Engineering Research Council for providing funding for this project.

Without my parents moral and financial support none of this would have been possible and it is to them that this thesis is dedicated.

CONTENTS

1 ABSTRACT

Since the mid 1900's it has been supposed that the global magnetic field surrounding a quiescent prominence provides the force required to prevent its collapse under the influence of the Sun's gravitational field. Many theoretical models of this magnetic field have been produced in which it is assumed that the prominence plasma is supported in a dip in the field lines by the associated magnetic tension force. It is the aim of this thesis to propose further models of the magnetic field in order to extend our knowledge and understanding of prominences.

In doing so we present three distinct models. The first is an extension of the twisted flux tube model for prominences proposed by Priest et al. (1989). Here we present analytical solutions to the magnetohydrostatic equilibrium equation within the tube using the so-called generating function method in which we select two distinct functional forms of the longitudinal field component. Unlike the solutions found by Priest et al., we allow for large deviations of the field from cylindrical symmetry. The prominence is represented by a finite vertical sheet of mass and current and we show that it is possible for such a sheet to be in static equilibrium everywhere along its vertical extent.

Next we consider the model of van Ballegooijen and Martens in which photospheric motions drive a reconnection process leading to the formation of a helical magnetic structure capable of supporting dense prominence plasma in the low points of the helical windings. Under the assumption of cylindrical symmetry we analyse two methods of solving the magnetohydrostatic equilibrium equation in which the positions of the field line footpoints at the photosphere are imposed. Using a combination of analytical and numerical techniques, we study the quasi-static evolution of the model as the height of the helical axis increases. Unlike the numerical analysis of van Ballegooijen and Martens we are able to produce inverse polarity configurations without the problem of singular field components at the helical axis.

Lastly we present an analysis of the interaction of a finite, vertical sheet of mass and current (representing a prominence) with an external constant-current force-free field. We formalise two distinct boundary-value problems in which the distribution of the normal

magnetic field component along the photosphere is imposed along with the distribution of either the normal magnetic field component across the prominence or the prominence surface current. In both cases we demonstrate for particular boundary conditions that it is possible for equilibrium solutions to exist of both normal and inverse polarity in which dense material is supported everywhere along the prominence sheet. In particular we are, for the first time, able to produce an inverse polarity equilibrium configuration in which the field components are locally bounded and closed field lines exist above the prominence sheet while an X-type neutral point lies below it.

2 INTRODUCTION

2.1 Chapter summary

In this chapter we provide much of the background information for the subsequent chapters. Section 2.2 introduces the basic equations of magnetohydrodynamics used to describe the interaction of plasmas and magnetic fields on a large scale. In section 2.3 we consider the hydrostatic form of the equations which will be of particular use in our current field of study. Section 2.4 summarises the more important observations of quiescent solar prominences in relation to this study. This is by no means a complete review and considerably greater detail may be found in the chapters of Priest (1988). In section 2.5 we describe some of the more notable analytical models for the global magnetic field surrounding prominences in an attempt to understand the mechanism by which they are supported against the effect of the Sun's gravitational field. Again, more detailed reviews may be found in Anzer (1988) or Priest (1990).

2.2 The equations of magnetohydrodynamics

Many solar phenomena are believed to owe their existence to the subtle interaction between the ionised plasma of which the Sun is composed, and the Sun's magnetic field. All the physical processes with which we will be concerned occur on length-scales much larger than those on which individual particles interact, allowing us to treat the plasma as a continuous fluid. The equations which govern these processes are known as the equations of magnetohydrodynamics (universally abbreviated to MHD) and an outline of their derivation is presented below.

We start from Maxwell's equations of electromagnetism, written

$$\nabla \times \mathbf{B} = \mu \mathbf{j} + \frac{1}{c^2}\frac{\partial \mathbf{E}}{\partial t} \qquad (2.1)$$

$$\nabla . \mathbf{B} = 0 \qquad (2.2)$$

$$\nabla \times \mathbf{E} = -\frac{\partial \mathbf{B}}{\partial t} \qquad (2.3)$$

$$\nabla . \mathbf{E} = \rho_c / \varepsilon \qquad (2.4)$$

where **B** is the magnetic induction (more usually referred to as the

magnetic field), **E** the electric field, **j** the current density and ρ_c the charge density. μ is the magnetic permeability and ε the permittivity, usually approximated by μ_0 and ε_0, their values in a vacuum, so that the speed of light $c = (\mu_0 \varepsilon_0)^{-1/2}$.

Here we must make an assumption concerning the features we wish to study. We will only consider those processes in which the plasma velocity is non-relativistic, a reasonable restriction for most solar phenomena. Assuming the magnitudes of the terms on both sides of equation (2.3) to be equal, a comparison of the magnitudes of the terms in equation (2.1) then shows that the second term on the right-hand side is negligible compared with the term on the left and so we may rewrite this equation as

$$\nabla \times \mathbf{B} = \mu \mathbf{j} \tag{2.5}$$

Consistency with equation (2.5) requires the plasma to be essentially electrically neutral so that

$$\rho_c << n e \tag{2.6}$$

where n is the particle number density and e the electron charge.

Plasma which is moving with velocity **v** in a magnetic field is subject to a total electric field of $\mathbf{E} + \mathbf{v} \times \mathbf{B}$. Ohm's law states that the current density is proportional to this electric field and may be written

$$\mathbf{j} = \sigma (\mathbf{E} + \mathbf{v} \times \mathbf{B}) \tag{2.7}$$

where σ is the electrical conductivity.

We can now eliminate the electric field and current density from equations (2.3), (2.5) and (2.7) to determine a relationship between the primary variables of the magnetic field and the plasma velocity. We find that

$$\frac{\partial \mathbf{B}}{\partial t} = \nabla \times (\mathbf{v} \times \mathbf{B}) - \nabla \times (\eta \nabla \times \mathbf{B}) \tag{2.8}$$

where $\eta = 1/\mu\sigma$ is known as the magnetic diffusivity. Assuming η to be uniform throughout the plasma and using equation (2.2) gives

$$\frac{\partial \mathbf{B}}{\partial t} = \nabla \times (\mathbf{v} \times \mathbf{B}) + \eta \nabla^2 \mathbf{B} \tag{2.9}$$

which is known as the induction equation and determines the magnetic field, subject to equation (2.2), when the plasma velocity is prescribed.

The first term on the right-hand side of the induction equation represents changes in the magnetic field due to the coupling of the field and plasma velocity while the second results from the effects of magnetic diffusion. The ratio of the magnitudes of these

terms is known as the magnetic Reynolds number R_m which, for a typical plasma velocity v_0 and length-scale l_0, becomes

$$R_m = v_0 \, l_0 / \eta \qquad (2.10)$$

For many solar applications R_m is very much bigger than unity allowing us to neglect the diffusion term in equation (2.10) in an approximation known as the perfectly conducting limit. A consequence of this limit is Alfven's frozen-flux theorem which states that in a perfectly conducting plasma, magnetic field lines move with the plasma as if they were frozen to it.

The motion of the plasma is described by the equations of continuity and motion. Conservation of mass yields the continuity equation

$$\frac{D\rho}{Dt} + \rho \, \nabla . \mathbf{v} = 0 \qquad (2.11)$$

where ρ is the plasma density and

$$\frac{D}{Dt} = \frac{\partial}{\partial t} + \mathbf{v} . \nabla \qquad (2.12)$$

is the convective time derivative. Conservation of momentum, under the assumption of equation (2.6), gives the equation of motion which can be written as

$$\rho \frac{D\mathbf{v}}{Dt} = - \nabla p + \mathbf{j} \times \mathbf{B} + \rho \, \mathbf{g_c} + \rho \, \nu \left(\nabla^2 \mathbf{v} + \frac{\nabla (\nabla . \mathbf{v})}{3} \right) \qquad (2.13)$$

where p is the plasma pressure, $\mathbf{g_c}$ the acceleration due to gravity and ν the coefficient of kinematic viscosity, which is assumed to be uniform throughout the plasma. The terms on the right-hand side of equation (2.13) represent, respectively, the forces due to plasma pressure gradients, the Lorentz force, the gravitational force and viscosity.

At this stage it is helpful to note that using equation (2.5), the Lorentz force can be decomposed into two parts written

$$\mathbf{j} \times \mathbf{B} = \frac{(\mathbf{B} . \nabla) \mathbf{B}}{\mu} - \nabla \left(\frac{B^2}{2\mu} \right) \qquad (2.14)$$

representing a magnetic tension along the field lines of magnitude B^2/μ and a magnetic pressure of magnitude $B^2/2\mu$. The result is a tension force perpendicular to curved field lines and a pressure force acting from regions of greater magnetic field strength towards those with lower field strength. Note that since the Lorentz force is perpendicular to the field the components of the two forces along the field lines must cancel.

The plasma pressure is for simplicity assumed to be given by

the ideal gas law

$$p = \rho R T / \mu_a \qquad (2.15)$$

where T is the temperature, μ_a the mean atomic weight of the plasma and R the gas constant. A useful quantity to introduce at this point is the plasma beta defined as

$$\beta = 2 \mu p / B^2 \qquad (2.16)$$

which is just the ratio of plasma pressure to magnetic pressure.

The last of our fundamental equations is an energy equation

$$\rho T \frac{Ds}{Dt} = - L \qquad (2.17)$$

where s is the entropy per unit mass of the plasma and L is the energy loss function due to all sources and sinks present. This is simply a statement of the first law of thermodynamics and may be rewritten in terms of the plasma pressure and density as

$$\frac{\rho^\gamma}{\gamma - 1} \frac{D}{Dt}\left(\frac{p}{\rho^\gamma}\right) = - L \qquad (2.18)$$

where γ is the ratio of the specific heat of the gas at constant pressure to that at constant volume. Note that if the temperature is assumed to be constant, equation (2.18) is redundant.

Two velocities associated with the plasma are the sound speed

$$c_s = (\gamma p / \rho)^{1/2} \qquad (2.19)$$

and the Alfven speed

$$v_A = B / (\mu \rho)^{1/2} \qquad (2.20)$$

which is the velocity at which transverse waves propagate along the magnetic field lines due to the magnetic tension associated with them.

In summary, the basic equations used throughout our study are the induction equation

$$\frac{\partial \mathbf{B}}{\partial t} = \nabla \times (\mathbf{v} \times \mathbf{B}) + \eta \nabla^2 \mathbf{B} \qquad (2.9)$$

the continuity equation

$$\frac{D\rho}{Dt} + \rho \nabla . \mathbf{v} = 0 \qquad (2.11)$$

the equation of motion

$$\rho \frac{D\mathbf{v}}{Dt} = - \nabla p + \mathbf{j} \times \mathbf{B} + \rho \mathbf{g_c} + \rho \nu \left(\nabla^2 \mathbf{v} + \frac{\nabla(\nabla . \mathbf{v})}{3}\right) \qquad (2.13)$$

the ideal gas law

$$p = \rho R T / \mu_a \qquad (2.15)$$

and the energy equation

$$\frac{\rho^{\gamma}}{\gamma-1}\frac{D}{Dt}\left(\frac{p}{\rho^{\gamma}}\right) = -L \qquad (2.18)$$

These equations determine **v**, **B**, ρ, p and T subject to the condition

$$\nabla.\mathbf{B} = 0 \qquad (2.2)$$

In addition **j** and **E** are given by Ampere's law

$$\mathbf{j} = \nabla \times \mathbf{B} / \mu \qquad (2.5)$$

and Ohm's law

$$\mathbf{E} = -\mathbf{v} \times \mathbf{B} + \mathbf{j} / \sigma \qquad (2.7)$$

2.3 The equations of magnetohydrostatics

If we consider the special case of a structure which does not evolve in time, so that time derivatives and velocities are identically zero, both the induction and continuity equations become redundant. The inertial and viscous terms drop out of the equation of motion to leave

$$\mathbf{0} = -\nabla p + \mathbf{j} \times \mathbf{B} + \rho\, \mathbf{g_c} \qquad (2.21)$$

known as the equation of magnetohydrostatic equilibrium. If gravity acts in the negative y-direction, then resolving the forces along a field line yields

$$p = p_0 \exp\left(-\int_0^y \frac{1}{H(y')}\, dy'\right) \qquad (2.22)$$

where p_0 is the pressure at y = 0 and H(y) is the pressure scale height, given by the ideal gas law as

$$H(y) = R\, T(y) / \mu_a\, g_c \qquad (2.23)$$

It now becomes clear that gravitational forces are negligible compared to pressure gradient forces when the vertical extent of the structure under consideration is much less than the scale height. In addition, pressure forces are negligible by comparison with the Lorentz force when the plasma beta is very much smaller than unity. The above conditions allow us to define the important concept of a force-free field in which the magnetic forces dominate pressure gradient and gravitational forces so that the magnetohydrostatic equilibrium equation reduces to

$$\mathbf{j} \times \mathbf{B} = \mathbf{0} \qquad (2.24)$$

which must be solved subject to

$$\nabla.\mathbf{B} = 0 \qquad (2.2)$$

Despite the seemingly innocuous form of the above equations, solutions

for **B** are surprisingly difficult to obtain. However, progress can be assisted by considering the field to be invariant in one direction. For example, consider the cartesian coordinate system (x,y,z) in which the field components depend only on x and y so that they may be expressed in terms of a scalar flux function A(x,y) as

$$\mathbf{B} = \left(\frac{\partial A}{\partial y}(x,y),\ -\frac{\partial A}{\partial x}(x,y),\ B_z(x,y)\right) \tag{2.25}$$

immediately satisfying equation (2.2). Writing equation (2.24) in component form after substituting for **j** from equation (2.5), it is easily shown that

$$B_z = B_z(A) \tag{2.26}$$

and

$$\nabla^2 A + \frac{d}{dA}\left(\frac{B_z^2(A)}{2}\right) = 0 \tag{2.27}$$

It should be noted that the above expressions may also be obtained for a z-invariant cylindrical polar coordinate system (r,θ,z) in which the field can be written in terms of $A(r,\theta)$ as

$$\mathbf{B} = \left(\frac{1}{r}\frac{\partial A}{\partial \theta}(r,\theta),\ -\frac{\partial A}{\partial r}(r,\theta),\ B_z(r,\theta)\right) \tag{2.28}$$

Note also that using the above expressions for **B** it can be verified that $(\mathbf{B}.\nabla)A = 0$, implying that A (and hence B_z) is constant along field lines.

Many authors have expended a great deal of effort in the search for solutions to equation (2.27) after the form of $B_z(A)$ has been imposed and this approach will frequently be referred to in subsequent chapters. The simplest choice, $B_z(A) = \alpha$ ($\alpha \in \Re$), causes equation (2.27) to reduce to Laplace's equation and corresponds to potential fields. Another well-known form is $B_z(A) = \alpha A$ for which equation (2.27) reduces to the linear Helmholtz equation, yielding so-called constant-α (or linear) force-free fields. Less studied is the form $B_z(A) = \alpha A^{1/2}$ for which equation (2.27) becomes Poisson's equation, corresponding to constant-current force-free fields.

Although all solar processes are dynamic on small length-scales, many can be described, to a first degree of approximation, by the magnetohydrostatic equations as explained below. A comparison of the magnitudes of the terms in the full equation of motion for a typical plasma velocity v_0 and length-scale l_0 gives the ratio of inertial effects to viscous effects as

$$Re = v_0 l_0 / \nu \tag{2.29}$$

where Re is known as the Reynolds number. For many aspects of solar theory, this is very much larger than unity, allowing viscous effects to be neglected. Furthermore, the inertial term itself may be neglected if the plasma velocity is very much smaller than the sound speed, Alfven speed and gravitational free-fall speed $(2g_c l_0)^{1/2}$. Such a system, which evolves slowly in time, is assumed to pass through a series of essentially static equilibrium states, approximated by the magnetohydrostatic equilibrium equation, in what is known as a quasi-static evolution.

2.4 Summary of prominence observations

Throughout the following chapters we will concern ourselves with only one of the many types of solar phenomena, namely quiescent solar prominences. The term prominence may be used to describe any large, transient structure composed of condensed plasma and located in the lower solar atmosphere. There have been many attempts to classify them morphologically, but for the purposes of this work it suffices to distinguish between those phenomena which are long-lived with little global change over a number of days (quiescent prominences) and those which evolve rapidly over time-scales of minutes (active prominences). Henceforth, we shall concern ourselves only with the properties of quiescent prominences and the term prominence refers only to this type.

Although observations of prominences have been recorded intermittently since the 13th century, it was not until the mid 19th century that observations backed up by photographical techniques provided for a scientific study of their properties. In Hα photographs of the solar disc they appear as dark filaments since they absorb much of the line-of-sight emission from the photosphere. When observed in Hα at the limb using a coronagraph they appear bright against a less emissive coronal background. They are in fact huge, elongated, vertical sheets of relatively cool, dense plasma located in the upper chromosphere and lower corona.

The review of Martin (1990) shows that they tend to be formed in the zone between two large-scale regions of opposite photospheric polarity, in which the transverse magnetic field is highly sheared, causing the Hα fibrils to align themselves along what is known

as the filament channel, and in which small areas of opposing polarity converge towards the channel and cancel. A small, low, dark filament is formed and this grows and rises steadily over the course of several days.

In their mature state, they are generally 60 - 600 Mm long, 10 - 100 Mm in height and 4 - 15 Mm in width, with a typical prominence measuring 200 Mm by 50 Mm by 6 Mm. For an idea of scale, the solar radius is approximately 700 Mm. The temperature is thought to be in the range 5000 - 10000 K and the particle density 10^{16} - 10^{17} m^{-3} though the distribution of these quantities within the prominence is a matter of great uncertainty. For comparison, the coronal environment in which prominences are located, possesses a temperature of approximately $2x10^6$ K and a particle density of roughly 10^{15} m^{-3}.

Prominences tend to reach down to the photosphere in a set of regularly spaced feet, thought to be located at the supergranule boundaries, which are connected by arches. High-resolution photographs reveal that prominences are composed of many fine, vertical threads.

The magnetic field through the prominence is of the order 1-30 G (typically 3 - 15 G) (Kim, 1990) and is inclined at approximately 3^0 to the horizontal (Athay et al., 1983) and about 20^0 to the longitudinal prominence axis (Tandberg-Hanssen and Anzer, 1970; Leroy et al., 1983; Kim, 1990). Again the distribution of the field is uncertain but the observations of Leroy et al. (1983) conclude that the magnetic field strength often decreases slightly with height. A highly important observation concerning the magnetic field was the realisation by Babcock and Babcock (1955) that prominences always overlie the polarity inversion line between two large-scale regions of opposite line-of-sight polarity in the photosphere.

Mass motions are observed within the prominence with upwards velocities typically less than 5 km s^{-1} and horizontal velocities of 10 - 20 km s^{-1} (Schmieder, 1990).

An end on view of a prominence at the limb reveals a region of reduced density surrounding the prominence known as the coronal cavity and this is embedded in an arcade of hot loops, typically 400 Mm in width. A helmet streamer, stretching radially outwards, is frequently seen to overlie the arcade.

Prominences can remain in this mature phase with little

global change for anything up to 9 months. During this time, they tend to drift towards the nearest pole, simultaneously becoming stretched and aligned E - W due to differential rotation. Often, several mature prominences are seen at a high latitude, forming a polar crown. Eventually they either disperse as the material drains down to the photosphere or they erupt radially outwards at speeds of about 100 km s^{-1}, often revealing a twisted, helical structure as they do so. Such an eruption is often referred to as a disparition brusque and in two-thirds of cases the prominence reforms in the same place over the course of about a week.

2.5 Summary of prominence models

Many authors have attempted to model prominences by one of two approaches, considering either the global properties of the prominence in order to determine how the dense material is supported, or the internal structure to see how the cool plasma remains in thermal equilibrium. For the present work we are predominantly interested in the first of these and ask: how can cool, dense plasma be supported against the effects of the Sun's gravitational field acting to pull it down to the photosphere? The observation of Babcock and Babcock (1955), that prominences always lie above the polarity inversion line between regions of opposite polarity in the photosphere, indicates that the magnetic field plays a crucial role in this support. Since a mature prominence exhibits little global change over time-scales much larger than free-fall or Alfven times, the plasma must be in approximate equilibrium and this is described by the magnetohydrostatic equilibrium equation

$$\mathbf{0} = -\nabla p + \mathbf{j} \times \mathbf{B} + \rho \mathbf{g}_c \qquad (2.21)$$

Throughout the remainder of this chapter, we adopt the cartesian coordinate system (x,y,z) in which the x-z plane through $y = 0$ represents the photosphere and the upper-half plane $y > 0$ is the corona. The x-axis is perpendicular to the prominence sheet and z is measured along the longitudinal prominence axis. Gravity is assumed to be uniform and acts in the negative y-direction so that

$$\mathbf{g}_c = -g_c \mathbf{e}_y \quad \text{where} \quad g_c > 0 \qquad (2.30)$$

Let us consider briefly the work of Kippenhahn and Schluter (1957) in which they consider plasma of uniform temperature, whose

pressure and density depend only on the horizontal coordinate, x. The horizontal magnetic field components B_x and B_z are assumed constant whilst the vertical field component B_y also depends solely on x. Resolving equation (2.21) vertically and horizontally gives

$$\frac{d}{dx}\left(p + \frac{B_y^2}{2\mu}\right) = 0 \qquad (2.31)$$

and

$$\frac{B_x}{\mu}\frac{dB_y}{dx} - \rho g_c = 0 \qquad (2.32)$$

Equation (2.31) represents a balance between the magnetic and plasma pressures, whilst equation (2.32) tells us that the effect of the magnetic tension force due to a changing B_y is to balance the gravitational force acting on the plasma. These equations must be solved subject to the boundary conditions

$$p \to 0 \text{ as } |x| \to \infty \quad \text{and} \quad B_y(0) = 0 \qquad (2.33)$$

It should be noted that a direct consequence of the first boundary condition is that

$$|B_y| \to B_{y\infty} \text{ as } |x| \to \infty \qquad (2.34)$$

Integrating equation (2.31) gives

$$p = \frac{B_{y\infty}^2 - B_y^2}{2\mu} \qquad (2.35)$$

and using equation (2.15) to substitute for ρ, equation (2.32) can be integrated to give

$$B_y = B_{y\infty} \tanh \frac{B_{y\infty}\, x}{2\, B_x\, H} \qquad (2.36)$$

with

$$p = \frac{B_{y\infty}^2}{2\mu} \operatorname{sech}^2 \frac{B_{y\infty}\, x}{2\, B_x\, H} \qquad (2.37)$$

where H is given by equation (2.23)

The distribution of the vertical field component and the plasma pressure with x are shown in Figures 2.1(a) and 2.1(b), respectively. The projection of the field lines in the x-y plane is illustrated in Figure 2.1(c). Examination of these plots shows that the maximum pressure (and hence density, since they are directly proportional) is located at $x = 0$, which is where a reversal in the vertical magnetic field component occurs. It follows that we can support dense material in a field line dip in which the magnetic tension and gravitational forces balance and the magnetic pressure force acts to compress the plasma towards the centre of the dip.

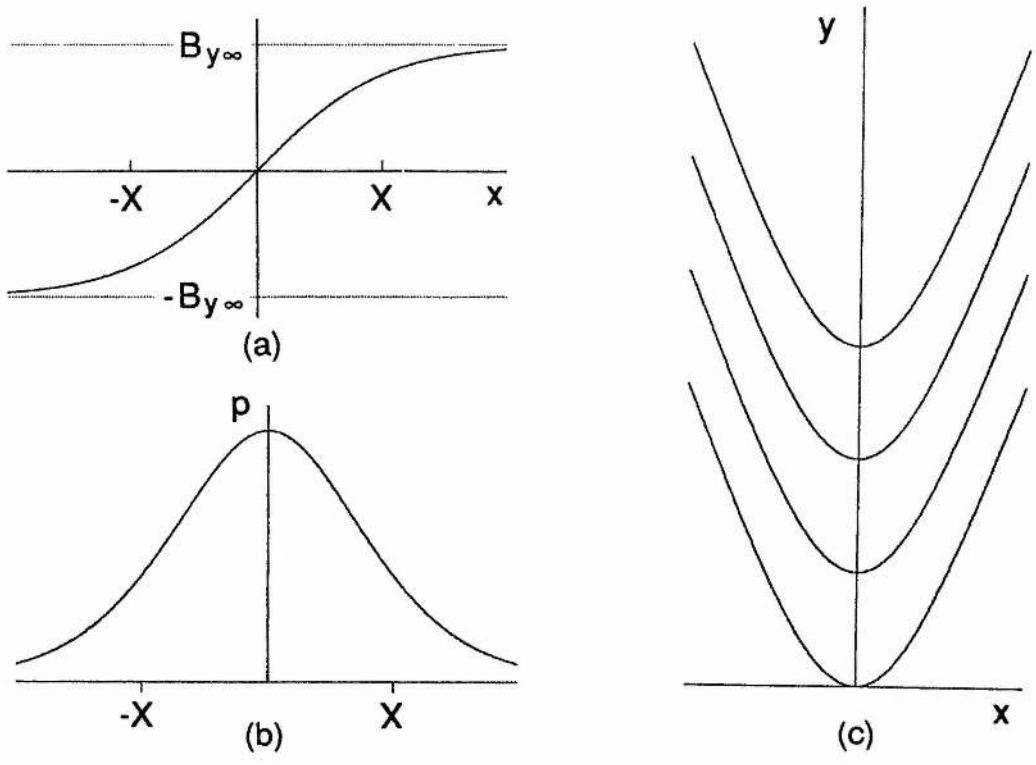

Figure 2.1 The distribution of (a) the vertical field component and (b) the plasma pressure with x in the Kippenhahn and Schluter prominence model. (c) The magnetic field projection in the x-y plane. X = $2B_xH/B_{y\infty}$.

Many authors, then, have been concerned with modelling the global structure of the external magnetic field to obtain configurations in which it is possible to support the prominence in a field line dip. To a first approximation, the fine structure and feet are neglected and, because the prominence is relatively long and thin, it is frequently modelled as a longitudinally invariant (i.e. independent of z), infinitesimally thin, vertical slab of current and plasma (a current sheet), lying directly above a polarity inversion line at the photosphere. Because no allowance is made for any z-dependence (but components in this direction are allowed) we can consider the system projected onto a single upper-half x-y plane, taken without loss of generality to be that passing through z = 0. The current sheet will then lie on the y-axis between the base of the sheet at $(0,y_1)$ and the upper limit $(0,y_2)$. The polarity inversion line will of course be located at (0,0).

Across such a sheet, we assume that since the sheet is infinitesimally thin, B_x and B_z do not change sign and so

$$[B_x] = [B_z] = 0 \qquad (2.38)$$

where $[B_a] = B_a(0^+,y) - B_a(0^-,y)$, denotes the change in B_a across the sheet. However, the vertical field component B_y is discontinuous across the sheet and integrating equation (2.32) across the sheet gives the balance between the gravitational and magnetic tension forces as

$$m\, g_c = B_x\, [B_y]\, /\mu = B_x\, j_\Sigma \qquad (2.39)$$

where m is the sheet mass density per unit length and $\mathbf{j}_\Sigma$ is the surface current along the sheet, given by equation (2.5) as

$$\mathbf{j}_\Sigma = j_\Sigma\, \mathbf{e}_z = [B_y]/\mu\, \mathbf{e}_z \qquad (2.40)$$

Thus, given the vertical and tangential field components at the current sheet, equation (2.39) determines the mass which is supported in the given magnetic field configuration. Note that for a physically acceptable model, this mass must, of course, be positive. This will only be the case if the magnetic tension force is upwards at every point along the sheet.

Since the plasma beta within the corona is very much less than unity (typically 10^{-2}) and the coronal scale height (about 100 Mm) divided by this beta is very much larger than the vertical extent of a prominence (about 50 Mm), we can neglect the plasma pressure and gravitational forces in the magnetohydrostatic equilibrium equation and consider the coronal field to be force-free. The simplest example of such a field is the potential case and many authors have assumed a potential coronal field in their models of the global field structure.

Kippenhahn and Schluter (1957), for instance, modelled the external magnetic field as that due to equal potential line dipoles lying on the photosphere outside an infinite, vertical current sheet ($y_1 = 0$, $y_2 = \infty$). The field is symmetrical about $x = 0$ and is given in the first quadrant by a negative dipole lying at $x = 1$ and a positive one at $x = -a$ ($0 < a < 1$), and in the second quadrant by a positive dipole lying at $x = -1$ and a negative one at $x = a$. The resulting field is sketched in Figure 2.2 and the field line dip along the sheet in which dense material may be supported is clearly visible. Such a model, in which the magnetic field passes through the prominence sheet from the region of positive to negative photospheric polarity, is said to have normal polarity or to be an N-type configuration.

A more realistic representation of a prominence is gained if it is modelled as a finite current sheet. Anzer (1972) considered the problem in which the normal field components are imposed as functions of position at the photosphere and across a current sheet which

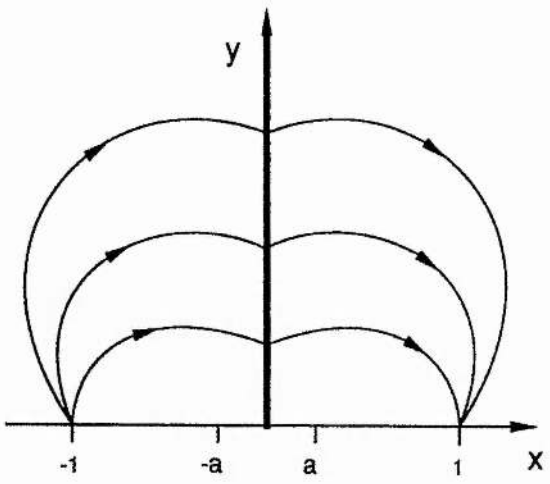

Figure 2.2 The global magnetic field configuration for the Kippenhahn and Schluter prominence model.

stretches from the photosphere ($y_1 = 0$) to a finite height, as sketched in Figure 2.3. Assuming a potential field to exist outside the sheet, the resulting mixed boundary-value problem can be solved to obtain the field throughout the corona. Unfortunately the numerical solutions which are presented are unphysical due to a downwards Lorentz force acting in the lower part of the sheet and so no support of dense matter is possible.

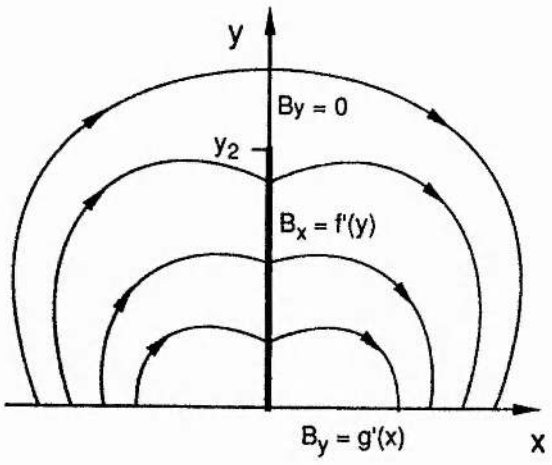

Figure 2.3 The boundary-value problem analysed by Anzer.

The work of Kuperus and Raadu (1974) is particularly remembered for the introduction of an alternative topology to that of Kippenhahn and Schluter. They represent the prominence by a current

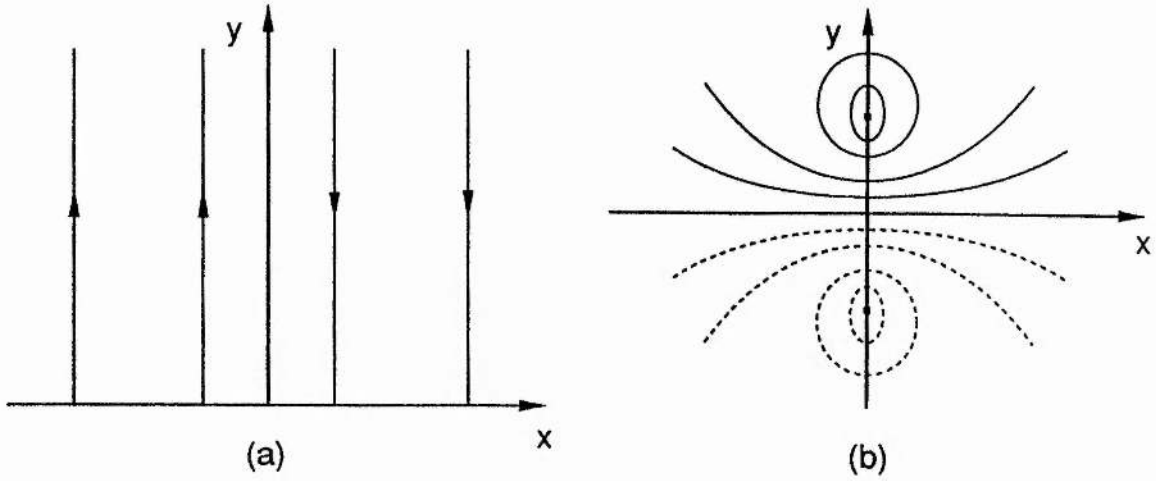

Figure 2.4 The magnetic fields combined in the Kuperus and Raadu model. (a) The background vertical field. (b) The field due to the prominence filament located at $(0,y_1)$ and the image filament located at $(0,-y_1)$.

filament which is embedded in a purely vertical background field which changes sign at $x = 0$. No Lorentz force is provided by such a field, but it is conjectured that the filament induces photospheric currents which can be mimicked by an equal and opposite sub-photospheric line-current lying at $(0,-y_1)$ as shown in Figure 2.4. The repulsive force between the two filaments opposes the gravitational force acting on the mass of the upper one, resulting in a unique equilibrium position for the prominence. The resultant magnetic field is sketched in Figure 2.5.

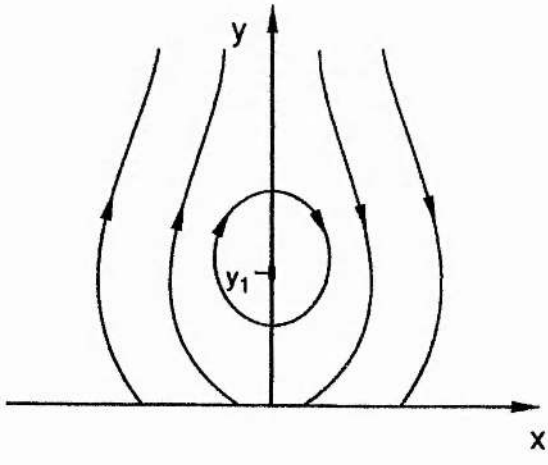

Figure 2.5 The resultant magnetic field of the Kuperus and Raadu model.

Prominences are, however, not well represented by current filaments since their vertical extent is appreciable and so keeping the same field

topology, but extending the prominence to a current sheet, yields the configuration shown in Figure 2.6(a), or more generally we could allow for that illustrated in Figure 2.6(b) in which an X-type neutral point is present below the sheet. Such configurations, in which the field passes through the prominence from the region of negative polarity to that of positive polarity are said to have inverse polarity or to be I-type. Leroy (1988), in a review of the magnetic fields observed in prominences, states that high-altitude, mature, quiescent prominences found in the polar crown tend to be I-type whereas low-lying prominences close to active regions tend to be N-type. It is interesting to note that thermal shielding of the prominence from its much hotter environment is conveniently explained by the closed regions in fields of an I-type topology since thermal conduction across field lines is comparatively weak.

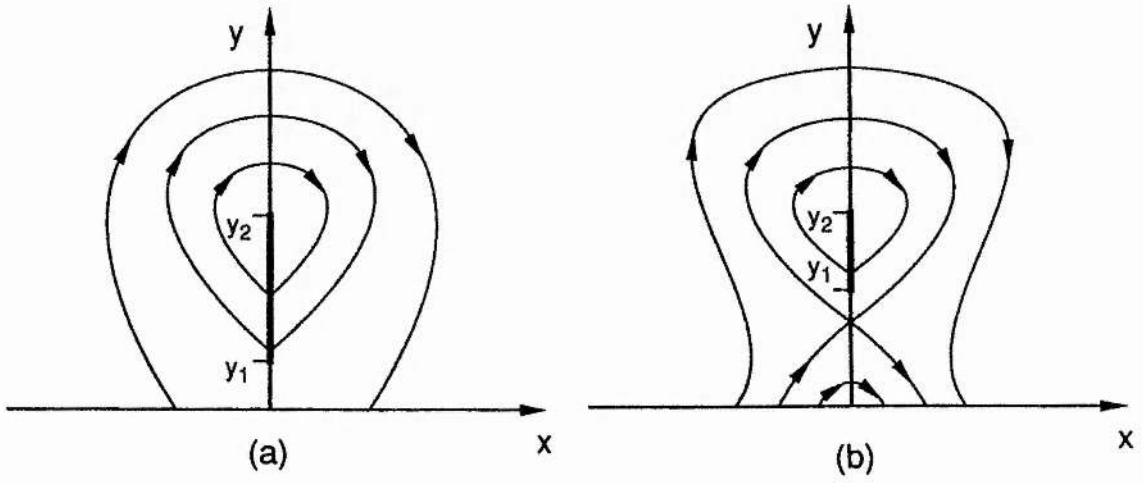

Figure 2.6 Extended current sheet configurations of an inverse polarity.

Van Tend and Kuperus (1978) and Kuperus and Van Tend (1981) extended the work of Kuperus and Raadu (1974) by allowing for an additional background field. Given the form of this field they found that increasing the current I could result in no neighbouring equilibrium position for some critical current, possibly leading to a dynamic evolution such as prominence eruption if the current is increased beyond this critical value.

Malherbe and Priest (1983) used complex variable theory to model the prominence as a cut in the upper-half complex plane extending along the imaginary axis from $\eta = iy_1$ to $\eta = iy_2$ where $\eta = x + iy$. An analytic function of η outside the cut can then describe a

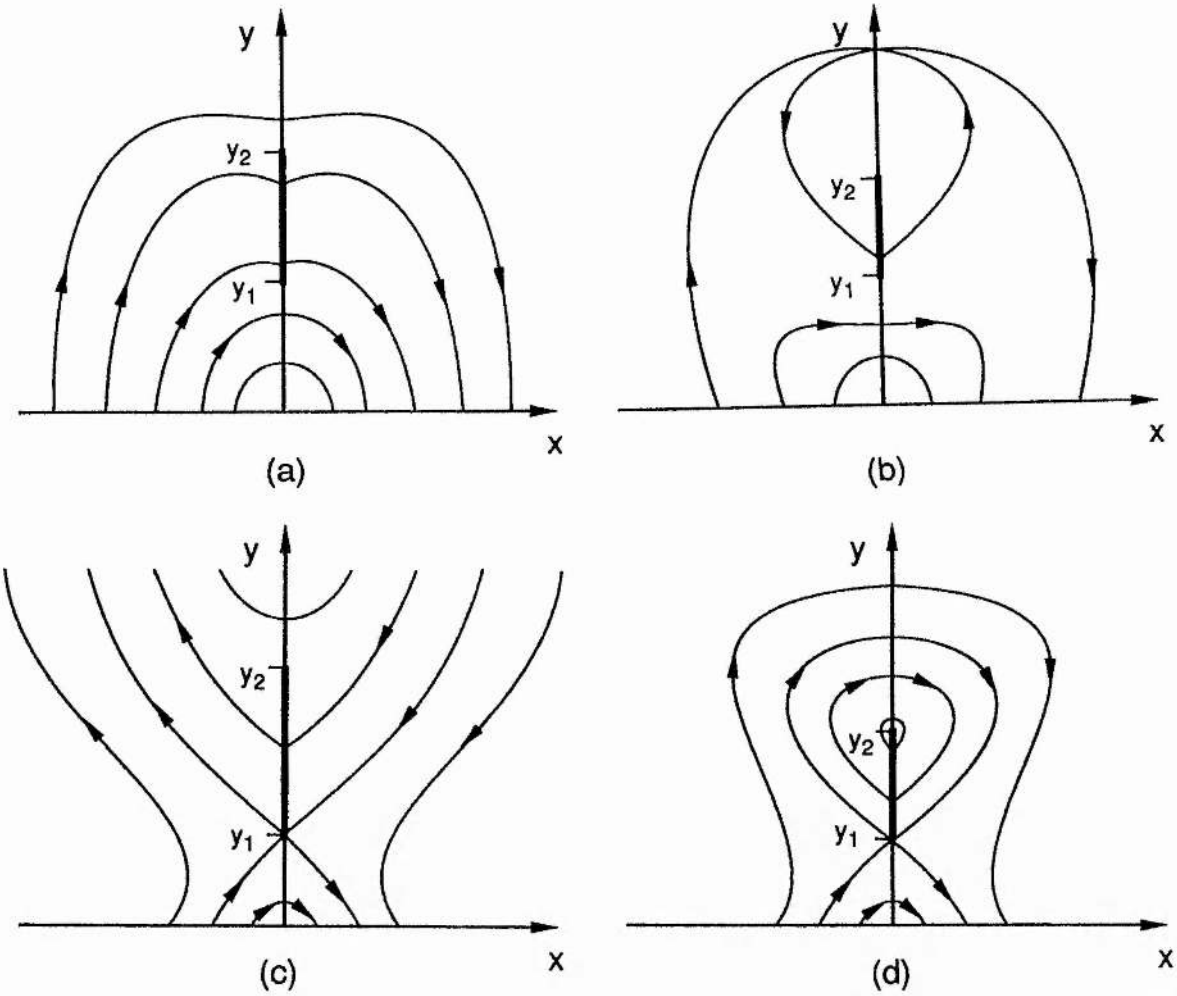

Figure 2.7 Examples of the configurations found by Malherbe and Priest. (a) and (b) show N-type while (c) and (d) show I-type configurations.

potential coronal field written in the form $B_y + iB_x$ and examples of both the N- and I-type configurations they generated are given in Figure 2.7. It should be noted, however that in the finite I-type configuration sketched in Figure 2.7(d), the field is singular and the Lorentz force is downwards at the upper end of the sheet, demonstrating a lack of equilibrium at this point. In addition, all the fields they presented are singular at the polarity inversion line.

An approach such as that of Malherbe and Priest (1983) does not allow observed forms of the photospheric and prominence magnetic fields to be used in the construction of a prominence model. Rather they are a direct result of the chosen analytical function of η. Accordingly, Demoulin et al. (1989) generalised the work of Anzer (1972) by considering the case of a current sheet which is detached from the photosphere, with a purely horizontal field across the y-axis above and

below the sheet. Assuming a potential coronal field, the solution of the resultant boundary-value problem shows that it is possible to generate N-type equilibrium configurations (see Figure 2.8) but they were unable to find any I-type configurations in which the magnetic tension force was upwards everywhere along the sheet allowing for the support of dense material.

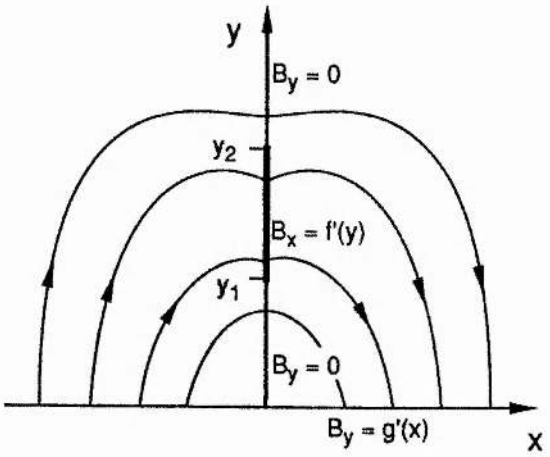

Figure 2.8 The configuration for normal polarity models generated from the boundary-value problem considered by Demoulin et al.

One of the major problems with all of the models so far described is the assumption of a potential field outside the prominence whereas observations repeatedly confirm the presence of a strong longitudinal magnetic field component. Although such a component may be introduced by simply superimposing a uniform B_z upon any of the above models, it may be more naturally introduced by assuming a more general force-free field than a potential one exists outside the prominence. As a first step, Kuperus and Van Tend (1981) discussed the effects the introduction of a force-free field may have on the equilibrium of a current filament.

Amari and Aly (1989) considered the interaction of a current filament with a linear force-free field in which the first harmonic of the force-free arcade was imposed as the background field and the current strength I and direction could be varied. They found that whatever the value of I, a unique equilibrium position $(0,y_1)$ always exists for both N- and I-type configurations, examples of which are sketched in Figure 2.9. However, a generalisation of the background field to include a further harmonic of the force-free arcade, showed

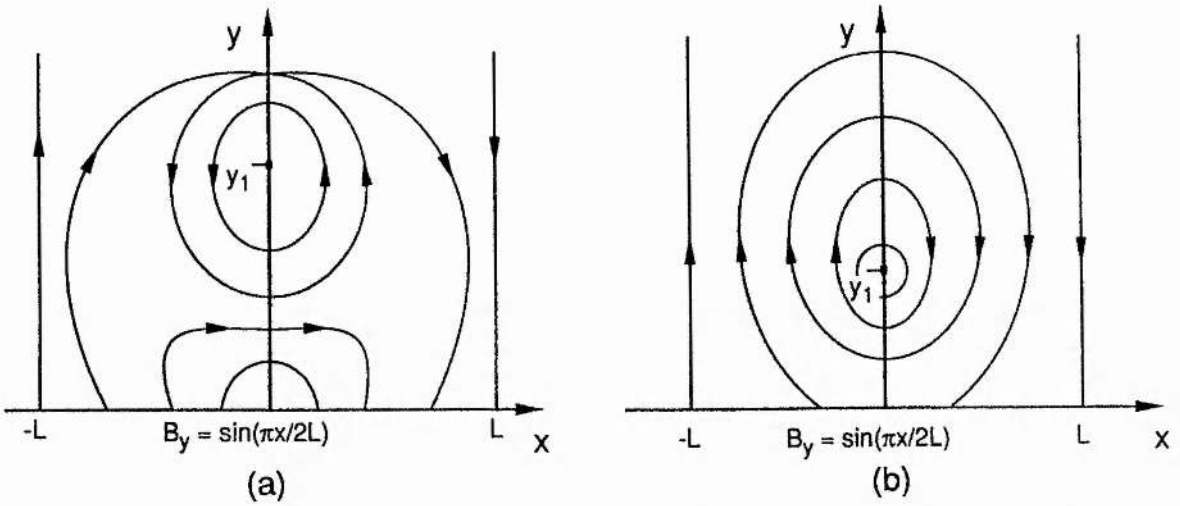

Figure 2.9 Equilibrium configurations generated from the boundary-value problem considered by Amari and Aly for a current filament in a linear force-free field. (a) shows a normal polarity and (b) an inverse polarity model.

that increasing I can result in a loss of equilibrium since the equilibrium position is no longer a monotonically increasing function of I (Demoulin and Priest, 1988). Amari and Aly (1990a) extended their work to consider a finite current sheet interacting with a linear force-free field. They imposed the same photospheric boundary condition as in the current filament case and along the prominence they imposed the distribution of the surface current. Solving the associated boundary-value problem, they found that only N-type configurations can be in equilibrium (see Figure 2.10) only if the physical parameters satisfy

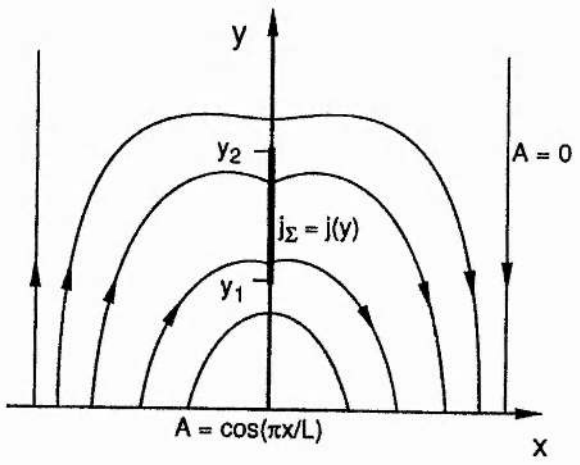

Figure 2.10 The normal polarity model produced by Amari and Aly in which a current sheet interacts with a linear force-free field.

certain constraints. They also found that in the I-type model, a downwards magnetic tension force is always present at the top of the sheet. The physical reason for such a phenomena is that there is a self-pinching effect within the sheet due to the interaction of a small element of the sheet with neighbouring elements which tends to create a downwards force in the upper parts of the sheet (Anzer, 1985; Anzer and Priest, 1985; Amari and Aly, 1990a).

It should be noted that in the above models, little attempt is made to explain how such a magnetic field arises. Rather, they simply demonstrate that dense plasma can be supported if a field line dip is present. For N-type configurations, it has been suggested that plasma condensing at the top of an arcade type structure, due to a thermal instability, may cause the field lines to sag down and create the dip. However, it is likely that the cooling plasma would drain down along the field lines before it is able to produce a dip itself since the cooling time for coronal plasma is considerably longer than its free-fall time. An alternative suggestion is that cool plasma is ballistically injected from the chromosphere along the field lines of an arcade. This would, however, require the plasma to come to rest at the top of the arcade which is a somewhat contrived situation. It would thus seem that a dip must exist before the formation of a prominence can occur (Priest et al., 1989). Amari et al. (1991) showed that it is not possible to create a dip simply by shearing a z-invariant arcade, irrespective of the shear profile. However, they did find that very long, flat field lines can be produced which may reduce the free-fall time sufficiently in order to allow cooling plasma to create the dip. In the case of I-type configurations, a field line dip naturally exists at the base of the helical windings. However, it is thought that not enough material exists in the closed field region to produce a prominence of appreciable size although recent disputes concerning the filling factor of prominences may remove this objection. It is difficult to imagine injection of material along the helical field lines but this is not ruled out as a possible means of formation.

Recently, models have been presented which attempt to describe the formation and subsequent evolution of a prominence through a series of force-free equilibria (i.e. a quasi-static evolution). For example, Priest, Hood and Anzer (1989) modelled the field surrounding the prominence as a large-scale, curved flux tube, initially

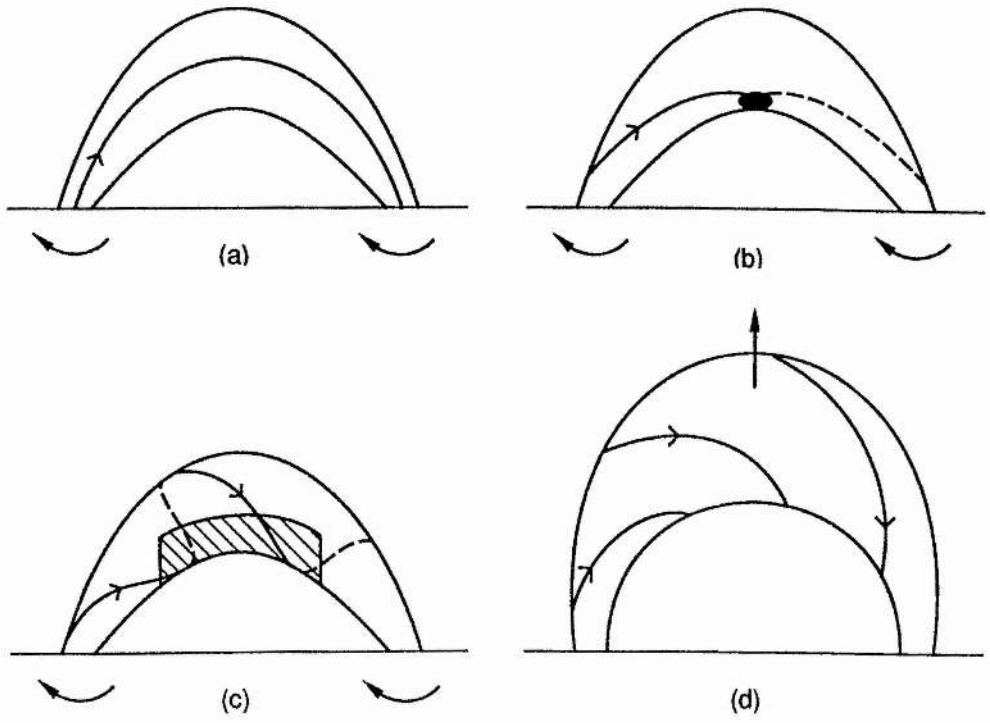

Figure 2.11 The evolution of the Twisted Flux Tube model for prominences. (a) The initial arcade type field. (b) The first field line attains a dip. (c) The prominence grows as more field lines acquire a dip. (d) The twist becomes so large that the prominence erupts. (From Priest et al., 1989).

composed of arcade-type field lines overlying a polarity inversion line. The suggested evolution is sketched in Figure 2.11. As twisting proceeds, individual field lines within the tube may acquire an upward curvature near the summit of the tube, producing a dip in which dense material can collect and be supported. Further twisting results in more and more field lines acquiring a dip, allowing the prominence to grow in length while being stretched along the polarity inversion line due to shearing photospheric motions parallel to this line. Ultimately the twist becomes so large that the tube becomes unstable and the prominence erupts, filling the tube with plasma and revealing the helical structure for the first time.

Van Ballegooijen and Martens (1989) present an alternative method by which a helical structure may be formed via a reconnection process driven by converging photospheric motions acting on a sheared arcade (see Figure 2.12). An initial potential arcade-type field, straddling a polarity inversion line, is sheared due to photospheric motions which are parallel to, but oppositely directed either side of,

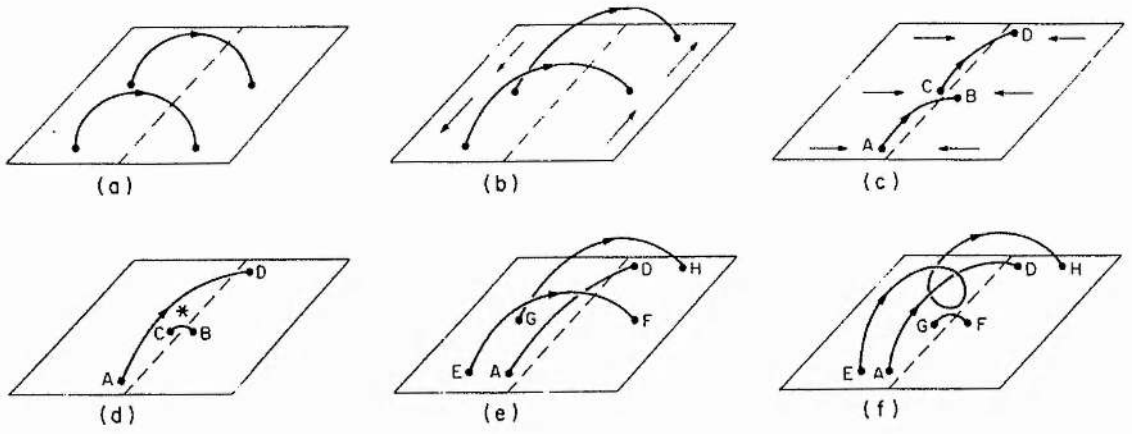

Figure 2.12 The evolution of an initial arcade-type field due to photospheric motions. (a) The initial potential field. (b) Flows along the polarity inversion line produce a sheared field. (c) Converging flows act to enhance the shear whilst bringing the footpoints towards the line. (d) Reconnection produces one long loop AD and a shorter one BC which submerges. (e) Overlying loops converge towards the line. (f) Reconnection leads to a helical field line EH and a small loop FG which submerges. (From van Ballegooijen and Martens, 1989).

the line. Converging motions normal to the line act to bring the footpoints of the sheared field lines closer towards the line so that strong current gradients are produced and the effects of magnetic diffusion are no longer negligible. This allows the field lines to reconnect, producing a short, highly curved field line, which submerges due to its associated magnetic tension forces, and a long field line around which subsequently reconnected field lines wrap themselves. Thus a helical structure is formed along the polarity inversion line in which dense material can collect at the lowest points of the helical windings. Eventually, the overlying arcade becomes unable to confine the helical structure, allowing it to erupt.

Finally, we should note that in this present work we are concerned with an analytical approach to modelling the global structure of the magnetic field in the neighbourhood of a prominence. For this reason, the numerical models that exist for prominence formation and evolution and the few models of the prominence feet and fibril structure have not been considered in this discussion.

3 PROMINENCE SHEETS SUPPORTED IN A TWISTED MAGNETIC FLUX TUBE

3.1 Chapter summary

The Twisted Flux Tube model for the support of solar prominences by Priest et al. (1989), described in section 2.5., is here extended to consider large deviations of the tube from cylindrical symmetry. The work of Priest et al. (1989) is briefly summarised in section 3.2 and the development of the mathematical model and the conditions for its solution are outlined in section 3.3. In sections 3.4 and 3.5, we present analytical solutions to the magnetohydrostatic equilibrium equation for the force-free magnetic field structure around the prominence, given two functional forms of the field component parallel to the prominence axis. An interesting extension to these solutions is considered in section 3.6 and the results are summarised and discussed in section 3.7.

3.2 Introduction

The proposal of prominence formation in a twisted flux tube by Priest et al. (1989), described in section 2.5, helped to answer some of the fundamental questions concerning these phenomena. In particular, the model demonstrates how field lines may acquire a dip in which the prominence material may subsequently collect. Additionally, the model is essentially three-dimensional and the strong longitudinal field component (indicated by the observations of Anzer and Tandberg-Hanssen, 1970; Leroy et al., 1983 and Kim, 1990) is introduced in a completely natural fashion.

It was suggested that the twisting motions arise from the effects of Coriolis forces on a diverging supergranule flow in which the field line footpoints are anchored. Twist of one sense will produce N-type configurations while twist of the opposite sense produces I-type configurations. Initially, the twist may be of either sign, but after a long time Coriolis forces tend relentlessly to produce I-type configurations as observed in most mature prominences (Leroy, 1988).

In order to make analytical progress, Priest et al. (1989) assume that the tube is uniform along its length and possesses a small

inverse aspect ratio so that it may be approximated by a straight tube of constant cross-sectional area. The tube is considered as an isolated entity but is presumed to be enclosed by a potential field which matches onto the field at the boundary of the tube. The prominence is represented by a vertical sheet of mass and current located at the low points of the helical windings within the tube. It is assumed that the deformation of the tube from cylindrical symmetry, due to the prominence sheet, is relatively small. A study of the sheet equilibrium is then possible by considering the linearised form of equation (2.27) and it is shown that equilibrium solutions can exist in which the sheet is supported against gravity.

In this chapter we proceed with an analysis similar to that of Priest et al. (1989) but here we allow for large deviations of the tube.

3.3 Mathematical development

In this section, a summary of the assumptions made in setting up the model and the basic equations which result is given. In order to investigate the magnetic field structure in the region of the prominence, a section across the tube, perpendicular to the axis is considered. Following Priest et al. (1989) we assume a small inverse aspect ratio for the tube. The large-scale curvature can then be neglected as a first approximation and we define a cylindrical polar coordinate system (r,θ,z) for the tube as illustrated in Figure 3.1. The prominence is considered to be an infinitesimally thin, vertical sheet of mass and current lying on the line $\theta = \pm\pi$ with the upper end point of the prominence located at $r = 0$.

Within the tube, in the neighbourhood surrounding the prominence, the magnetic field is assumed to be z-invariant and force-free. Following section 2.3, the field may then be expressed in terms of a flux function $A(r,\theta)$ as

$$\mathbf{B} = (B_r, B_\theta, B_z) = \left(\frac{1}{r}\frac{\partial A}{\partial \theta}(r,\theta), -\frac{\partial A}{\partial r}(r,\theta), B_z(r,\theta)\right) \quad (2.28)$$

where A satisfies

$$\nabla^2 A + \frac{d}{dA}\left(\frac{B_z^2(A)}{2}\right) = \nabla^2 A + F(A) = 0 \quad (2.27)$$

In Priest et al. (1989), a solution for $A(r,\theta)$ of the above equation in the presence of a prominence sheet was obtained by

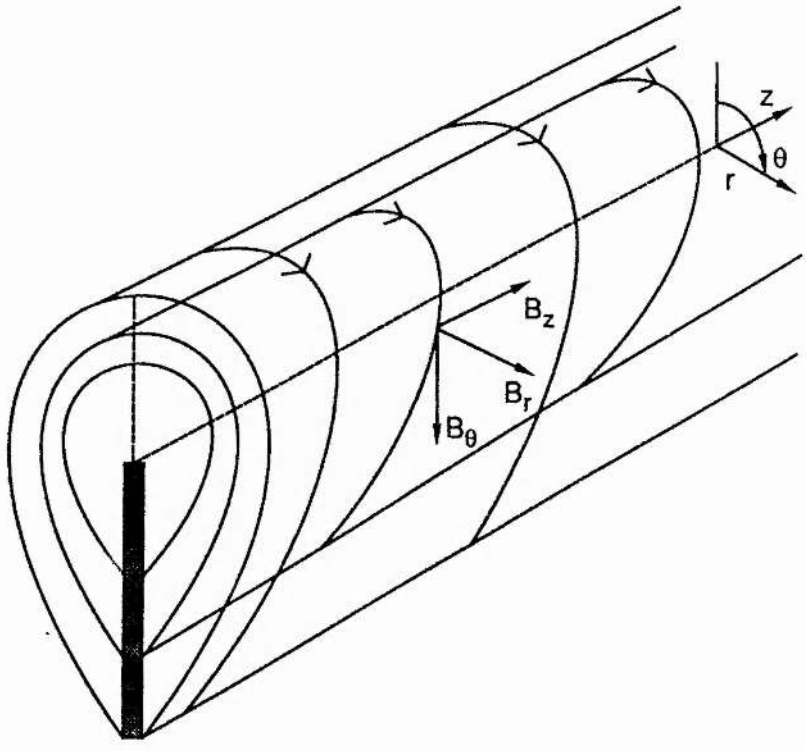

Fig. 3.1 The notation used for a flux tube in which a prominence sheet is supported along the line $\theta = \pi$.

considering this field to be a perturbation $A_1(r,\theta)$ about a cylindrically symmetric field $A_0(r)$ in which no current sheet is present. Thus

$$A(r,\theta) = A_0(r) + A_1(r,\theta) \qquad (3.1)$$

where $A_0(r)$ satisfies

$$\nabla^2 A_0 + F_0(A_0) = 0 \qquad (3.2)$$

However, the function $F_0(A)$ for the cylindrical field is not necessarily the same as the function $F(A)$ for the perturbed system since the function $B_z(A)$ in the presence of a prominence sheet may not be the same as in the absence of the sheet before the prominence forms. Let us denote by $F_1(A)$ the difference between these functions so that

$$F(A) = F_0(A) + F_1(A) \qquad (3.3)$$

A Taylor expansion to first order then gives us

$$F(A) \approx F_0(A_0) + F_1(A_0) + F'_0(A_0)A_1 \qquad (3.4)$$

and subtracting equation (3.2) from equation (2.27) then yields

$$\nabla^2 A_1 + F'_0(A_0)A_1 = - F_1(A_0) \qquad (3.5)$$

The linearised equation (4.13) in Priest et al. (1989) neglected the term on the right-hand side of equation (3.5), making the assumption that

F(A) and hence $B_z(A)$ does not change as the model evolves from the original symmetric state in which no prominence exists to the perturbed state containing the prominence sheet.

Now the amount of plasma per unit length in a volume element with section r dr dθ is

$$M = \rho\, r\, dr\, d\theta \qquad (3.6)$$

and the corresponding axial magnetic flux threading the element is

$$f = B_z\, r\, dr\, d\theta \qquad (3.7)$$

These may be integrated over θ to give the mass and flux between neighbouring flux surfaces. If one starts with a cylindrical flux tube and then supposes that the prominence forms to give a flux tube with a current sheet, the question is: how does $B_z(A)$ change? This is a nontrivial question, which is outside the scope of this chapter to answer. B_z will depend on several factors, such as the end conditions where the flux tube comes down and concentrates towards sources in the photosphere or the details of the prominence formation process. Furthermore, initially the density is spread fairly uniformly over azimuth (θ), but after formation it is concentrated in the current sheet. The total flux (f integrated over r and θ) will be unlikely to change during formation but its distribution in r and θ may well alter. If it does not do so and the density and mass outside the sheet remain constant (due to a mass inflow by evaporation or injection to provide the prominence mass) then we can see from the above two equations that $B_z(A)$ will be unaltered. If on the other hand the density ρ decreases (because of, for instance, prominence condensation from the corona) then, if M is conserved, r dr dθ would increase and B_z would decrease.

In this chapter we will not incorporate such complications. We will, however, consider much larger deviations away from cylindrical symmetry than Priest et al. (1989). In doing so we can choose between two possibilities. We could consider our model as describing the evolution from a cylindrically symmetric state $A_0(r)$ to a perturbed state $A(r,\theta)$ during which the function $F_0(A)$ changes by $F_1(A)$. Assuming $F_0(A)$ and $F_1(A)$ then to be known, we may solve equation (3.2) to obtain $A_0(r)$ and then equation (3.5) to obtain $A_1(r,\theta)$ and hence obtain the final state $A(r,\theta)$ from equation (3.1). This approach is difficult to implement in practise because the function $F_1(A)$ cannot easily be determined.

Alternatively, we shall consider our model to describe only the final state of the system without reference to the initial state. Thus F(A) corresponds now to the functional form of $B_z(A)$ in the presence of a particular prominence sheet and the solution of equation (2.27) for $A(r,\theta)$ describes the field everywhere outside this sheet. This greatly simplifies the mathematical analysis of the model as we no longer need to introduce the arbitrary function $F_1(A)$. We are however, unable to determine the original cylindrically symmetric field from which the final system was derived (unless of course we assume that $B_z(A)$ does not alter during the evolution). This is the course which we will pursue in this chapter.

The field is assumed to be symmetrical about the vertical axis and so above the prominence sheet we have

$$B_r = 0 \text{ on } \theta = 0 \qquad (3.8)$$

It should be noted that a change in the direction of B_θ or B_z within the tube is physically unrealistic and so, as r is increased from zero for a particular value of θ, we have the condition that B_θ and B_z remain of constant sign within the extent of the tube. Furthermore, for a physically reasonable model it is necessary that the field components are bounded at all points within the tube.

The mass in the prominence sheet is assumed to be in static equilibrium between the action of a downward uniform gravitational field and a necessarily upward magnetic tension force provided by **B**. For this force to be in the required direction there must be a field line dip at $\theta = \pm\pi$ for all r so that (c.f. section 2.5)

$$\left(\frac{dr}{d\theta}\right)_{\theta\to\pi-} = \left(\frac{B_r}{r\,B_\theta}\right)_{\theta\to\pi-} > 0 \qquad (3.9)$$

If this is indeed the case then the local force balance equation gives the mass density per unit length m as

$$m(r) = [B_r](r)\; B_\theta(r,\pi) / \mu\, g_c \qquad (3.10)$$

where $[B_r]$ is the jump in B_r across the prominence from $\theta = -\pi$ to $\theta = +\pi$. The total mass per unit length M may then be determined from

$$M = \int_0^{r_\pi} m \; dr \qquad (3.11)$$

where r_π is the radius of the outermost field line at $\theta = \pi$.

In the following two sections, we seek solutions to equation (2.27) for $A(r,\theta)$, the field around the prominence when it has already formed, after prescribing one of two functional forms of $B_z(A)$. The

field **B** must satisfy the four properties outlined above, namely

a) The deformation of the tube is symmetric about the vertical axis (equation (3.8)).

b) There is no sign change in either B_z or B_θ within the extent of the tube.

c)There are no singularities of the field components in the neighbourhood of the prominence.

d) There exists a field line dip along the line $\theta = \pi$ in which a prominence may be supported (equation (3.9)).

3.4 Solution with $B_z = \pm cA$

If this form of B_z is assumed we have the so-called constant-α field and equation (2.27) becomes

$$\nabla^2 A + c^2 A = 0 \qquad (3.12)$$

to which separable solutions of the form $A(r,\theta) = R(r)f(\theta)$ may be sought so that equation (3.12) becomes

$$\frac{r}{R}\frac{d}{dr}\left(r\frac{dR}{dr}\right) + c^2r^2 = -\frac{1}{f}\frac{d^2f}{d\theta^2} = K^2 \qquad (3.13)$$

The constant K^2 is assumed to be positive since negative values give imaginary solutions for R.

The solution for $f(\theta)$, subject to the condition of symmetry about the vertical axis is

$$f(\theta) = \cos(K\theta) \qquad (3.14)$$

Rewriting the radially dependent part of equation (3.13) with $s = cr$ yields Bessel's equation of order K with solution

$$R(r) = b\,J_K(cr) \qquad (3.15)$$

where the Bessel function of the second kind $Y_K(cr)$ has been excluded since it tends to infinity as r tends to zero, hence violating condition (c) above.

Combining equations (3.14) and (3.15) gives a solution for A as

$$A(r,\theta) = b\,J_K(cr)\,\cos(K\theta) \qquad (3.16)$$

but, noting that equation (3.12) is linear, a general solution to this equation can be obtained by adding together all possible solutions. This general solution may be written

$$A(r,\theta) = \frac{B_0}{c}\left(J_0(cr) + \sum_{n=1}^{\infty} b_n \cos(K_n\theta) J_{K_n}(cr)\right) \qquad (3.17)$$

on taking the term for which $K_n = 0$ outside the sum. For each n we must have $K_n \geq K_l$, the lowest value of K_n for which there are no singularities in the field components in the neighbourhood of the prominence. Also we require that there be no change of sign in the B_θ component for small values of r.

The field components are obtained from equation (2.28) and so may be expressed as

$$B_r = -B_0 \sum_{n=1}^{\infty} b_n K_n \sin(K_n\theta) J_{K_n}(cr)/(cr) \tag{3.18}$$

$$B_\theta = B_0 \left(J_1(cr) - \sum_{n=1}^{\infty} b_n \cos(K_n\theta) \left(\frac{K_n J_{K_n}(cr)}{cr} - J_{K_n+1}(cr) \right) \right) \tag{3.19}$$

$$B_z = \pm B_0 \left(J_0(cr) + \sum_{n=1}^{\infty} b_n \cos(K_n\theta) J_{K_n}(cr) \right) \tag{3.20}$$

Clearly, B_0 (assumed to be positive without loss of generality) is the strength of the longitudinal field at $r = 0$. The parameters K_n describe how rapidly the field changes with θ and the b_n represent the departure of the field from a cylindrically symmetric case (given by $b_n = 0$ for all n). Note that this symmetrical case is not necessarily the one from which the final state with the prominence sheet is generated.

By considering the series expansion of $J_K(x)$ close to $x = 0$, it will be seen that singularities of the field components B_r and B_θ are avoided by taking $K_n \geq 1$ for all n and that a sign change in B_θ is avoided for small r by taking $K_n \geq 2$ for all n. Thus we find $K_l = 2$.

Taking as a particular solution to equation (3.12)

$$A = B_0 \{J_0(cr) + b \cos(K\theta) J_K(cr)\} / c \tag{3.21}$$

gives field components

$$B_r = - B_0 K b \sin(K\theta) J_K(cr) / (cr) \tag{3.22}$$

$$B_\theta = B_0 \{J_1(cr) - b \cos(K\theta)[K J_K(cr) / (cr) - J_{K+1}(cr)]\} \tag{3.23}$$

$$B_z = \pm B_0 \{J_0(cr) + b \cos(K\theta) J_K(cr)\} \tag{3.24}$$

where $K \geq 2$.

For a fixed value of θ, B_z generally changes sign at a smaller value of r than B_θ and so the curve $B_z = 0$ in the r-θ plane forms the outermost possible field line (since A and hence B_z are constant on field lines). Thus the field is purely azimuthal on the outermost allowable field line.

To satisfy the criterion that a field line dip is present at $\theta = \pm\pi$, we must have $B_r(r,\pi) > 0$ since B_θ is positive for small r. This implies that $b < 0$ for $2i < K < 2i+1$ and $b > 0$ for $2i+1 < K < 2i+2$ where $i = 1,2,3,...$ Note that for $K = 2,3,4,...$ $dr/d\theta$ evaluated at $\theta = \pi$ is zero since B_r vanishes along this line and no dip exists.

Examples of such fields are illustrated in Figure 3.2. Note especially the field line dip along the line $\theta = \pi$ in which the prominence sheet is supported. Figure 3.3 shows the variation of B_θ with distance along the vertical axis. For $2 \leq K < 3$ notice that B_θ decreases as K increases since the θ-dependent term decreases passing from a positive to a negative value. The increase in the allowed radial extent of the tube and hence the prominence height may also be seen. For $3 \leq K < 4$ and $\theta = 0$, the second term in the expression for B_θ becomes smaller in magnitude as K is increased and hence B_θ increases. However for $\theta = \pi$ the $\cos(K\pi)$ term will increase with K, again becoming positive, and so cause B_θ to decrease. For any fixed value of K, an increase in the magnitude of b serves to magnify the effect of the θ-dependent term.

The mass density per unit length for the prominence within the current sheet is obtained from equation (3.10) as

$$m = \frac{m_0 J_K(cr)}{cr}\left(J_1(cr) - b\cos(K\pi)\left(\frac{KJ_K(cr)}{cr} - J_{K_n+1}(cr)\right)\right) \quad (3.25)$$

where

$$m_0 = -2\sin(K\pi)\, K\, b\, B_0^2 / \mu\, g_c \quad (3.26)$$

The variation of m along the prominence is shown in Figures 3.4(a) to 3.4(d). Clearly since B_r and B_θ both vanish at $r = 0$, m will do likewise. Since B_r also vanishes along the prominence sheet for integer values of K, m will remain zero for all values of r. The increase in the maximum allowable extent of the tube in the direction of the prominence height as K increases from one integer value to the next is also clearly shown. Increasing the magnitude of b obviously increases m. The total mass per unit length is calculated from equation (14) where r_π is the value of r at which B_z changes sign at $\theta = \pi$. The variation of mass with K and b evaluated numerically is shown in Figure 3.4(e).

It can be shown as follows that these solutions are the only separable solutions to equations (2.24) and (2.2) that satisfy all the conditions outlined above. Following the work of Priest and Milne (1979), assume separable solutions for the field components exist such that

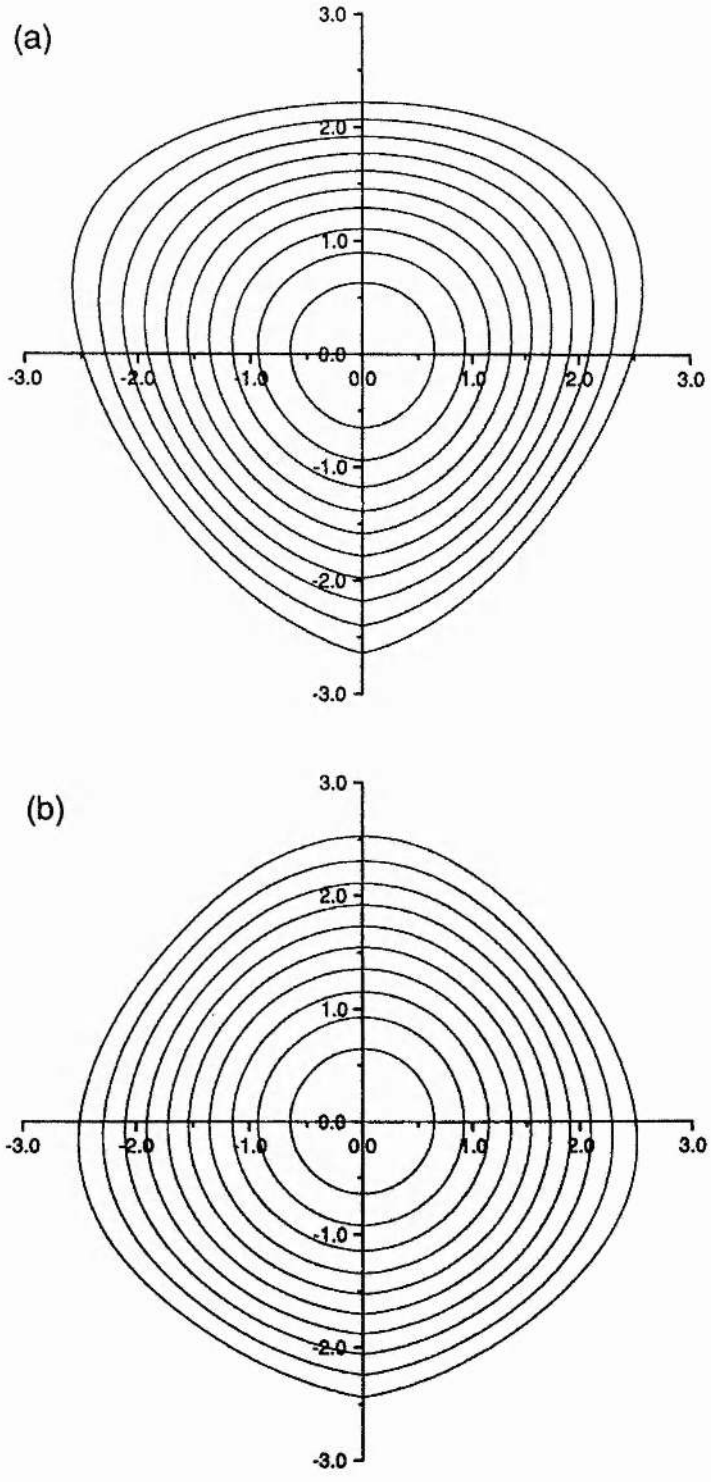

Fig. 3.2 Magnetic field configurations for the solution in which $B_z = cA$. (a) K = 2.8, b = -0.5, c = 1.0, (b) K = 3.8, b = 0.5, c = 1.0.

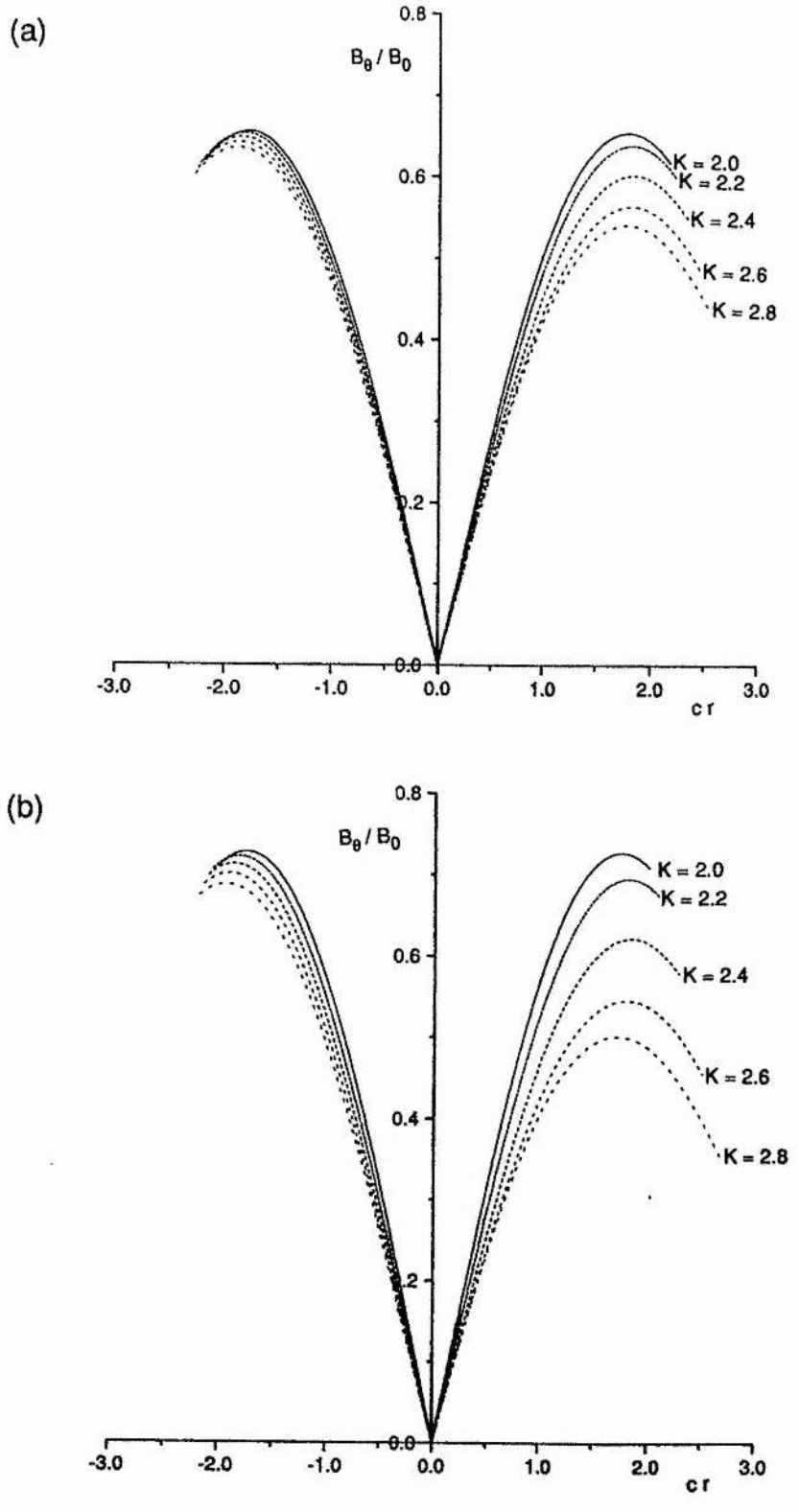

Fig. 3.3 The variation of B_θ with cr along the symmetry axis. Negative values of cr refer to the line $\theta = 0$, and positive values are along the prominence. (a) b = -0.3, $2.0 \leq K \leq 2.8$, (b) b = -0.6, $2.0 \leq K \leq 2.8$.

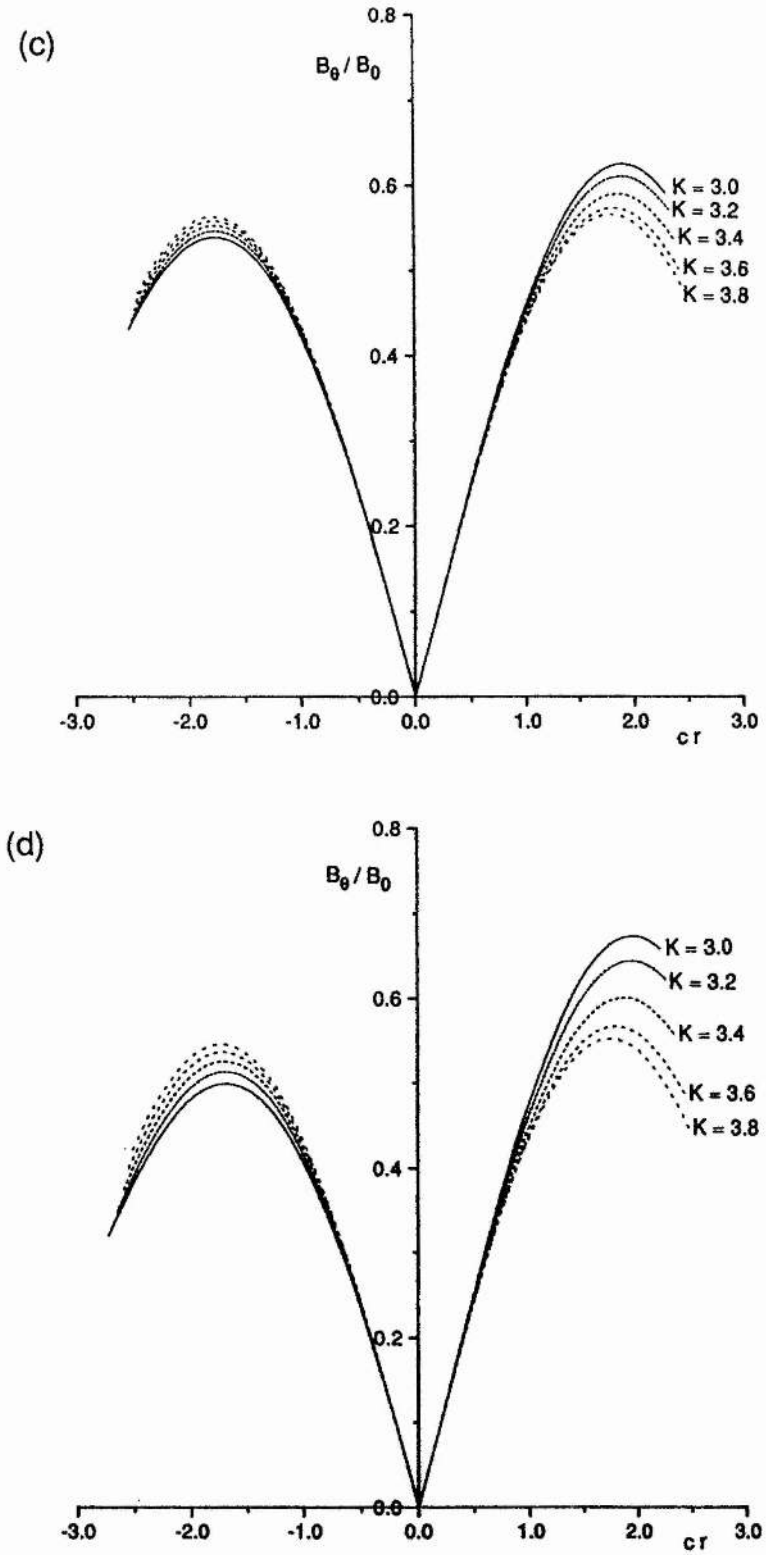

Fig. 3.3 The variation of B_θ with cr along the symmetry axis. Negative values of cr refer to the line $\theta = 0$, and positive values are along the prominence. (c) b = 0.3, $3.0 \leq K \leq 3.8$, (d) b = 0.6, $3.0 \leq K \leq 3.8$.

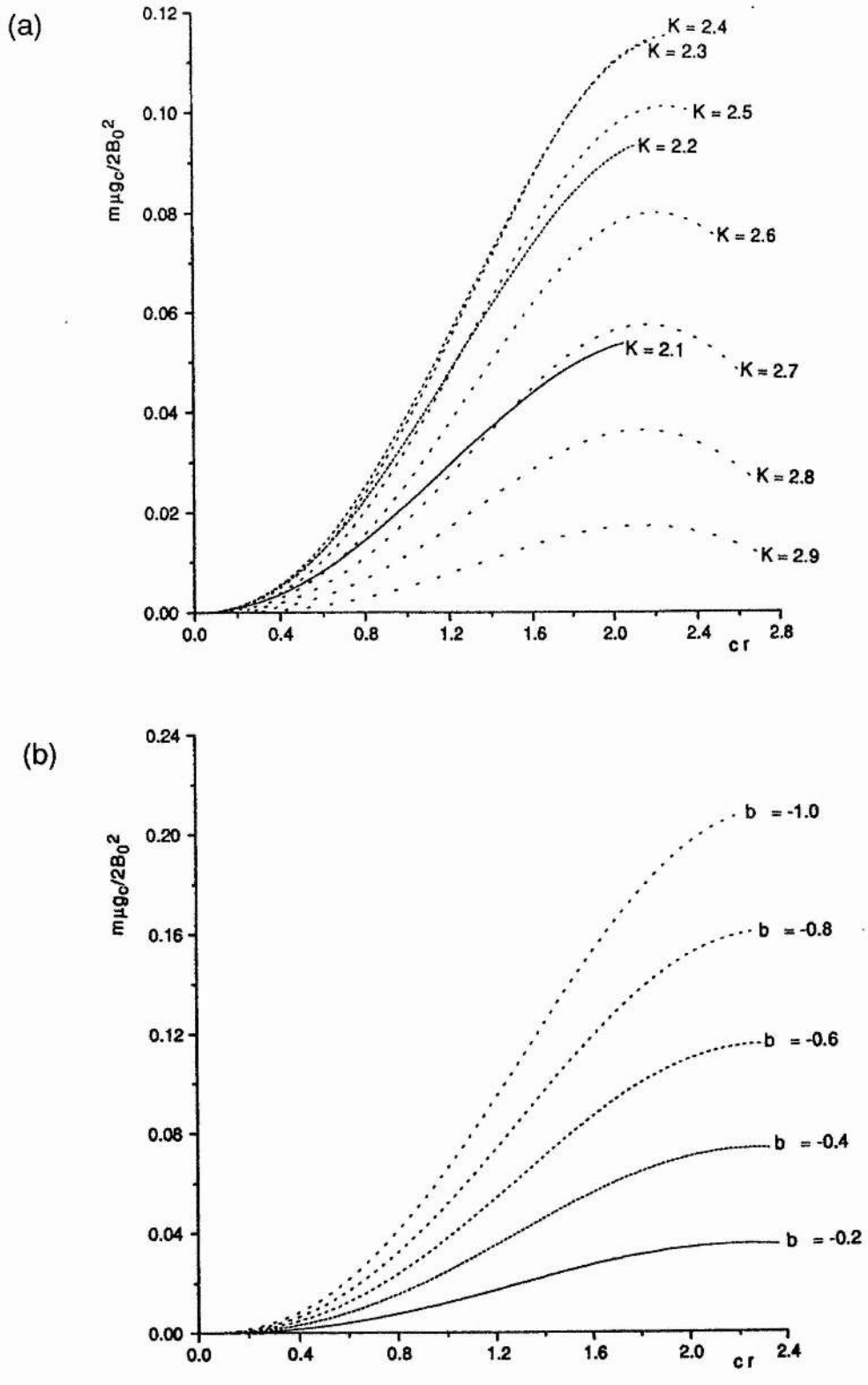

Fig. 3.4 The variation of m with cr for different values of K and b. (a) b = -0.6 and (b) K = 2.4.

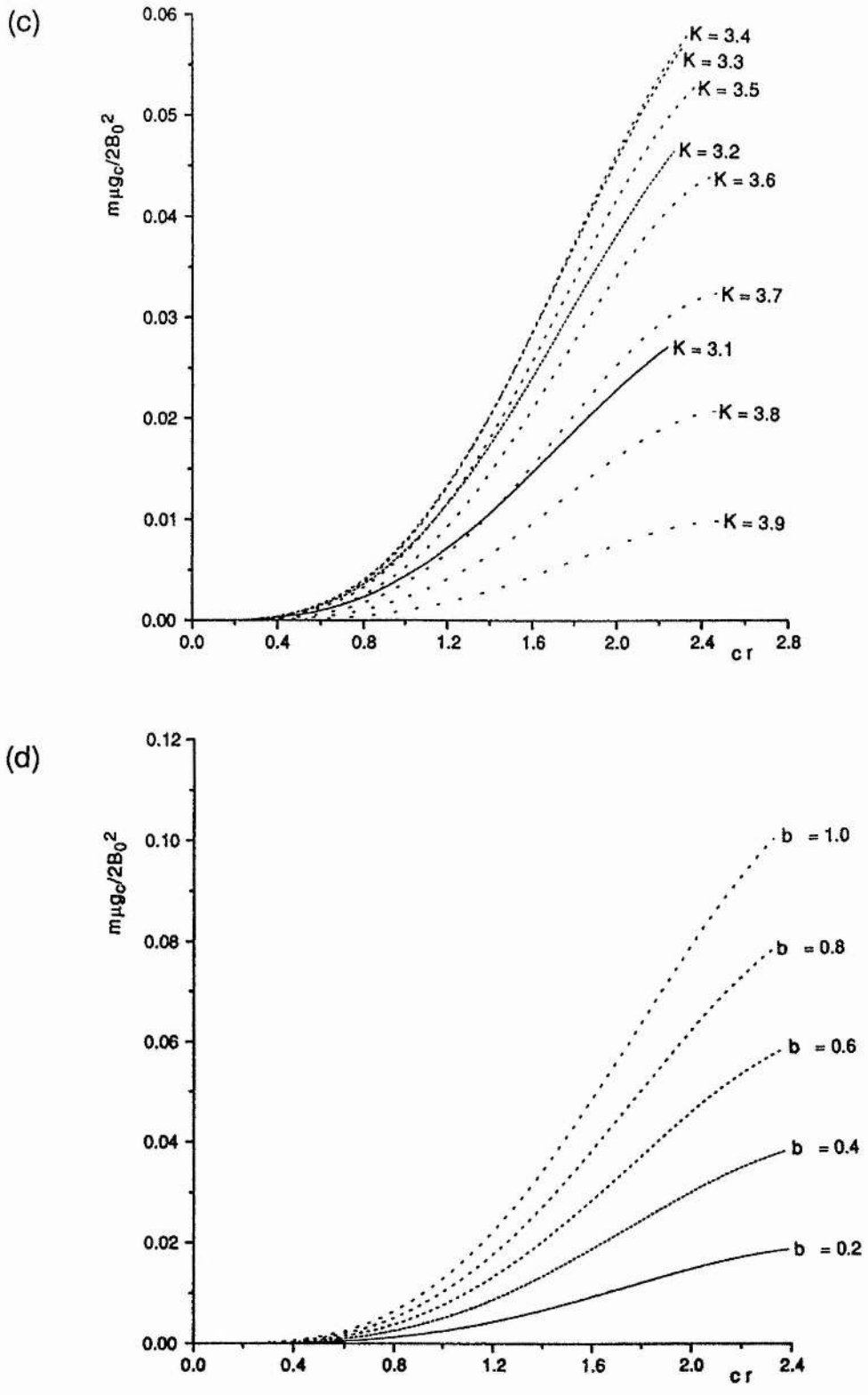

Fig. 3.4 The variation of m with cr for different values of K and b. (c) b = 0.6 and (d) k = 3.4.

(e)

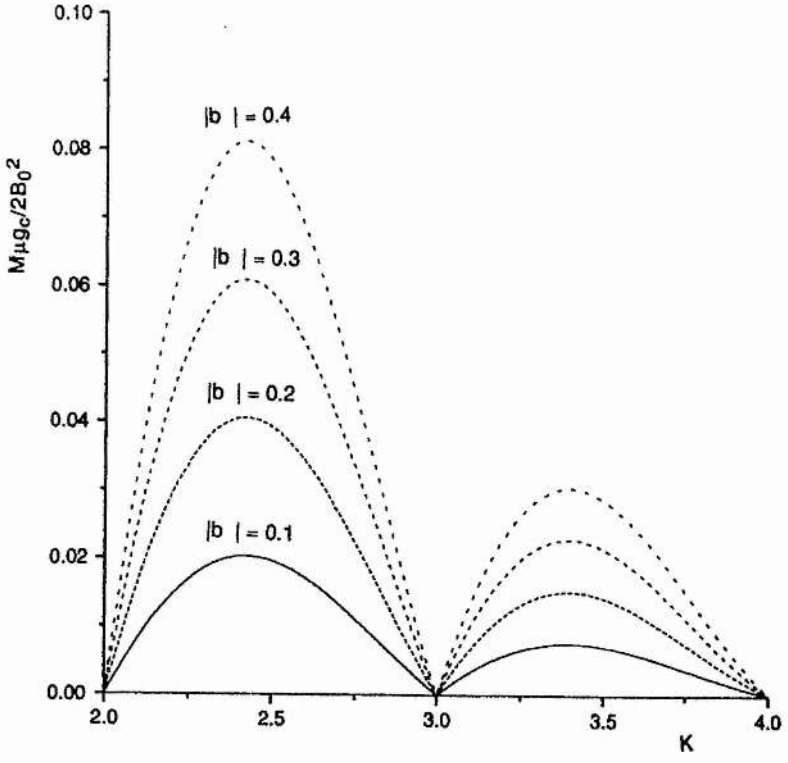

Fig. 3.4 (e) The variation of M with K for different values of b and for c = 1.0.

$$B_r = R_r(r)F_r(\theta), \quad B_\theta = R_\theta(r)F_\theta(\theta), \quad B_z = R_z(r)F_z(\theta) \tag{3.27}$$

The r- and z-components of equation (2.24) along with equation (2.2) then give

$$\frac{rR_z}{R_rR_\theta}\frac{dR_z}{dr} + \frac{F_\theta^2}{F_z^2}\frac{1}{R_r}\frac{d}{dr}(rR_\theta) = l = \frac{F_\theta}{F_z^2}\frac{dF_r}{d\theta} \tag{3.28}$$

$$\frac{rR_r}{R_zR_\theta}\frac{dR_z}{dr} = m = -\frac{F_\theta}{F_rF_z}\frac{dF_z}{d\theta} \tag{3.29}$$

$$\frac{1}{R_\theta}\frac{d}{dr}(rR_r) = n = -\frac{1}{F_r}\frac{dF_\theta}{d\theta} \tag{3.30}$$

In order to make equation (3.28) separable, one of the following conditions must apply.

a) F_θ/F_z = constant

This just gives rise to the solutions outlined above for $B_z = cA$.

b) $dR_z/dr = 0$

Priest and Milne give the solutions

$$B_r = b\sin(\sqrt{(nl)}\theta)\, r^{-1+\sqrt{(nl)}} \tag{3.31}$$

$$B_\theta = b\cos(\sqrt{(nl)}\theta)\, r^{-1+\sqrt{(nl)}} \tag{3.32}$$

$$B_z = B_0 \tag{3.33}$$

B_θ will not change sign for $|\sqrt{(nl)}| < 1/2$ but for there to be no singularity of B_r and B_θ at the origin $\sqrt{(nl)} > 1$. These two conditions cannot both be satisfied simultaneously and so no physically realistic solutions of this form exist.

c) $\frac{1}{R_r}\frac{d}{dr}(rR_\theta) = \text{constant}$

Here two types of solution exist depending on whether or not the constant is zero or non-zero. The case where the constant is zero was studied by Birn et al. (1978) who obtained the solutions

$$B_r = r^{-1}\, c\, \tanh(c\theta) \tag{3.34}$$

$$B_\theta = r^{-1} \tag{3.35}$$

$$B_z = r^{-1}\, c\, /\, \cosh(c\theta) \tag{3.36}$$

but the field components are all singular at $r = 0$ and so are not acceptable.

For a non-zero constant, k say, Priest and Milne give the solutions

$$R_r = r^{-1+k}, \qquad R_\theta = r^{-1+k}, \qquad R_z = \pm r^{-1+k} \tag{3.37}$$

$$F_r = -\frac{1}{k}\frac{dF_\theta}{d\theta}, \qquad F_z = \lambda\, |F_\theta|^{(k-1)/k} \tag{3.38}$$

where F_θ is a solution of

$$\frac{d^2F_\theta}{d\theta^2} + k^2F_\theta + \lambda^2\, k\,(k-1)\, F_\theta\, |F_\theta|^{-2/k} = 0 \tag{3.39}$$

Clearly, singularities of the field components can only be prevented by taking $k > 1$. The solution of the θ-dependent equations for F_θ with $\lambda = 0$, subject to the condition of symmetry, is simply

$$F_\theta = F_0 \cos(k\theta) \tag{3.40}$$

which changes sign for $|k| > 1/2$. With $\lambda \neq 0$ however, we have the condition $k > 1$ already in order to prevent singularities and the addition of the extra term increases the rate of change of F_θ with θ since the term is positive. Thus F_θ will always change sign for θ in the range $[-\pi,\pi]$ and so all the separable solutions are physically unrealistic except for the linear one.

3.5 Solution with $B_z = \pm 2\, c\, A^{1/2}$

Assuming this form of B_z, equation (2.27) becomes

$$\nabla^2 A + 2\, c^2 = 0 \tag{3.41}$$

which is just Poisson's equation with a uniform source. Since it has

been shown that separable solutions are irrelevant for forms of B_z other than $B_z = cA$, we seek instead a particular integral to equation (3.41) by assuming such a solution to be dependent on r alone. A general solution to equation (3.41) is then obtained by adding this particular integral to the complementary function of the homogenous equation

$$\nabla^2 A = 0 \tag{3.43}$$

which is just Laplace's equation.

Thus a particular integral for equation (3.42) is obtained from

$$\frac{1}{r}\frac{d}{dr}\left(r\frac{dA_p}{dr}\right) = -2c^2 \tag{3.44}$$

which has solution

$$A_p = -\frac{c^2 r^2}{2} \tag{3.45}$$

while a complementary function to equation (3.43) can be found by seeking separable solutions of the form $A_c(r,\theta) = R(r)f(\theta)$ so that equation (3.43) becomes

$$\frac{r}{R}\frac{d}{dr}\left(r\frac{dR}{dr}\right) = -\frac{1}{f}\frac{d^2 f}{d\theta^2} = K^2 \tag{3.46}$$

The solution for the θ-dependent part, subject to the condition of symmetry is

$$f(\theta) = \cos(K\theta) \tag{3.47}$$

The r-dependent part may be written

$$r^2 R'' + r R' - K^2 R = 0 \tag{3.48}$$

namely an Euler equation with solution

$$R(r) = b\, r^K \tag{3.49}$$

neglecting the term in r^{-K} which would give a singularity at $r = 0$.

The resulting general solution for equation (3.41) can thus be written

$$A(r,\theta) = A_p + A_c = -\frac{c^2 r^2}{2} + b_0 + \sum_{n=1}^{\infty} b_n \cos(K_n\theta) r^{K_n} \tag{3.50}$$

where A_c is obtained by combining equations (3.47) and (3.49) and summing all possible solutions. On replacing $c^2 = \sqrt{2}B_0/2l$ and $b_0 = \sqrt{2}B_0 l/4$, A may be expressed as

$$A(r,\theta) = \frac{\sqrt{2}B_0}{4l}(l^2 - r^2) + \sum_{n=1}^{\infty} b_n \cos(K_n\theta) r^{K_n} \tag{3.51}$$

where for each n, $K_n \geq K_l$, the lowest value of K_n for which no singularities occur in the field components and no sign change occurs in

B_θ for small r.

The field components, given by equation (2.28), may be written

$$B_r = - \sum_{n=1}^{\infty} b_n \sin(K_n\theta) K_n r^{K_n-1} \qquad (3.52)$$

$$B_\theta = \frac{\sqrt{2}B_0 r}{2l} - \sum_{n=1}^{\infty} b_n \cos(K_n\theta) K_n r^{K_n-1} \qquad (3.53)$$

$$B_z = \pm \left(B_0^2 \left(1 - \frac{r^2}{l^2}\right) + \frac{2\sqrt{2}B_0}{l} \sum_{n=1}^{\infty} b_n \cos(K_n\theta) r^{K_n} \right)^{1/2} \qquad (3.54)$$

Clearly, B_0 (assumed to be positive without loss of generality) is the strength of the longitudinal field at r = 0. Once again the parameters K_n describe the rate at which the field changes with θ, while the b_n represent the departure of the field from a cylindrically symmetric field (again, not necessarily the original one) and l scales the tube radius such that B_z changes sign when r = l in the cylindrically symmetric case. To avoid singularities in the field components, $K_n \geq 1$ for all n but a sign change in B_θ is only avoided by taking $K_n \geq 2$ for all n. This implies that $K_1 = 2$, a point not taken into account in some of the solutions presented in Priest et al. (1989).

Note that the imposition of an observed distribution of B_θ along the prominence does not allow the determination of unique values for the K_n and b_n. This distribution with r is only of use in the following limited way. It must be assumed that there exist only a finite number (N, say) of values of K_n and that these are known along with values of B_0 and l. Then, measurements of B_θ at N points along the prominence will yield a set of N simultaneous equations from equation (3.53) which can be solved for the N unknowns $b_1, b_2, \ldots, b_N$. These then determine the field throughout the neighbouring region. It is difficult to apply such a method to the solutions presented in section 3.4 due to the oscillatory nature of Bessel functions.

Taking as a particular solution to equation (3.41)

$$A = \sqrt{2}\, B_0 (l^2 - r^2) / (4\, l) + b\, r^K \cos(K\theta) \qquad (3.55)$$

gives field components

$$B_r = - r^{K-1}\, b\, K \sin(K\theta) \qquad (3.56)$$

$$B_\theta = B_0\, r / (\sqrt{2}\, l) - r^{K-1}\, b\, K \cos(K\theta) \qquad (3.57)$$

$$B_z = \pm \{B_0^2 (1 - r^2/l^2) + 2\sqrt{2}\, B_0\, b\, r^K \cos(K\theta)/l\}^{1/2} \qquad (3.58)$$

where $K \geq 2$. As r tends to ∞, the magnitudes of the field components

all grow without bound and so the solution is only valid locally in the neighbourhood of the prominence.

Note that these solutions for the field components are identical to those found in Priest et al. (1989) with ε replaced by b. Here, however, there is no constraint on the magnitude of b. We now realise that the linearised solutions found in Priest et al. (1989) are also valid in the nonlinear regime. As r is increased from zero for a fixed value of θ, B_z and also B_θ (if b cos(Kθ) is positive) will change sign. As argued earlier, in general the curve $B_z = 0$ will form the outermost possible field line and hence give the limit to the possible radial extent of the tube.

Since B_θ is positive for small r, a field line dip exists at $\theta = \pm\pi$ if, from equation (12), $B_r(r,\pi) > 0$ and so $b < 0$ for $2i < K < 2i+1$ and $b > 0$ for $2i+1 < K < 2i+2$ where $i = 1,2,3,...$ Once again note that for $K = 2,3,4,...$ $dr/d\theta$ evaluated at $\theta = \pm\pi$ is zero and so no dip exists. Examples of such fields may be seen in Figure 3.5. The variation of B_θ with distance along the vertical axis is shown in Figure 3.6 in which B_θ has been rewritten

$$\frac{\sqrt{2}B_\theta}{B_0} = \tilde{r} - \tilde{b}\,\tilde{r}^{K-1}K\cos(K\theta) \qquad (3.59)$$

where

$$\tilde{r} = r/l, \quad \tilde{b} = \frac{\sqrt{2}}{B_0}\,b\,l^{K-1} \qquad (3.60)$$

As K is increased from one integer value to the next, the strength of B_θ along the prominence decreases as the second term in this expression becomes more negative. Again, increasing the magnitude of b enhances the effect of this second term.

From equation (3.10), the mass density per unit length may be written

$$m = \frac{-2Kb\sin(K\pi)}{\mu g_c}\left(\frac{\sqrt{2}B_0 r^K}{2l} - bKr^{2K-2}\cos(K\pi)\right) \qquad (3.61)$$

or

$$\frac{m\mu g_c}{B_0^2} = -K\tilde{b}\sin(K\pi)\left(\tilde{r}^{\,K} - \tilde{b}K\tilde{r}^{2K-2}\cos(K\pi)\right) \qquad (3.62)$$

Once more this will always be positive since $B_r > 0$ along $\theta = \pi$ and $B_\theta > 0$ for all r and θ within the tube. The variation of m along the prominence is shown in Figures 3.7(a) and 3.7(b). As expected, m vanishes for integer values of K since B_r is then zero, and the allowable tube radius increases with K between two integer values. The total

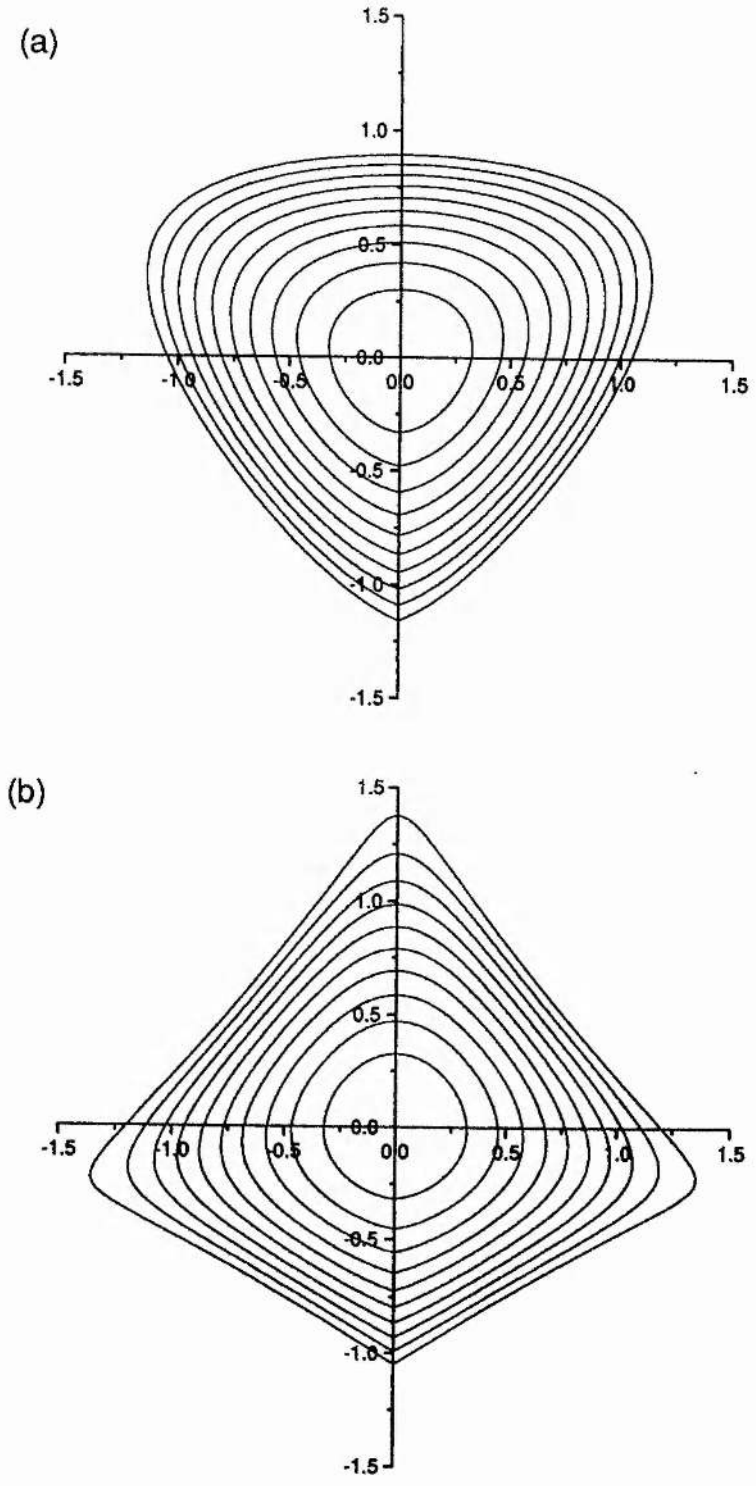

Fig. 3.5 Magnetic field configurations for the solution in which $B_z = 2cA^{1/2}$. (a) K = 2.8, b = -0.5, B_0 = 5.0, l = 1.0, (b) K = 3.8, b = 0.5, B_0 = 5.0, l = 1.0.

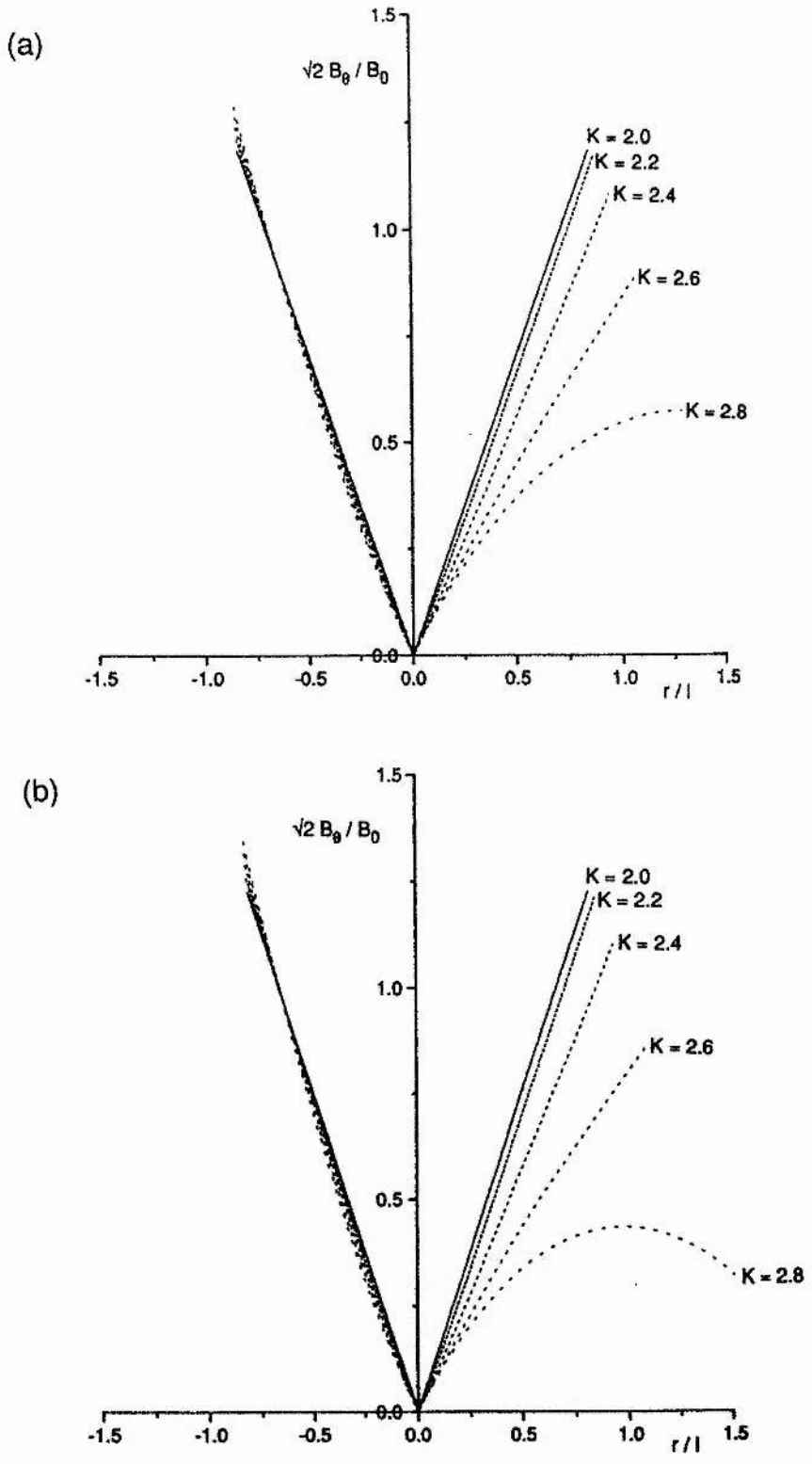

Fig. 3.6 The variation of B_θ with r/l for different values of K keeping $\sqrt{2}bI^{K-1}/B_0$ fixed. (a) $2.0 \leq K \leq 2.8$, $\sqrt{2}bI^{K-1}/B_0 = -0.2$, (b) $2.0 \leq K \leq 2.8$, $\sqrt{2}bI^{K-1}/B_0 = -0.25$.

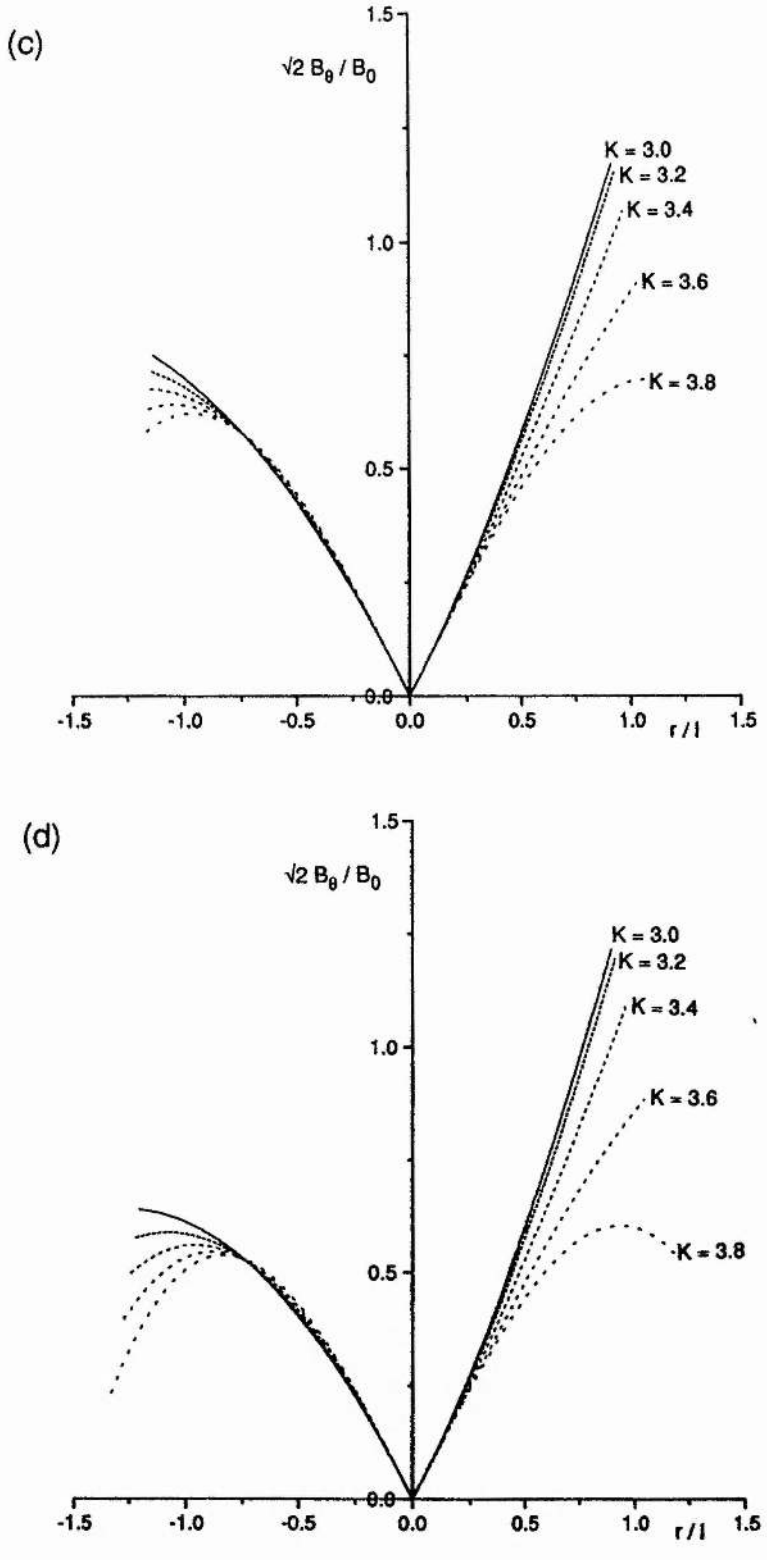

Fig. 3.6 The variation of B_θ with r/l for different values of K keeping $\sqrt{2}bl^{K-1}/B_0$ fixed. (c) $3.0 \leq K \leq 3.8$, $\sqrt{2}bl^{K-1}/B_0 = 0.1$, (d) $3.0 \leq K \leq 3.8$, $\sqrt{2}bl^{K-1}/B_0 = 0.13$.

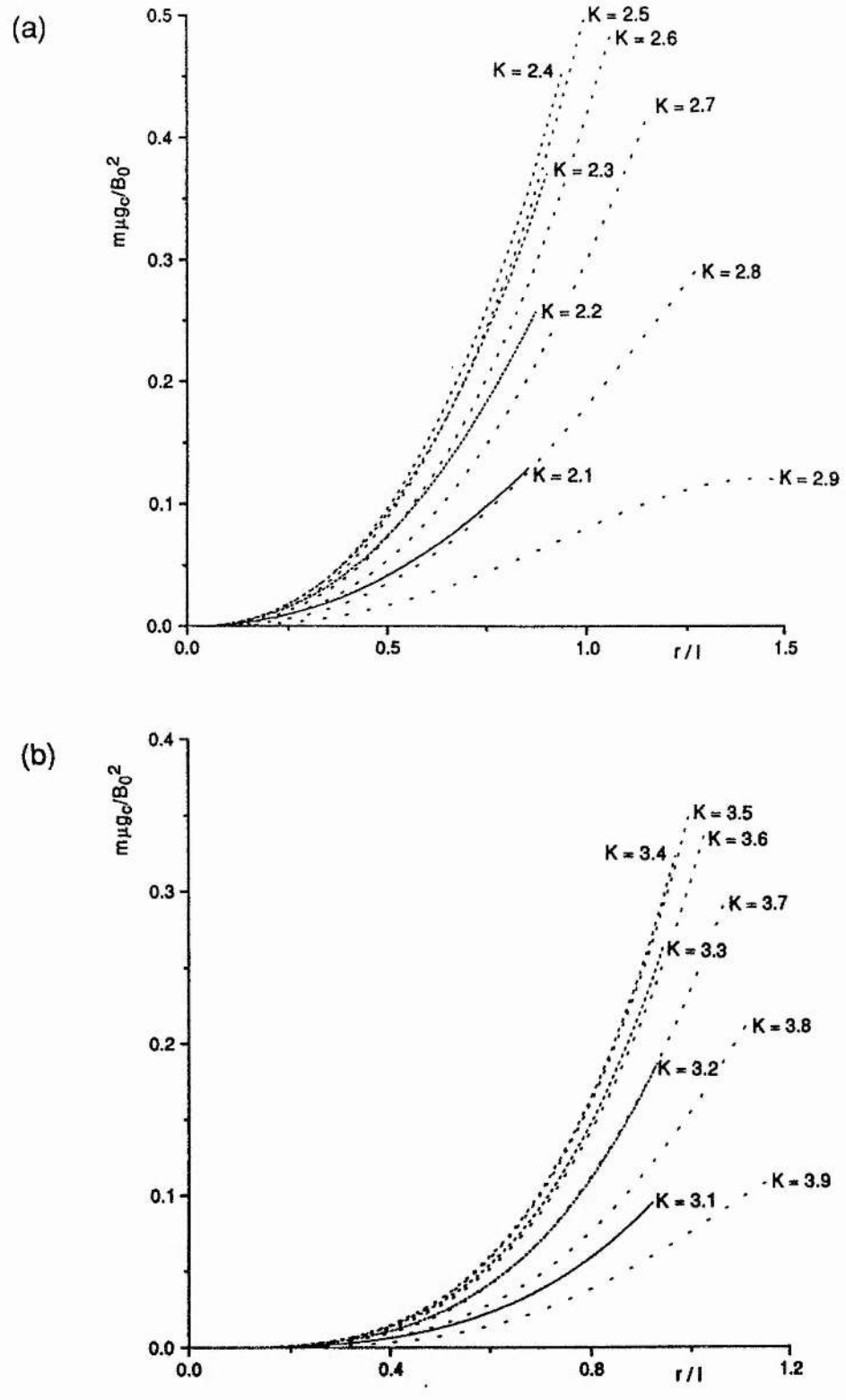

Fig. 3.7 The variation of m with r/l for different values of K keeping $\sqrt{2}bl^{K-1}/B_0$ fixed. (a) $2.1 \leq K \leq 2.9$, $\sqrt{2}bl^{K-1}/B_0 = -0.2$, (b) $3.1 \leq K \leq 3.9$, $\sqrt{2}bl^{K-1}/B_0 = 0.1$.

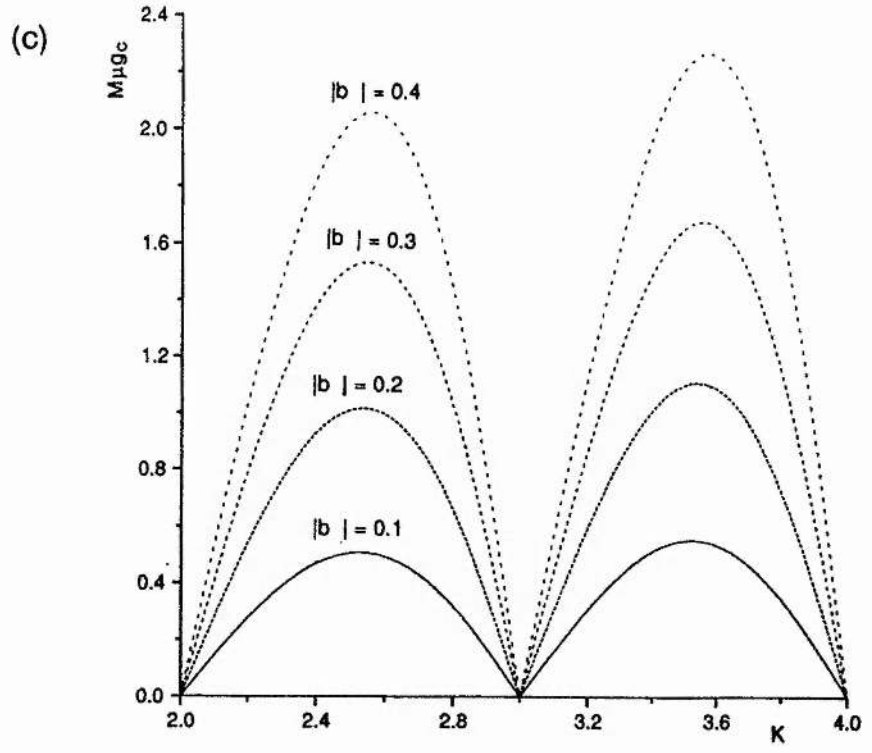

Fig. 3.7 (c) The variation of M with K for different values of b. $B_0 = 5.0$ and $l = 1.0$.

mass per unit length is obtained from equation (3.11) as

$$M = \frac{-2Kb\sin(K\pi)}{\mu g_c}\left(\frac{\sqrt{2}B_0 r_\pi^{K+1}}{2l(K+1)} - \frac{bKr_\pi^{2K-1}\cos(K\pi)}{2K-1}\right) \qquad (3.63)$$

where r_π is the value of r at which $B_z = 0$ for $\theta = \pi$. The variation of M with K and b is shown in Figure 3.7(c).

3.6 Inclusion of further terms from the series solution

One of the problems with the fields considered so far (given by equations (3.21) to (3.24) and (3.55) to (3.58)) is that in all cases we must cut the model off at a particular field line in order to prevent a sign change in the longitudinal field component. This action necessarily results in the particular field line possessing a discontinuity in the radial field component at the base of the prominence sheet unless B_r, and hence the prominence mass, tend to zero at this point. Such a discontinuity would propagate into any potential field that is assumed to surround the tube raising the question: why is no material supported in this dip?. In the fields we have already constructed, the mass does not vanish at the base of the sheet, yet it is possible to overcome such a problem by the inclusion of additional terms from the series solution

for $A(r,\theta)$. As an example, let us consider a further term from the solution found in section 3.5 for $B_z = 2cA^{1/2}$ (equations (3.51) to (3.54)) such that

$$A = \sqrt{2}B_0(l^2-r^2)/(4l) + b_1 r^{K_1}\cos(K_1\theta) + b_2 r^{K_2}\cos(K_2\theta) \quad (3.64)$$

$$B_r = -r^{K_1-1}b_1K_1\sin(K_1\theta) - r^{K_2-1}b_2K_2\sin(K_2\theta) \quad (3.65)$$

$$B_\theta = B_0 r/(\sqrt{2}l) - r^{K_1-1}b_1K_1\cos(K_1\theta) - r^{K_2-1}b_2K_2\cos(K_2\theta) \quad (3.66)$$

$$B_z = \pm\{B_0^2(1-r^2/l^2) + 2\sqrt{2}\,B_0\,b_1 r^{K_1}\cos(K_1\theta)/l + 2\sqrt{2}\,B_0\,b_2 r^{K_2}\cos(K_2\theta)/l\}^{1/2} \quad (3.67)$$

where $2 < K_1 < K_2$. Since $B_\theta > 0$ for small r, we see that for prominence equilibrium we require that $B_r(r,\pi)$ is also positive for small r and therefore that $b_1\sin(K_1\pi) < 0$. Because we are looking for a field in which $B_r(r,\pi)$ vanishes at some r, $b_2\sin(K_2\pi)$ must then be positive. Choosing the b_i and K_i i = 1,2 such that the above conditions are met, it is found that there exists a unique value of $r = r_c$ say, such that $B_r(r,\pi) = 0$. This then will be the point at which the field is cut off so that the mass density vanishes and there is no field discontinuity at the lower end point of the sheet. r_c is given explicitly by

$$r_c = \left(-\frac{b_1}{b_2}\frac{K_1}{K_2}\frac{\sin(K_1\pi)}{\sin(K_2\pi)}\right)^{\frac{1}{K_2-K_1}} \quad (3.68)$$

If $B_\theta(r,\pi) \geq 0$ for all $r \leq r_c$ then the sheet will be in equilibrium along its entire length, yielding a physically relevant prominence model.

To illustrate the above technique, let us take an example in which $K_1 = 2.5$, $K_2 = 3.5$, $b_1 = b_2 = -1$, giving $r_c = 5/7$ as the unique value of r at which the radial field component vanishes on the current sheet. If we cut the model off at the corresponding field line and take $l = r_c$, then equation (3.67) shows that $B_z(r_c,\pi)$ also vanishes and so the potential field surrounding the tube will be purely azimuthal. Figure 3.8(a) shows the variation of the field components with r along the current sheet with the corresponding distribution of m being shown in Figure 3.8(b).

A similar technique can be applied to the solution found for $B_z = cA$ by taking a further term. Once again, B_θ is positive for small radii and so for equilibrium we require $B_r(r,\pi)$ to be positive at small r. For $2 < K_1 < K_2$, $J_{K_1}(cr) < J_{K_2}(cr)$ for small enough r and so $b_1\sin(K_1\pi)$ must be negative for equilibrium. However, because of the oscillatory

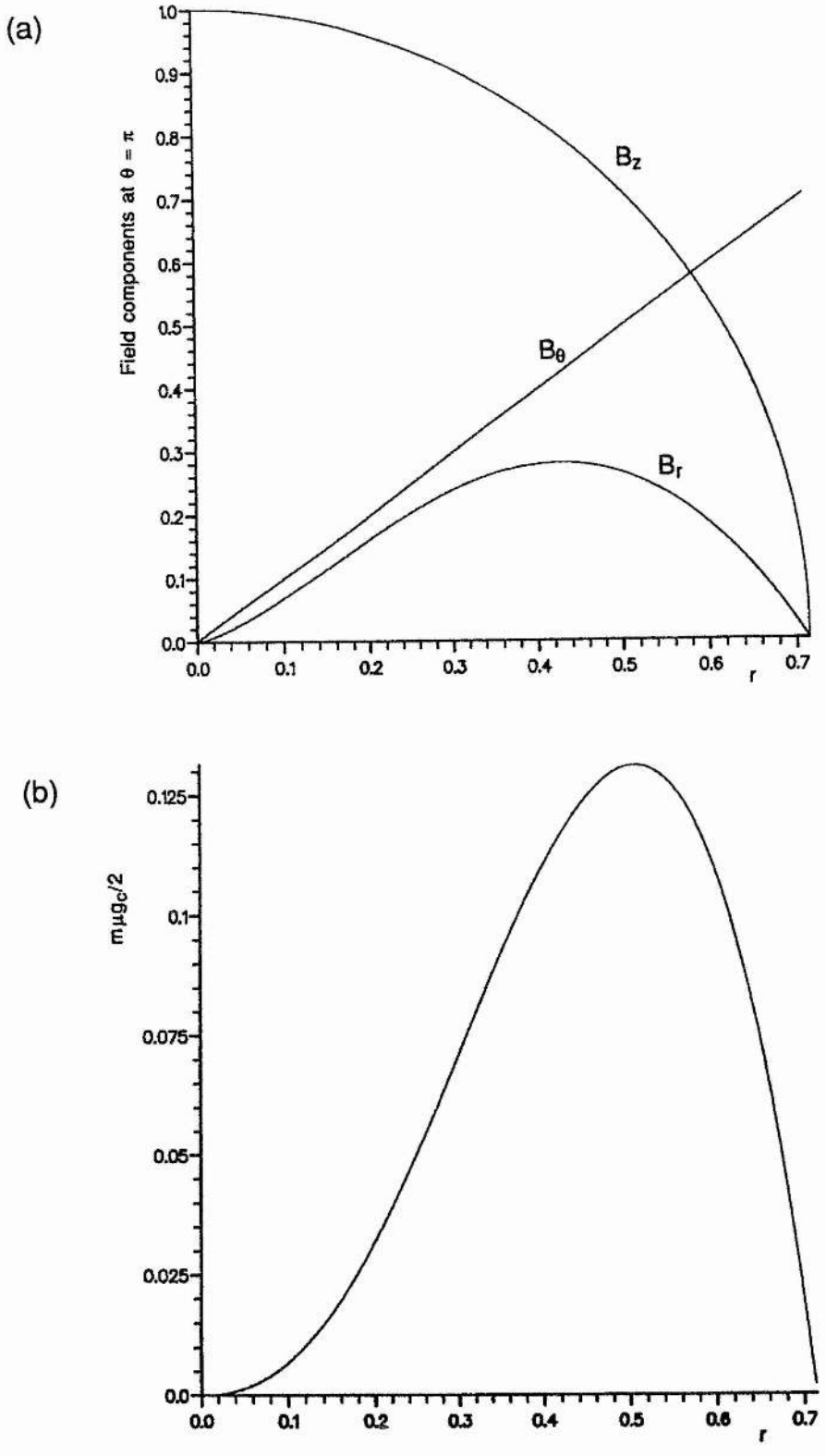

Fig. 3.8 The effect of including a further term from the series solution in which $B_z = 2cA^{1/2}$. (a) The variation of the magnetic field components along the prominence sheet. (b) The variation of m along the prominence sheet.

property of Bessel functions there is now no restriction on the sign of b_2. In this case there is also no unique zero of $B_r(r,\pi)$ but we can denote by $r = r_c$ the value of r at the first zero of $B_r(r,\pi)$ which must be found numerically. The model is again assumed to be cut off at the corresponding field line and enclosed by a potential field. Once again we must then ensure that $B_\theta(r,\pi) \geq 0$ for all $r \leq r_c$ so that the sheet is everywhere in equilibrium.

3.7 Discussion

We have represented a prominence as a sheet of mass and current embedded in the force-free magnetic field of a large-scale, twisted magnetic flux tube. In sections 3.4 and 3.5, analytical solutions to the system of equations arising from the model, subject to the conditions outlined in section 3.3, have been described for two functional forms of the longitudinal field component in the presence of the prominence sheet, namely $B_z = cA$ and $B_z = 2cA^{1/2}$. In section 3.6 we have shown how the simple model may be refined to give more physically relevant solutions.

The major problems with many of the inverse polarity models described in section 2.5 are; a) the presence of a singularity in the field at the line current or the ends of the current sheet representing the prominence (e.g. Malherbe and Priest, 1983); and b) the self-pinching of the current sheet which may result in a net downwards force in part of the sheet so that the prominence is not in equilibrium. However, most of these models have only considered a potential field outside the prominence.

A potential field may be represented by

$$\nabla^2 A = 0 \tag{3.69}$$

which has general solution

$$A = \sum_{n=1}^{\infty} a_n \sin(K_n\theta) K_n r^{K_n} \tag{3.70}$$

subject to the condition of symmetry about the vertical axis. Once more, all $K_n \geq K_l$ where K_l is the smallest value of K_n for which the field components are nonsingular and no field reversal occurs in B_z and B_θ. The field components are, from equation (2.28),

$$B_r = \sum_{n=1}^{\infty} a_n \sin(K_n\theta) K_n r^{K_n - 1} \tag{3.71}$$

$$B_\theta = \sum_{n=1}^{\infty} a_n \cos(K_n\theta) K_n r^{K_n-1} \qquad (3.72)$$

$$B_z = B_0 \qquad (3.73)$$

Clearly, to prevent a sign change in B_θ, $|K| < 1/2$. However, singularities are avoided in B_r and B_θ at $r = 0$ only for $K > 1$. Since these conditions cannot both be satisfied simultaneously we see that a potential field is unacceptable for the model.

In previous, essentially two-dimensional potential field models, shear can only be introduced by superimposing a uniform B_z component along the prominence axis. The use of force-free fields, however, allows a varying B_z component and it has been demonstrated in this chapter that they may be constructed such that the magnetic tension force at the current sheet is directed upwards everywhere and no singularity occurs at the top of the sheet where the sheet strength becomes zero and the self-pinching effect vanishes. A reason for this may be that with potential fields the current is concentrated into infinitesimally small regions, whereas with force-free fields the current flows along the field lines and hence is distributed throughout the configuration.

One feature of the solutions presented in sections 3.4 to 3.6 is that the immediate environment of the tube is neglected and the tube is considered as an isolated entity. A photospheric boundary may be introduced somewhat artificially by cutting the model off below a certain prominence depth and assuming that the photospheric field satisfies the boundary condition implied by such action. Such an action is somewhat unsatisfactory, however, since we are unable to use observed values of the photospheric field in constructing a prominence model.

In conclusion, it is worth stressing some of the properties of the twisted flux tube model which can explain several observed prominence features. In particular, it explains how a dip can be formed in the magnetic structure which will enable an initial condensation of plasma to be supported. The growth of the prominence in time is allowed by the increasing twist within the tube, resulting in more and more field lines acquiring a dip. Simultaneously, shearing and converging photospheric motions either side of the polarity inversion line cause the tube and hence the prominence to become increasingly aligned with the line. Eventually the twist increases so much that the

tube becomes unstable and eruption ensues, during which the tube fills with prominence material, revealing the helical structure displayed in so many eruption photographs.

4 PROMINENCE SUPPORT IN HELICAL CORONAL FIELDS FORMED BY PHOTOSPHERIC MOTIONS

4.1 Chapter summary

In this chapter we expand upon the work of van Ballegooijen and Martens (1989) in which they suggest a process whereby helical magnetic fields may be formed, capable of supporting a prominence in the low points of the helical windings. In section 4.2 some of the observational inspiration for the model is reviewed. Section 4.3 describes the model and previous related work. In sections 4.4 and 4.5 we discuss two methods of following the evolution of a prominence lying within a helical field. The first method develops further the analytical solution of van Ballegooijen and Martens. Section 4.6 contains a summary and discussion of the results.

4.2 Introduction

Many models for the global magnetic field around prominences exist (see section 2.5) which have in common the idea of plasma being supported in a dip in the magnetic field lines. Support against the effect of the Sun's gravitational field comes from the tension force associated with the upwards curvature of the field lines of the dip which balances the gravitational force acting on the plasma. Indeed, Priest et al. (1989) and Demoulin and Priest (1989) suggest that the formation of a field line dip prior to prominence formation is essential, since condensing plasma is unlikely to create the dip itself. Amari et al. (1991) have further shown that it is not possible to create a dip simply by shearing a two-dimensional, line-tied force-free arcade.

The incentive to examine the field properties when the field line footpoints are subjected to shearing flows parallel to the polarity inversion line comes from observations indicating that the magnetic field in the neighbourhood of a prominence has a strong longitudinal component (Tandberg-Hanssen and Anzer, 1970; Leroy et al., 1983). Likewise, observations confirming the presence of converging photospheric motions perpendicular to the polarity inversion line (Martin et al. ,1985; Martin, 1986; Hermans and Martin, 1986) have

prompted interest in examining the effect such flows have on the coronal field. In a recent summary of observations, Martin (1990) suggests that a necessary condition for prominence formation is for small fragments of magnetic field of opposite polarity to flow towards the polarity inversion line and cancel as magnetic flux is removed by the submergence of field lines through the photosphere. Van Ballegooijen and Martens (1989) have modelled the effects of this motion by considering a reconnection process driven by converging motions acting on a sheared force-free arcade. A description of the model is to be found in section 2.5. It explains how a helical magnetic field structure, aligned with the polarity inversion line, may be produced which can represent an I-type model of a prominence, since condensed plasma can collect and be supported in the field line dips at the lowest points of the helical twists. As the converging motion continues, more flux is transferred from the arcade region to the helical region and the helical axis rises. Eventually, the overlying arcade is unable to contain the helical field and an eruption occurs during which the condensed plasma fills the helical field and reveals the twisted appearance seen in many prominence eruptions. Van Ballegooijen and Martens consider briefly a nonsingular analytical solution and in more detail a numerical solution which unfortunately has a field singularity at the helical axis.

In this chapter we present some analytical and numerical results on the effect of shearing and converging motions on a cylindrically symmetric force-free arcade. In doing so, we assume that a helical structure forms via the reconnection process described by van Ballegooijen and Martens but the results we obtain are without their unphysical singularities.

4.3 The mathematical model

We adopt the cartesian coordinate system (x,y,z) in which the corona occupies the half-space $y > 0$ above the photosphere, represented by the x-z plane through $y = 0$. We neglect the three-dimensional structure (reasonable for prominences with little overall curvature such as low-altitude prominences) and assume that all physical quantities are invariant under a translation parallel to the z-axis. Because the photospheric plasma is relatively dense, we assume

that the field line footpoints are line-tied; in other words, motions within the photosphere drag the footpoints with them. We assume that the coronal field is force-free and, following section 2.3, we can express such a field in terms of a flux function A(x,y) as

$$\mathbf{B} = (B_x, B_y, B_z) = \left(\frac{\partial A}{\partial y}(x,y), -\frac{\partial A}{\partial x}(x,y), B_z(x,y)\right) \qquad (2.25)$$

where A satisfies

$$\nabla^2 A + B_z(A)\frac{d}{dA}\left(B_z(A)\right) = 0 \qquad (2.27)$$

Equation (2.27), subject to two boundary conditions on $y = 0$, determines A(x,y), and hence the field components, in the region $y > 0$. However, this equation is in general a nonlinear second-order partial differential equation and as such is inherently difficult to solve. Despite this, progress has been made by considering equation (2.27) along with one of the following two sets of boundary conditions.

a) $B_y(x,0) = B_n(x)$ and $B_z = f(A)$

Here both the distribution of the normal photospheric magnetic field and the functional form of the axial field component are imposed. The first of these conditions implies from equation (2.25) that A is determined along the photosphere to within a constant. It follows that the second condition can be interpreted as imposing $B_z(x,0)$.

Certain functional forms for $B_z(A)$ (see section 2.3) make possible the analytical solution of equation (2.27). Other forms of $B_z(A)$ may be handled numerically (see Priest and Milne (1980) for a summary of both analytical and numerical solutions to this problem). One drawback of this approach is that the functional form of $B_z(A)$ cannot be prescribed from observational data. Furthermore, during the quasi-static evolution through a series of equilibria it would seem unlikely that the functional form of $B_z(A)$ is unchanged (see section 3.3 for a discussion of this point).

b) $B_y(x,0) = B_n(x)$ and $d = d(x)$

Here we impose the distribution of both the normal photospheric field component and the footpoint displacement in the longitudinal direction of the field lines. The second condition can here be interpreted as imposing d(A). Since both functions can in theory be determined by observational data, such an approach is almost certainly more relevant when following a quasi-static evolution than using the first set of boundary conditions. The relationship between the footpoint

displacement and the longitudinal field component is given on a field line by

$$\frac{dz}{B_z} = \frac{ds}{|\nabla A|} \tag{4.1}$$

where s is the distance along the field line projected in the upper x-y plane. Integrating equation (4.1) yields

$$B_z(A) = \frac{d(A)}{\int_\zeta \frac{ds}{|\nabla A|}} \tag{4.2}$$

where ζ represents integration along the field projection in the upper x-y plane. This expression for $B_z(A)$ may then be substituted into equation (2.27), which in theory can then be solved.

Unfortunately, solutions by this second method are extremely difficult to obtain even using numerical techniques. However, the equations become much more amenable to solution if one constrains all physical properties to depend not on two dimensions but simply on the radial distance r from some symmetry axis aligned in the longitudinal direction and intersecting the x-y plane at (0,h) above the polarity inversion line at (0,0) (see Figure 4.1). Field line projections onto the upper x-y plane will then appear either as circles for $r \leq h$ or arcs of circles for $r > h$. Hence we obtain two topologically distinct field regions in three dimensions: a helical region above the photosphere for $r \leq h$ and an arcade region with footpoints tied to the photosphere for $r > h$. Within the helical region we interpret d as the longitudinal displacement along the field line in one complete helical twist.

In the present analysis then, we represent the formation and subsequent evolution of the prominence by the following scenario. We begin with a sheared semi-circular equilibrium arcade with $h = 0$. A converging flow causing the field line footpoints to approach the polarity inversion line is represented here by increasing the height h of the helical axis. We assume that on the global length scale the reconnection process described by van Ballegooijen and Martens occurs solely at the polarity inversion line and that elsewhere resistive effects are negligible due to the high conductivity of coronal plasma, and so the field evolves through a series of quasi-static equilibria as an ideal MHD fluid. The reconnection process transfers field lines from the arcade to the helical region. Without considering the details of the process we assume that the reconnection occurs at the rate at which

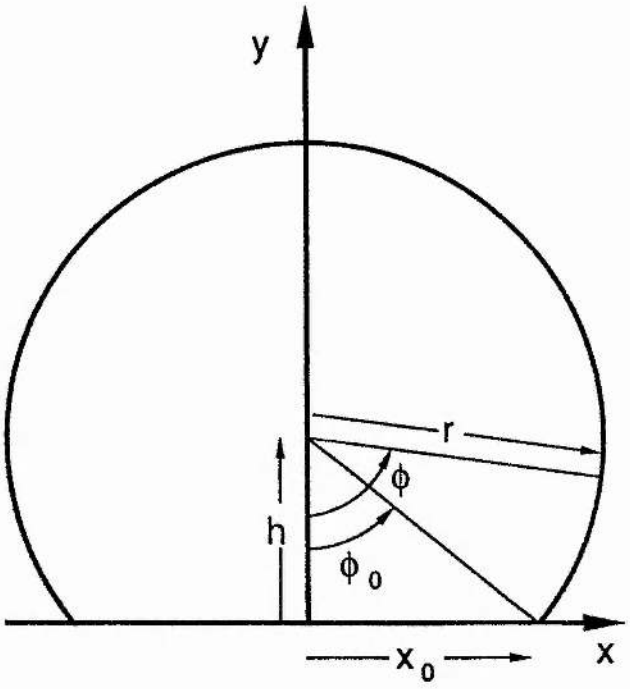

Fig. 4.1 The relationship between the cartesian and cylindrical polar coordinate systems. The z-axis is into the plane of the figure.

field lines are brought in towards the polarity inversion line so that no flux build-up occurs. Once field lines are transferred to the helical region it becomes possible to support condensed coronal plasma in the field line dips at the lowest points of the helical windings. In the present analysis we assume that no further deformation of the field lines occur as plasma collects in the dips since this would modify the cylindrically symmetric model, making the analysis considerably more difficult (see Priest et al. 1989 who make analytical progress by considering the linearised form of equation (2.27)).

Denote by φ the azimuthal angle about the helical axis where $\varphi = 0$ corresponds to the y-axis and $\varphi = \pm \varphi_0 = \pm \cos^{-1}(h/r)$ corresponds to the angles subtended by lines joining the helical axis to the two footpoints of an arcade field line. We then see that the field components can be written in terms of the scalar flux function A(r) as

$$\mathbf{B} = (0, B_\varphi(r), B_z(r)) = \left(0, -\frac{dA}{dr}, B_z(A)\right) \qquad (4.3)$$

immediately satisfying equation (2.2). Because we do not expect physically a change of sign in B_φ as r increases, it can be seen that A is then a monotonically decreasing function of r. The relationship between

d and B_z becomes simply

$$d = B_z \int_{\zeta} \frac{r\, d\varphi}{dA/dr} = \begin{cases} 2 B_z \pi r / B_\varphi & r \le h \\ 2 B_z (\pi - \varphi_0) r / B_\varphi & r > h \end{cases} \qquad (4.4)$$

Note that the restriction of one-dimensionality means that we have lost one degree of freedom and so we can impose the distribution of only one quantity. Priest and Milne (1980) chose to impose $B_n(x)$ to be the same for all values of h and considered an evolution through quasi-static equilibria brought about by a converging motion parallel to the x-axis. Although the mathematical problem is well defined in the arcade region and is straightforward to solve, this solution is just assumed to continue into the helical region. Thus unfortunately no control on the footpoint displacement is possible; it is purely a result of the mathematical solution. However, in order to take into account the effect of the helical field lines being tied to the photosphere at the ends of the prominence, we would expect to conserve the twist per unit length on each particular helical field line. This implies that once a field line enters the helical region, no further longitudinal displacement (i.e. change in d) is desirable and in general this is not the case when cylindrical symmetry and $B_n(x)$ are imposed. Van Ballegooijen and Martens (1989) considered briefly the problem when d(r,h) is imposed instead. Here no longitudinal (or indeed radial) deformation of the helical field lines occurs as h increases, provided that both d and A are functions of r only for $r \le h$. We will show in sections 4.4 and 4.5 that a series of fields in which the twist per unit length is conserved in the helical region can be generated in a straightforward manner. In addition to imposing d(r,h), we will consider the case of imposing d(A) which remains fixed as h increases. This implies that no further shearing motions occur during the evolution i.e. all footpoint motions are parallel to the x-axis.

In the following analysis then we proceed to examine the quasi-static evolution of an initial semi-circular sheared arcade as the height of the helical axis increases from 0. During the evolution we impose either d = d(r,h) or d = d(A).

4.4 Imposing the condition d = d(r,h)

Here we write the footpoint displacement as a function of

the radial distance r from the helical axis located at a height h above the photosphere. A convenient way of writing equation (2.27) when using this approach is

$$\frac{1}{2}\frac{d}{dr}\left(B_\varphi^2(1+\lambda^2/r^2)\right) + \frac{B_\varphi^2}{r} = 0 \qquad (4.5)$$

where

$$\lambda(r,h) = \begin{cases} \dfrac{d(r,h)}{2\pi} & r \le h \\ \dfrac{d(r,h)}{2(\pi - \cos^{-1}(h/r))} & r > h \end{cases} \qquad (4.6)$$

and

$$B_z = \frac{\lambda}{r} B_\varphi \qquad (4.7)$$

from equation (4.4). Some simple algebra shows that equation (4.5) can be expressed as

$$\frac{dB_\varphi}{dr}\left(1 + \frac{\lambda^2}{r^2}\right) + B_\varphi\left(\frac{1}{r} + \frac{\lambda}{r}\frac{d}{dr}\left(\frac{\lambda}{r}\right)\right) = 0 \qquad (4.8)$$

from which we obtain the solution (see van Ballegooijen and Martens, 1989, who had a typographical error)

$$B_\varphi = \frac{B_0 r}{\sqrt{\lambda^2+r^2}} \exp\left(-\int_0^r \frac{r\,dr}{\lambda^2+r^2}\right) \qquad (4.9)$$

where $B_0 = B_z(0)$ from equation (4.7). Thus for any given d(r,h) we calculate $\lambda(r,h)$ from equation (4.6) in both the helical and arcade regions. Equations (4.9) and (4.7) give the field components and equation (4.3) the distribution of A(r,h).

We will first consider a general distribution of $d(r) \sim r^m$ valid close to the symmetry axis and then examine a particular case.

4.4.1 Solution with $d(r) \sim r^m$ near $r = 0$

We consider the distribution of d(r,h) given by

$$d(r,h) = \begin{cases} 2b\pi r^m & r \le h \\ 2b(\pi - \cos^{-1}(h/r))r^m & r > h \end{cases} \qquad (4.10)$$

where $b > 0$. Immediately we see that in order to avoid a singularity at $r = 0$ we must have $m \ge 0$. This seemingly unusual looking form of d(r,h) is chosen to simplify the calculations henceforth. For such a form, the process of increasing h is in fact just equivalent to lowering the position of the photosphere in a predetermined helical field where $d(r) = 2b\pi r^m$.

The distribution of $\lambda(r,h)$ then becomes

$$\lambda(r) = b\, r^{m} \tag{4.11}$$

which is independent of h and hence for $m \neq 1$ (for which the integral in equation (4.9) is undefined) we obtain

$$B_{\varphi}(r) = \frac{B_0 b^{1/n} r^n}{(b^2+r^{2n})^{(1+n)/2n}} \tag{4.12}$$

and

$$B_z(r) = \frac{B_0 b^{(1+n)/n}}{(b^2+r^{2n})^{(1+n)/2n}} \tag{4.13}$$

where $n = 1 - m$. Notice that both components are only nonsingular at $r = 0$ for $0 < n \leq 1$ i.e. for $0 \leq m < 1$. However, although both components tend to zero as r increases, the footpoint displacement increases without bound and so this kind of distribution is only valid locally, i.e. in the neighbourhood of the helical axis. In order to obtain A(r), the expression for $B_{\varphi}(r)$ must be integrated. Making the substitutions $u = r^n$ and $t = \sinh^{-1}(u/b)$ yields

$$A(r) = A_0 - \frac{B_0}{n} b^{1/n} \int_0^{\sinh^{-1}(r^n/b)} (\tanh t)^{1/n}\, dt \tag{4.14}$$

where $A_0 = A(0)$. This expression can only be integrated analytically for values of n such that 1/n is an integer. However, a binomial expansion of equation (4.12), valid locally, i.e. for $|r^{2n}/b^2| < 1$, for all values of n gives

$$B_{\varphi}(r) = B_0\, b^{-1/n}\, r^n \left(1 + \sum_{k=1}^{\infty} \frac{r^{2nk} \prod_{j=1}^{k} [n(2j-1)+1]}{k! b^{2k} 2^k n^k} \right) \tag{4.15}$$

Integrating this expression term by term gives

$$A(r) = A_0 - B_0\, b^{-1/n} \left(\frac{r^{1+n}}{1+n} + \sum_{k=1}^{\infty} \frac{r^{\{n(2k+1)+1\}} \prod_{j=1}^{k} [n(2j-1)+1]}{k! b^{2k} 2^k n^k \{n(2k+1)+1\}} \right) \tag{4.16}$$

and this series may be summed numerically for any given value of n in the allowed range. Note that A is independent of h and so is d for $r < h$, which means that for field lines in the helical region we can express d as a function of A only. Therefore, once a field line has reconnected and entered the helical region, no further longitudinal displacement occurs and so the twist per unit length is conserved.

4.4.2 Solution with $d(r) \sim r^{1/2}$ near $r = 0$

In order to proceed analytically we need to select a value of n for which the integral in equation (4.14) can be evaluated. Such is the case for $n = 1/2$ and the footpoint displacement as a function of r for various values of h can be seen in Figure 4.2. Note that for $r < h$, represented by the dashed line, this displacement is independent of h. From equation (4.11)

$$\lambda(r) = b\, r^{1/2} \tag{4.17}$$

and so the solutions for the field components become

$$B_\varphi(r) = \frac{B_0 b^2 r^{1/2}}{(b^2+r)^{3/2}} \tag{4.18}$$

and

$$B_z(r) = \frac{B_0 b^3}{(b^2+r)^{3/2}} \tag{4.19}$$

The field components as functions of r for different values of b are illustrated in Figures 4.3(a) and 4.3(b). Note that at $r = b^2/2$, B_φ takes a maximum value of $2B_0/3^{3/2}$ which is independent of b and also that B_z is a monotonically decreasing function of r. Integrating the expression for B_φ gives

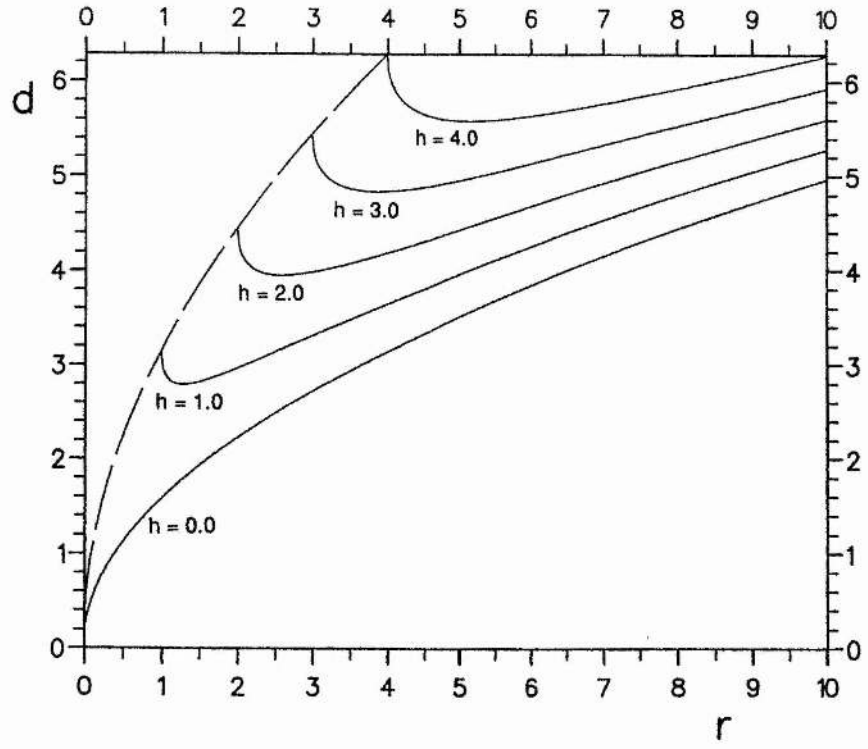

Fig. 4.2 The footpoint displacement as a function of r for different values of h for the case $d(r) = br^{1/2}$ in the helical region. The dashed line represents the displacement within the helical region.

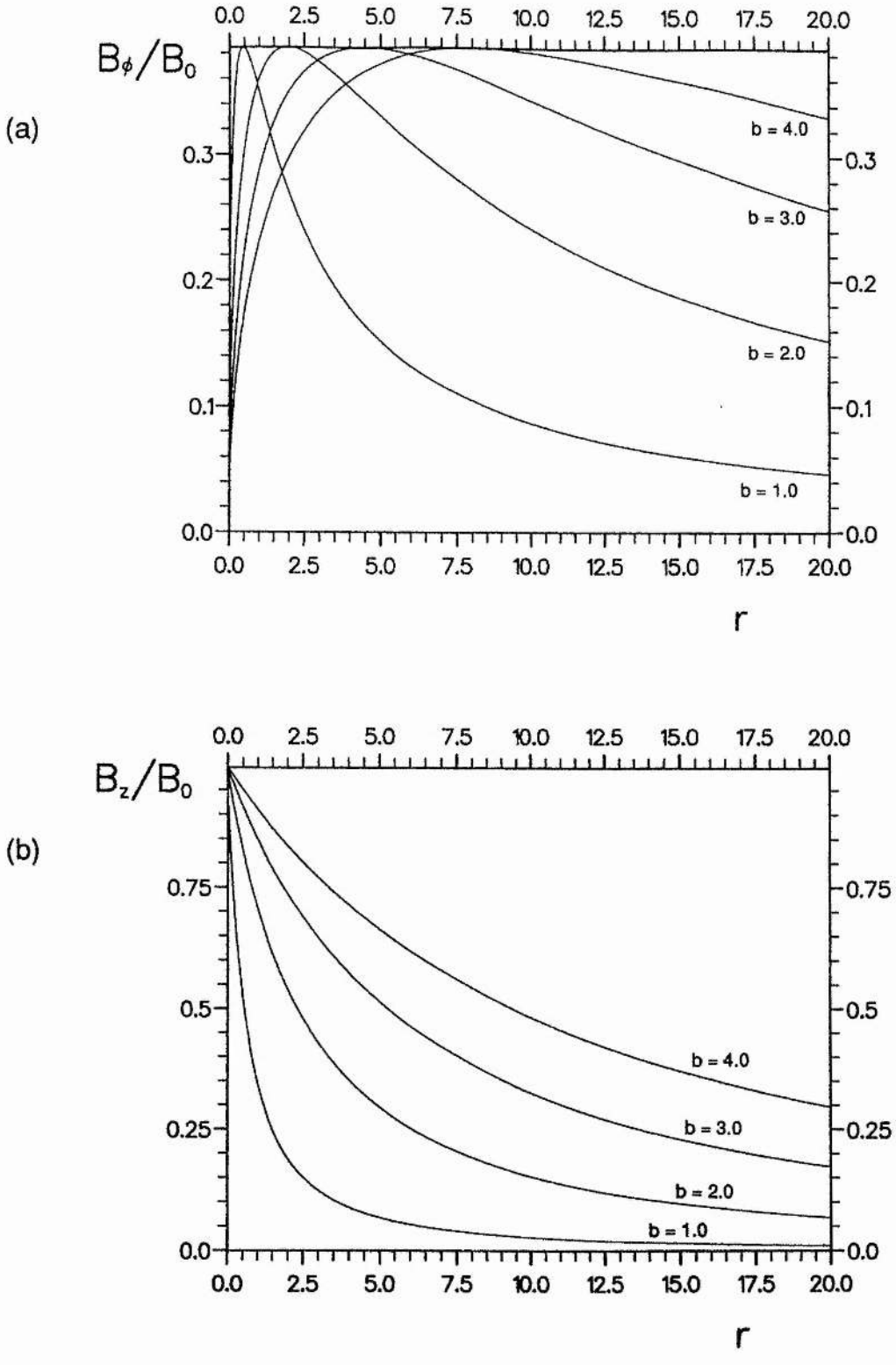

Fig. 4.3 (a) and (b) The distribution of the field components as functions of r for different values of b. Here m = 0.5.

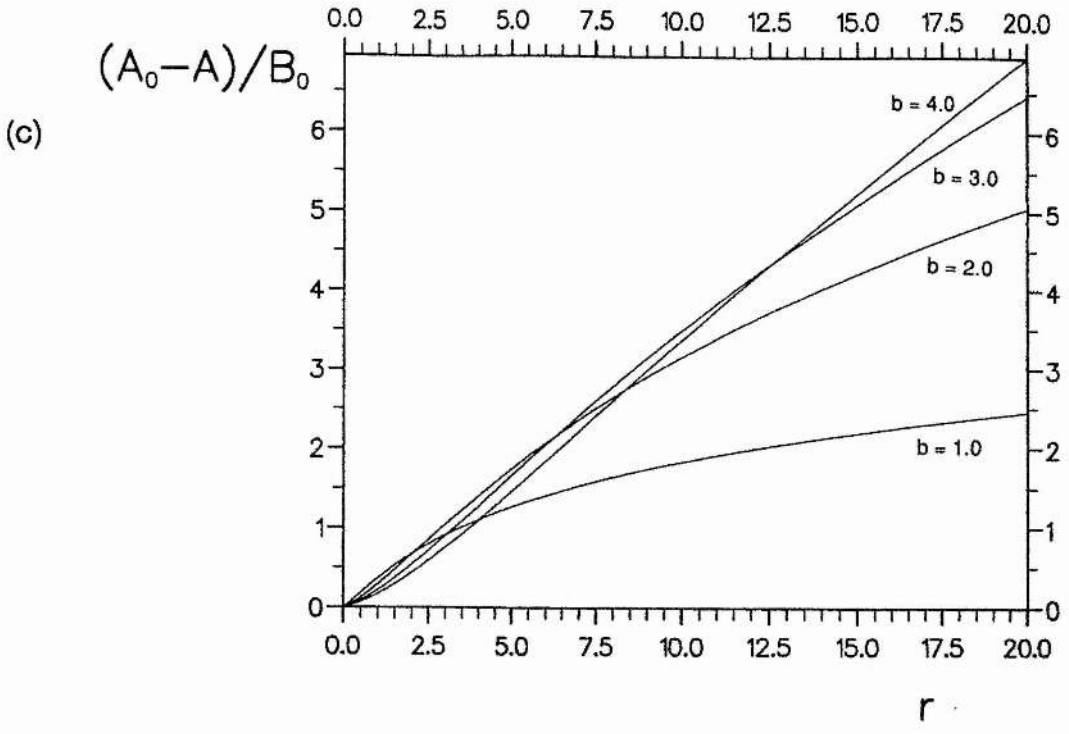

Fig. 4.3 (c) The distribution of the flux function as a function of r for different values of b. Here m = 0.5.

$$A(r) = A_0 - 2 B_0 b^2 \left(\sinh^{-1}\left(\left(\frac{r}{b^2}\right)^{1/2}\right) - \left(\frac{r}{r+b^2}\right)^{1/2}\right) \qquad (4.20)$$

and this is sketched as a function of r for different values of b in Figure 4.3(c) from which it is clearly seen that A is a monotonically decreasing function of r.

Writing r in terms of x and h we can follow the distribution of photospheric flux as h increases. This is shown in Figure 4.4(a) for a particular value of b. Note that as h increases, the flux at any value of x decreases as outer field lines are carried towards the polarity inversion line. It is also possible to follow the motion in the photospheric plane of the footpoints of particular field lines and this is shown in Figure 4.4(b). We can clearly see both the converging and shearing motions here. As h increases, the field line footpoints move towards the polarity inversion line and the shear displacement is enhanced. Lastly, Figure 4.5 shows a three-dimensional view of the field lines. As the symmetry axis rises so more and more field line footpoints are brought together to reconnect at the polarity inversion

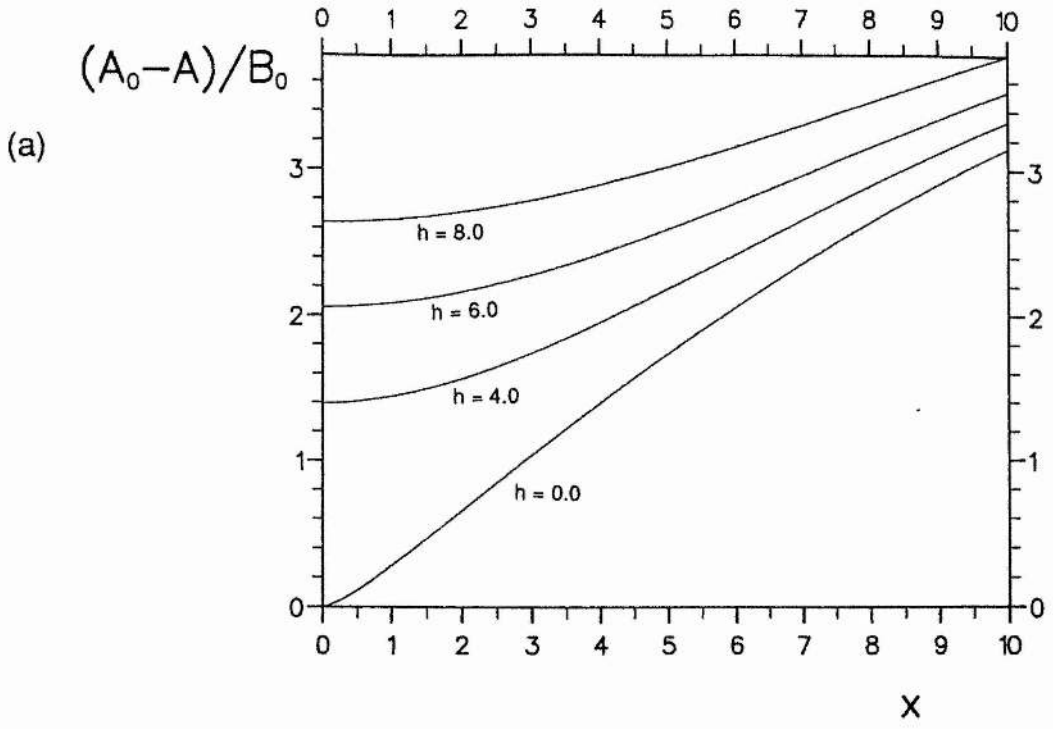

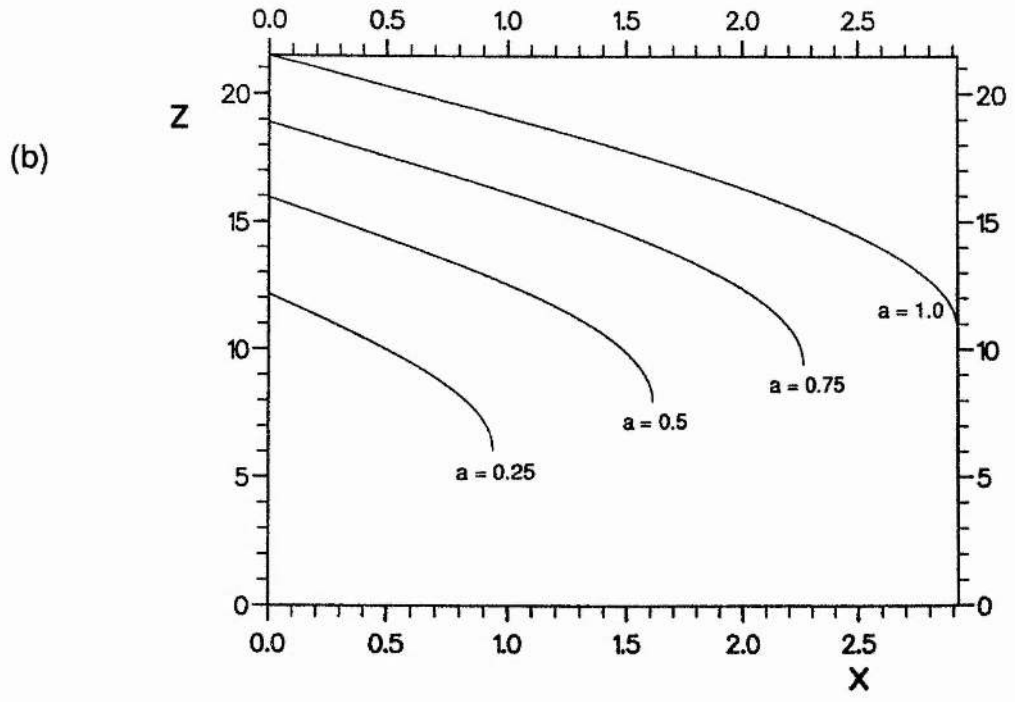

Fig. 4.4 (a) The photospheric distribution of the flux function for different values of the axis height. Here m = 0.5 and b = 2.0. (b) The footpoint paths in the photospheric plane as the height of the helical axis is increased. The paths are drawn for 4 different values of a = $(A_0-A)/B_0$, namely a = 0.25, 0.5, 0.75 and 1.0. Here m = 0.5 and b = 2.0.

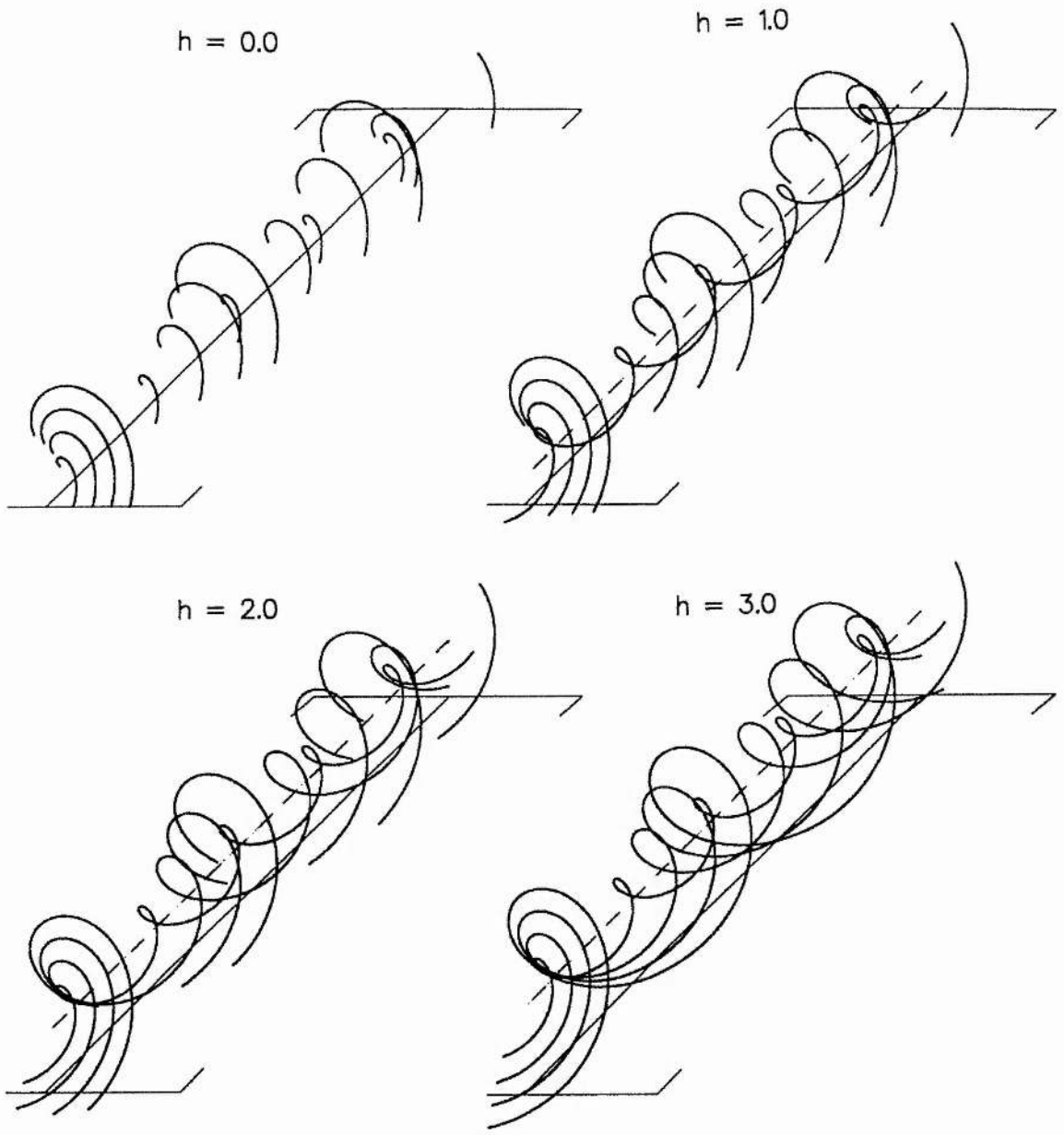

Fig. 4.5 The three-dimensional view of the field lines given by a = 0.25 (the inner line), 0.5, 0.75 and 1.0 (the outer line) as the helical axis, represented by the dotted line, rises. Here m = 0.5 and b = 2.0.

line, transferring flux from the arcade to the helical region.

4.5 Imposing the condition d = d(A)

We now impose the footpoint displacement such that it remains fixed on each field line throughout the ensuing evolution. When using this approach, we may write equation (2.27) as

$$\frac{d^2A}{dr^2}\left(r^3 + \frac{r\,d^2(A)}{4\pi^2}\right) + \frac{dA}{dr}\left(r^2 - \frac{d^2(A)}{4\pi^2}\right) + \left(\frac{dA}{dr}\right)^2 \frac{r\,d(A)}{4\pi^2}\frac{d}{dA}[d(A)] = 0 \qquad (4.21)$$

in the helical region and

$$\frac{d^2A}{dr^2}\left(r^3 + \frac{r\,d^2(A)}{4[\pi-\cos^{-1}(h/r)]^2}\right) + \frac{dA}{dr}\left(r^2 - \frac{d^2(A)\,\{[\pi-\cos^{-1}(h/r)] - h/(r^2-h^2)^{1/2}\}}{4[\pi-\cos^{-1}(h/r)]^3}\right) + \left(\frac{dA}{dr}\right)^2 \frac{r\,d(A)}{4[\pi-\cos^{-1}(h/r)]^2}\frac{d}{dA}[d(A)] = 0 \qquad (4.22)$$

in the arcade region. Equations (4.21) and (4.22) are both second-order nonlinear ordinary differential equations for A which in general can be solved numerically as an initial-value problem. The two boundary conditions for equation (4.21) are simply

$$A(r=0) = A_0 \qquad (4.23)$$

$$\frac{dA}{dr}(r=0) = 0 \qquad (4.24)$$

whilst the two boundary conditions for equation (4.22) are obtained from the solution for equation (4.21) at r = h.

Note from equation (4.21) that both A and dA/dr, and hence the field components, are independent of h once the field line has entered the helical region.

Note also that when d(A) and its derivative with respect to A are both zero, equations (4.21) and (4.22) reduce to

$$\frac{d^2A}{dr^2} + \frac{1}{r}\frac{dA}{dr} = 0 \qquad (4.25)$$

which simply gives the potential field solution.

In the examples that follow, equations (4.21) and (4.22) are both written as two simultaneous first-order ordinary differential equations and solved using a numerical routine.

4.5.1 Solution with d(A) = d(r) = d_0, a constant

In this example the footpoint displacement is the same on every field line. Within the helical region we are able to solve the equilibrium equation analytically for this form of the footpoint displacement. Rather than using equation (4.21), it is simpler to use the method described for the imposition of d(r,h) by putting $\lambda = d_0/2\pi$ in equation (4.9) which gives

$$B_\varphi = \frac{rB_0d_0/2\pi}{r^2+d_0^2/4\pi^2} \tag{4.26}$$

$$B_z = \frac{B_0d_0^2/4\pi^2}{r^2+d_0^2/4\pi^2} \tag{4.27}$$

From equation (4.3) we then see that

$$A = A_0 + \frac{B_0d_0}{4\pi} \ln\left(\frac{d_0^2/4\pi^2}{r^2+d_0^2/4\pi^2}\right) \tag{4.28}$$

In the arcade region equation (4.22) becomes

$$\frac{d^2A}{dr^2}\left(r^3 + \frac{r\,d_0^2}{4[\pi-\cos^{-1}(h/r)]^2}\right) + \frac{dA}{dr}\left(r^2 - \frac{d_0^2\{[\pi-\cos^{-1}(h/r)] - h/(r^2-h^2)^{1/2}\}}{4[\pi-\cos^{-1}(h/r)]^3}\right) = 0 \tag{4.29}$$

with the initial conditions for A and dA/dr at r = h given by equations (4.28) and (4.27) as A_h and $-B_{\varphi h}$, respectively. Note that equation (4.29) possesses a regular singular point at r = h. However, we can obtain a nonsingular analytical solution for A and dA/dr, valid close to r = h, by an expansion of equation (4.29) about this point. This gives

(a)

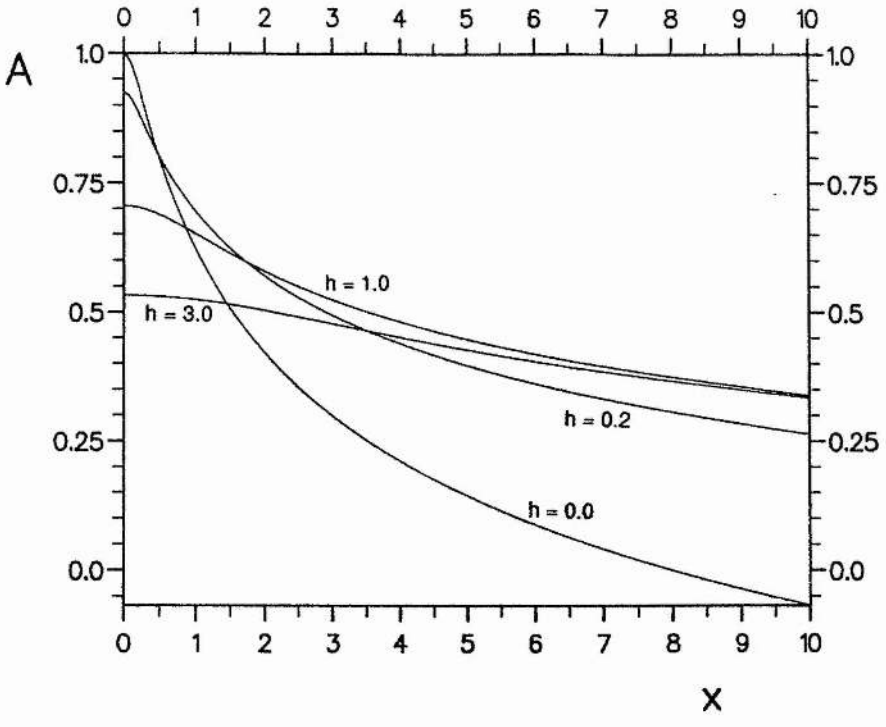

Fig. 4.6 (a) The photospheric distribution of the flux function for different values of the height of the helical axis for the case where d(r) = d(A) = d_0. The dashed line represents the helical region.

(b)

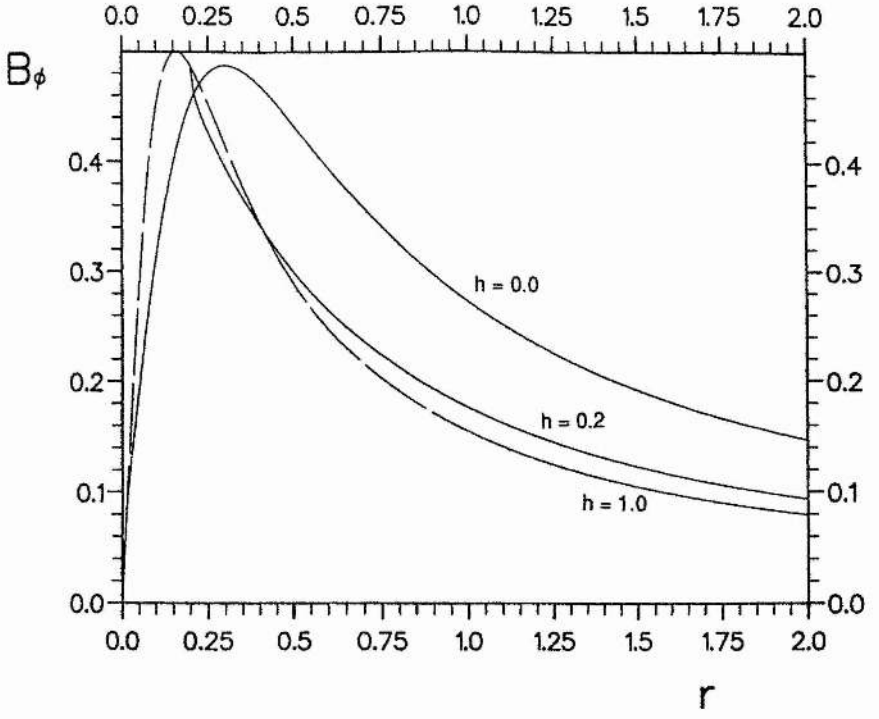

(c)

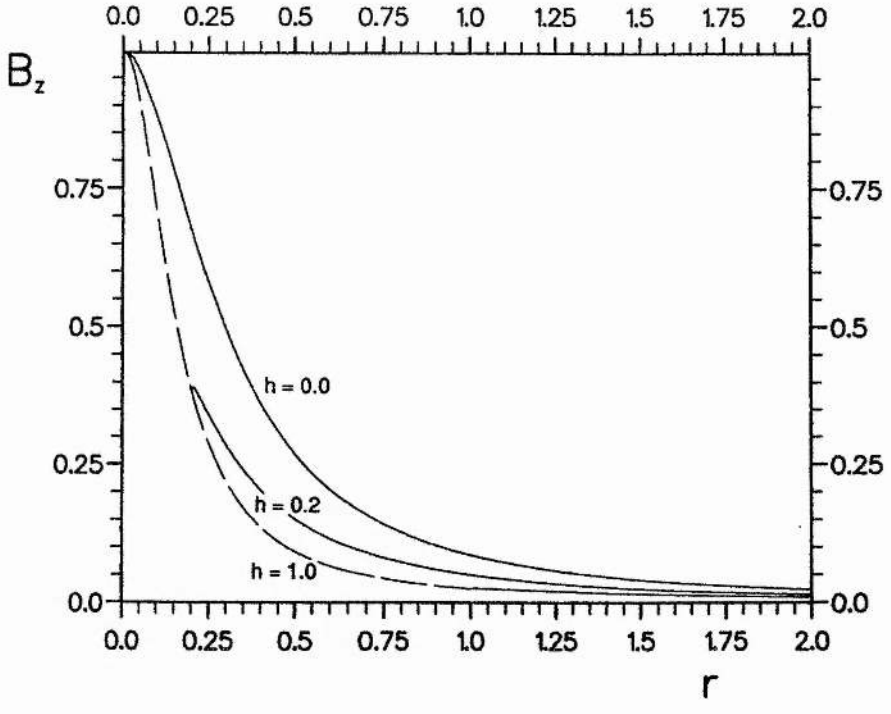

Fig. 4.6 (b) and (c) The distribution of the field components with r for different values of the height of the helical axis for the case where $d(r) = d(A) = d_0$. The dashed line represents the helical region.

$$\frac{dA}{dr} \approx - B_{\varphi h}\, e^{c(r-h)^{1/2}} \tag{4.30}$$

$$A \approx A_h - \frac{2}{c} B_{\varphi h}\left(e^{c(r-h)^{1/2}}\left((r-h)^{1/2} - \frac{1}{c}\right) + \frac{1}{c}\right) \tag{4.31}$$

where

$$c = - \frac{\sqrt{2}\, d_0^2}{\pi(4\pi^2 + d_0^2)h^{1/2}} \tag{4.32}$$

The above analytical solution is used for $r \leq h\,(1 + \varepsilon)$ where $\varepsilon << 1$. For $r > h\,(1 + \varepsilon)$ equation (4.29) is solved using a numerical routine. Thus for a particular value of d_0, we can find A and the field components at all radii for any $h \geq 0$. The distribution of A along the photosphere for

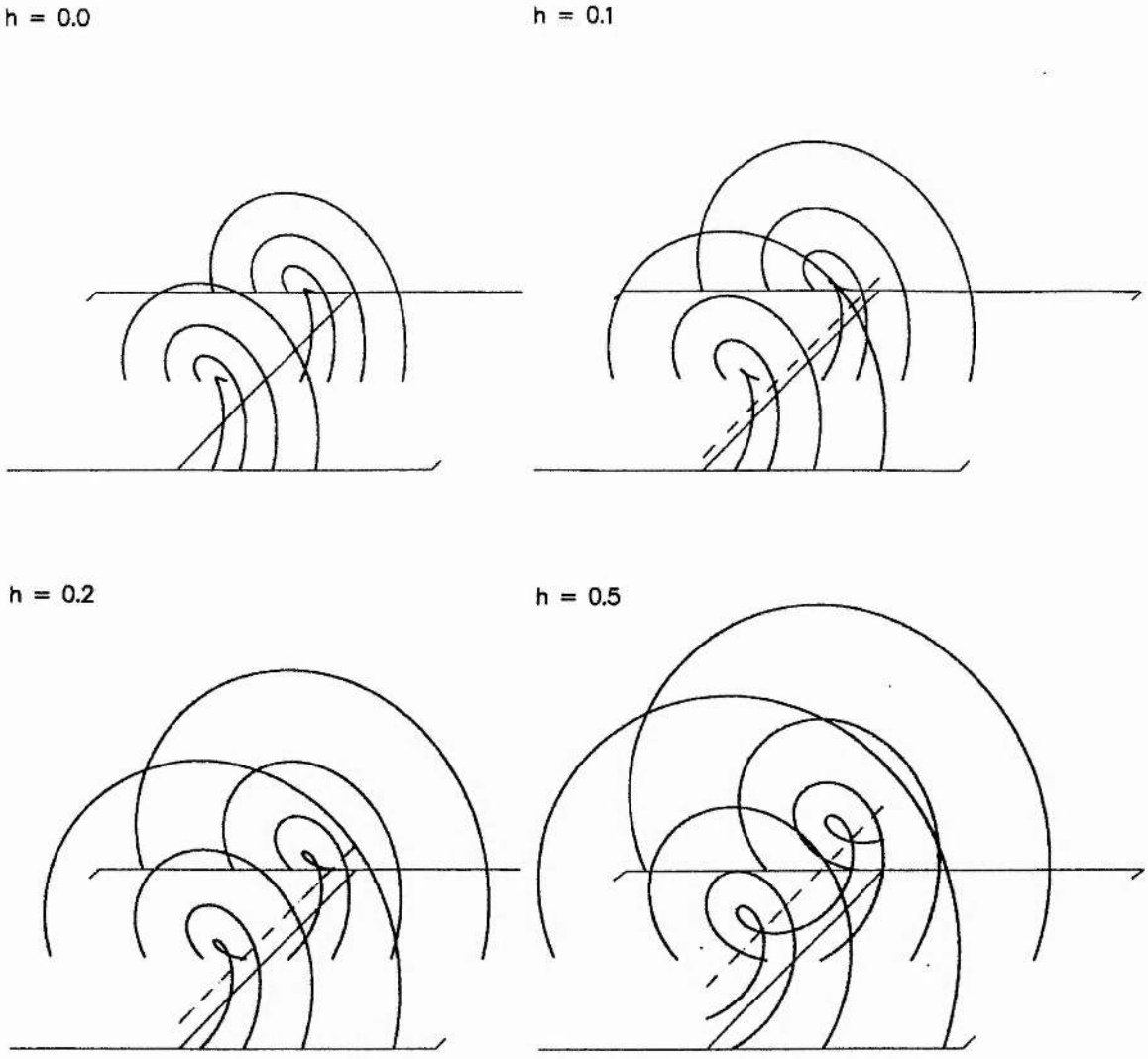

Fig. 4.7 The three-dimensional view of the field lines given by A = 0.9 (the inner line), 0.8, 0.7 and 0.6 (the outer line) as the height of the helical axis, represented by the dotted line, is increased.

various values of h is shown in Figure 4.6(a). We can see that as h increases, A decreases at points on the photosphere close to the polarity inversion line indicating local converging flows. However, further away from the polarity inversion line, the value of A actually increases with h in this example indicating the presence of diverging flows in the photosphere. The field components are plotted as functions of r in Figures 4.6(b) and 4.6(c). B_φ is obtained from the solution for dA/dr as given by the initial-value problem algorithm and B_z is then given by equation (4.4). We can clearly see that for $r < h$, indicated by the dashed line in the Figures, the field components are indeed independent of h. Figure 4.7 shows the three-dimensional representation of the field evolving with h. Note that although field lines with footpoints in the neighbourhood of the polarity inversion line are converging towards it as h increases, the outer field lines are in fact diverging from the inversion line and expanding radially.

4.5.2 Solution with $d(A) = e^A$

Since we have imposed that A is a monotonically decreasing function of r, we see that here the footpoint displacement is also decreasing with distance from the symmetry axis, tending towards a potential solution at infinity. Within the helical region the equilibrium equation becomes

$$\frac{d^2A}{dr^2}\left(r^3 + \frac{r\, e^{2A}}{4\pi^2}\right) + \frac{dA}{dr}\left(r^2 - \frac{e^{2A}}{4\pi^2}\right) + \left(\frac{dA}{dr}\right)^2 \frac{r\, e^{2A}}{4\pi^2} = 0 \qquad (4.33)$$

and this possesses a regular singular point at $r = 0$. A nonsingular analytical solution for A and dA/dr, valid close to $r = 0$, can be obtained from an expansion of equation (4.33) about this point which gives

$$\frac{dA}{dr} \approx -\frac{2\pi B_{z0} e^{A_0} r}{r^2(4\pi^2 - \pi B_{z0} e^{A_0}) + e^{2A_0}} \qquad (4.34)$$

$$A \approx A_0 + \frac{B_{z0} e^{A_0}}{B_{z0} e^{A_0} - 4\pi} \ln\left(1 - \frac{r^2(B_{z0} e^{A_0} - 4\pi)}{e^{2A_0}}\right) \qquad (4.35)$$

where A_0 and B_{z0} are the values of A and B_z at the helical axis. In the arcade region the equilibrium equation becomes

$$\frac{d^2A}{dr^2}\left(r^3 + \frac{r\, e^{2A}}{4[\pi - \cos^{-1}(h/r)]^2}\right) \qquad (4.36)$$

$$+\frac{dA}{dr}\left(r^2 - \frac{e^{2A}\{[\pi-\cos^{-1}(h/r)] - h/(r^2-h^2)^{1/2}\}}{4[\pi-\cos^{-1}(h/r)]^3}\right)$$
$$+\left(\frac{dA}{dr}\right)^2 \frac{r\, e^{2A}}{4[\pi-\cos^{-1}(h/r)]^2} = 0$$

Equation (4.36) possesses a regular singular point at r = h and so an expansion about this point is used to calculate the values of A and dA/dr close to this point. This gives

$$\frac{dA}{dr} \approx -\frac{(2h)^{1/2} B_{\varphi h}}{(2h)^{1/2} + 2B_{\varphi h}\pi(r-h)^{1/2}} \qquad (4.37)$$

$$A \approx A_h - \frac{(2h)^{1/2}}{\pi}\left((r-h)^{1/2} + \frac{(2h)^{1/2}}{2B_{\varphi h}\pi} \ln \frac{(2h)^{1/2} B_{\varphi h}}{(2h)^{1/2}+2B_{\varphi h}\pi(r-h)^{1/2}}\right) \qquad (4.38)$$

The distribution of A on the photosphere is shown in Figure 4.8(a) for various values of h. As in the previous example we can see that converging flows occur locally in the region of the polarity inversion line and diverging flows at larger distances. The field components are obtained in the same way as for the previous example and are plotted in Figures 4.8(b) and 4.8(c), the dashed line representing

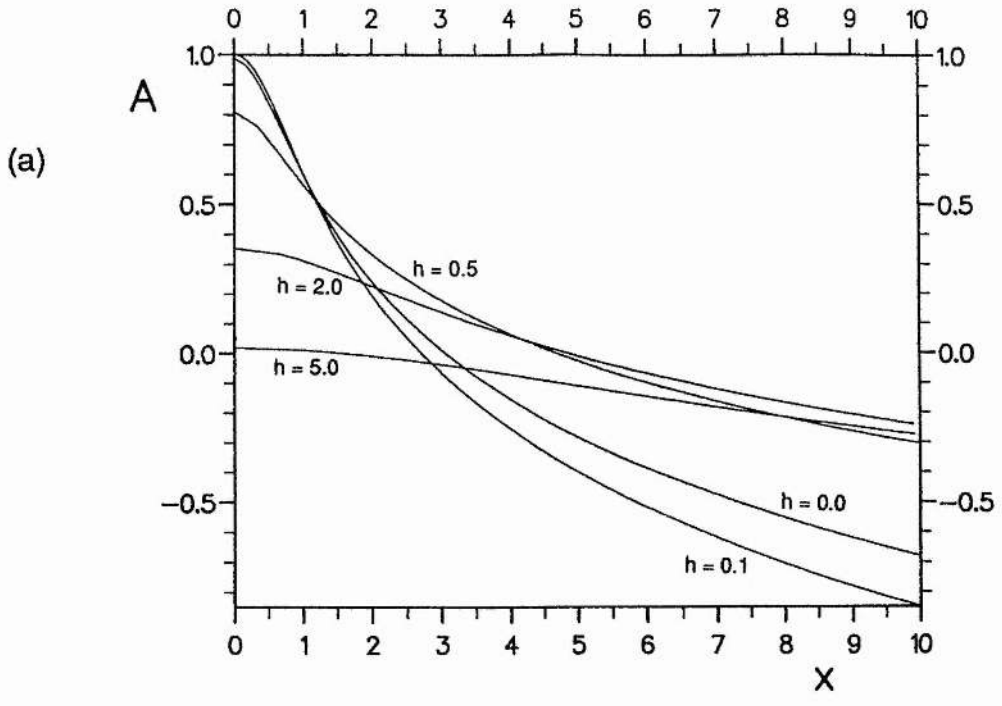

Fig. 4.8 (a) The photospheric distribution of the flux function for different values of the height of the helical axis for the case where $d(A) = e^A$. The dashed line corresponds to the helical region.

(b)

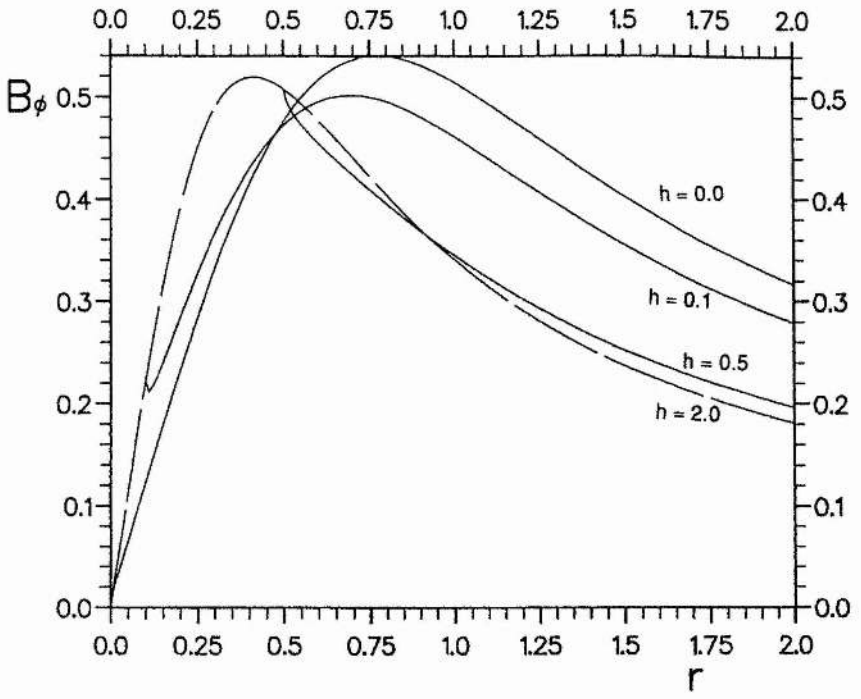

(c)

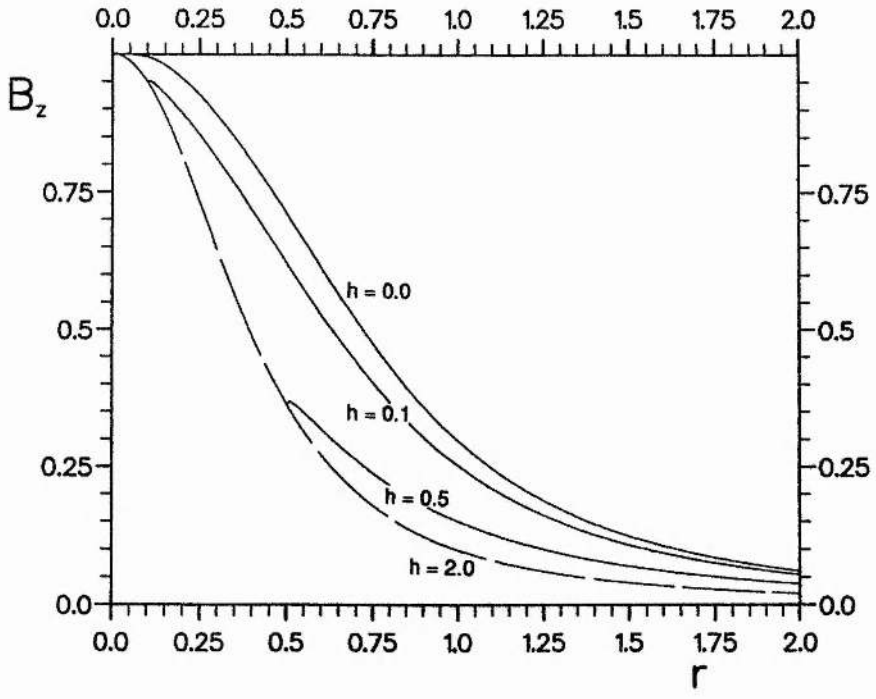

Fig. 4.8 (b) and (c) The distribution of the field components with r for different values of the height of the helical axis for the case where $d(A) = e^A$. The dashed line corresponds to the helical region.

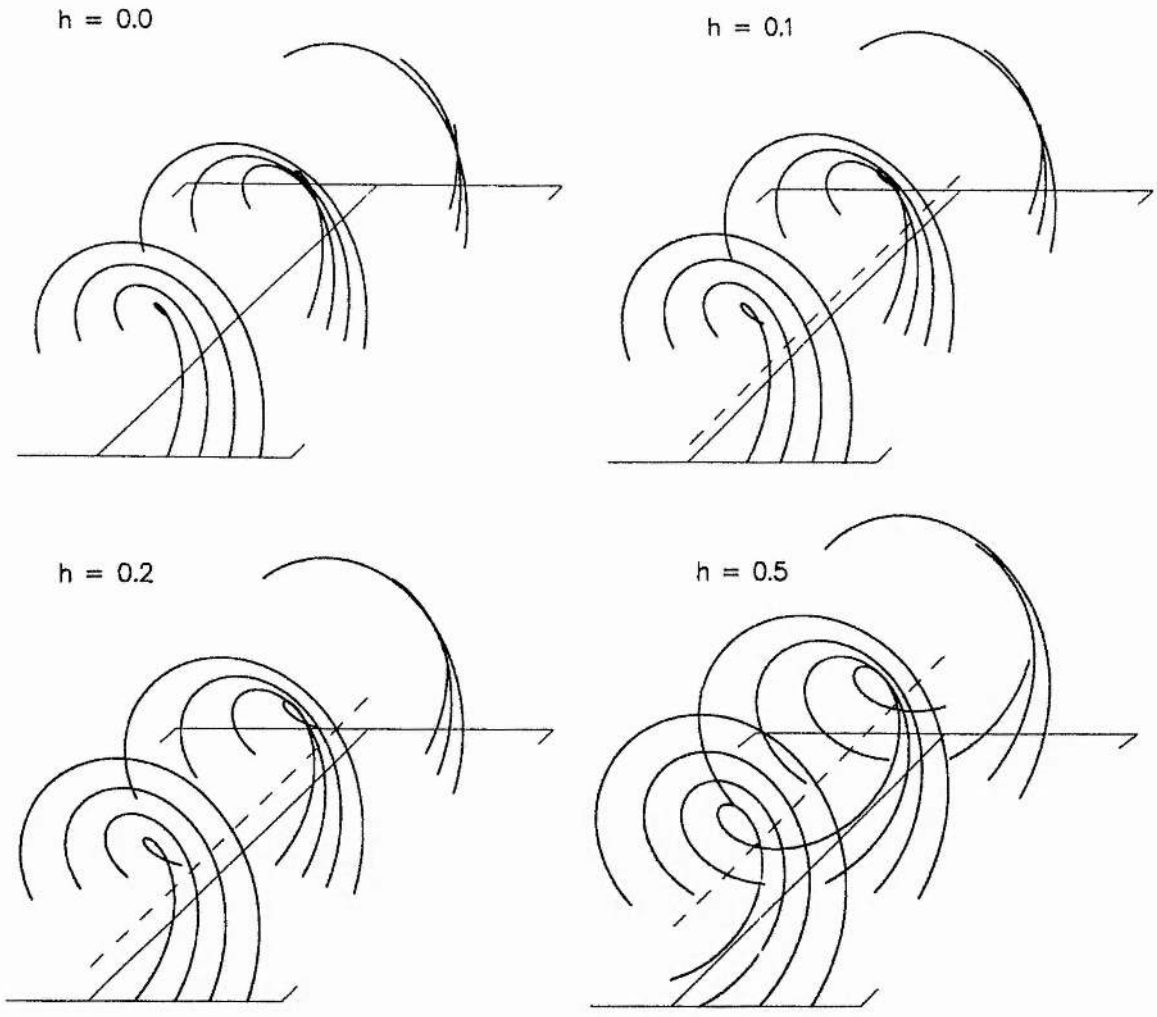

Fig. 4.9 The three-dimensional view of the field lines given by A = 0.9, 0.8, 0.7 and 0.6 (the inner line) as the height of the helical axis, represented by the dotted line, is increased.

the helical region in which the components are independent of h. Figure 4.9 shows how the three-dimensional field evolves as h increases and once more we can see that field lines whose footpoints are local to the polarity inversion line converge towards it as h increases, while the outer field lines diverge and expand radially.

4.6 Discussion

We have described two methods for constructing a series of cylindrically symmetric helical fields with overlying arcades in which the helical axis rises. This series can model the formation and evolution of a quiescent prominence supported at the low points of the

helical windings. In both cases we consider the physically relevant problem of imposing the footpoint displacement of the field lines in the arcade and the longitudinal displacement in one helical twist for the helical field lines. In addition, we avoid the presence of unphysical singularities in the field components

The first method involves imposing the footpoint displacement as a function of r and h. We have shown that it is possible to obtain analytical expressions for the field within both the helical and arcade regions, although in general these expressions must be obtained numerically. Although both shearing and converging photospheric motions take place as h increases, once a field line has entered the helical region there is no further longitudinal displacement if, in the helical region, d is a function of r only.

In the second method we impose the footpoint displacement as a function of A only. Although analytical solutions are no longer possible to find (except for the case d = constant), this method has the advantage of being equivalent to considering the action of flows perpendicular to the longitudinal axis of an initially sheared arcade.

As stated in section 4.3, we have assumed that throughout the evolution the field retains its cylindrical symmetry. Such a restriction does not allow us to arbitrarily impose the velocity components of the footpoints as a function of position. Instead we interpret the increasing height of the helical axis as an evolution in time and the footpoint velocity is a result of the calculations. An improvement on the present model would be to consider both r and φ variations about the helical axis. Such a problem, however, is not possible to solve analytically but may be examined using a z-invariant numerical MHD code.

5 PROMINENCE SHEETS SUPPORTED BY CONSTANT-CURRENT FORCE-FREE FIELDS. I - IMPOSITION OF NORMAL MAGNETIC FIELD COMPONENTS AT THE CURRENT SHEET AND THE PHOTOSPHERE

5.1 Chapter summary

In this and the following chapter, we present an analytical model for the magnetohydrostatic equilibrium of a sheet of mass and current in a constant-current force-free field. Section 5.2 contains a resumee of earlier related work followed by a mathematical description of the model along with the assumptions made in section 5.3. In section 5.4 we discuss the formulation of a boundary-value problem resulting from the model and solve it. An analysis of the solution in relation to the possibility of equilibrium, mass distribution and field topology for a bipolar photospheric field is then given. In section 5.5 we apply the method to a case in which simple forms of the boundary conditions are supplied and show the possibility of equilibrium configurations of both N-type and I-type. In section 5.6 we extend the model to allow for a quadrupolar photospheric field. Finally a discussion of the model is presented in section 5.7.

5.2 Introduction

In chapters 5 and 6 we describe two particular methods of generating longitudinally invariant magnetohydrostatic equilibria in which a finite, vertical sheet of mass and current is supported against gravity by an external constant-current force-free field. It is suggested that such a system can be used to model a globally stationary quiescent prominence, uniform along its long axis and of relatively small width. Indeed, as mentioned in section 2.5, such a system has been used before to model the support of prominences in potential fields (Anzer, 1972; Demoulin et al., 1989) and linear force-free fields (Amari and Aly 1990a). It is important to note, however, that in all these cases it was not possible to reproduce an I-type field topology in which the prominence sheet is in equilibrium at every point along its length.

In this present chapter it is assumed that the distribution of

the normal magnetic field components along the photosphere and across the prominence are given functions of position. This allows us to construct a mixed boundary-value problem (BVP) in the first quadrant, corresponding to the so-called "BVP3" described by Aly et al. (1989). This problem has already be studied by the aforementioned authors in the case of a potential coronal field and it is the aim of this chapter to extend their work by considering the case of a constant-current force-free field.

5.3 Mathematical description of the model

We adopt the cartesian coordinate system (x,y,z) in which the corona occupies the half-space $D = \{-\infty < x < \infty,\ y > 0,\ -\infty < z < \infty\}$ above the photosphere, denoted by $P = \{-\infty < x < \infty,\ y = 0,\ -\infty < z < \infty\}$. As in previous chapters, it is again assumed that all physical quantities are invariant under a translation parallel to the longitudinal axis of the prominence (the z-axis) and thus we need only consider the model in a single plane perpendicular to the prominence axis which we take, without loss of generality, to be that passing through the origin. Accordingly, we define by Ω the upper (coronal) half of the x-y plane passing through the origin so that $\Omega = \{-\infty < x < \infty,\ 0 < y < \infty,\ z = 0\}$.

The prominence is represented by Σ, an infinitesimally thin sheet of mass and current, finite in vertical extent, which intersects Ω along the curve Γ.

Outside the prominence the coronal magnetic field is assumed to be time-invariant and force-free and, following section 2.3, may be expressed in terms of a scalar flux function A(x,y) as

$$\mathbf{B} = \left(\frac{\partial A}{\partial y}(x,y),\ -\frac{\partial A}{\partial x}(x,y),\ B_z(x,y) \right) \qquad (2.25)$$

where A satisfies

$$\nabla^2 A + \frac{1}{2}\frac{d}{dA}\left(B_z^2(A)\right) = 0 \qquad (2.27)$$

Across the prominence, since we assume that the sheet is in equilibrium and is infinitesimally thin, we obtain

$$[B_z] = [B_n] = 0 \qquad (5.1)$$

where $[B_a]$ denotes the change in B_a across the sheet and B_n is the magnetic field component normal to the sheet. However, B_t (the tangential field component) is discontinuous across the sheet and so there exists a surface current $\mathbf{j}_\Sigma$ along it which from equation (2.5)

may be written (c.f. section 2.5)

$$\mathbf{j}_\Sigma = j_\Sigma \mathbf{e}_z = [B_t] / \mu \, \mathbf{e}_z \qquad (5.2)$$

The gravitational field $\mathbf{g}_c$ is taken to be constant and directed vertically downwards so that

$$\mathbf{g}_c = -g_c \mathbf{e}_y \qquad (5.3)$$

where $g_c > 0$. The prominence sheet is assumed to be in equilibrium between the vertically downwards force exerted upon its mass by gravity and the tension force due to the magnetic field (which then must clearly be in the positive y-direction) so that m, the sheet mass density per unit length, is given by

$$m \, g_c = j_\Sigma \, B_{n\Sigma} = [B_t] \, B_{n\Sigma} / \mu \qquad (5.4)$$

where $B_{n\Sigma}$ is the strength of the normal field component across the sheet. The total prominence mass per unit length, M, may then be determined from

$$M = \int_\Gamma m \, ds \qquad (5.5)$$

So far we have made no assumption about the nature of the z-invariant force-free field in the region outside the prominence. In order to proceed analytically we will select a particular functional form for the longitudinal field component $B_z(A)$. Equation (2.27) along with two boundary conditions described in the following section then defines a solvable boundary-value problem for A allowing us to compute the field everywhere in the corona.

5.4 Interaction of a prominence sheet with a constant-current force-free field

5.4.1 Formulation of the boundary-value problem

Throughout the ensuing sections we will assume that the functional form of the coronal field is the so-called constant-current force-free field. This field has the property that the longitudinal component of the coronal current (given everywhere in D/Σ by equation (2.5)) is of constant magnitude. The corresponding form of $B_z(A)$ is

$$B_z(A) = \pm 2 c \sqrt{A(x,y)} \qquad (5.6)$$

where c is a constant and $A \geq 0$. With this form of $B_z(A)$ equation (2.27) becomes

$$\nabla^2 A + 2 c^2 = 0 \qquad \text{in } D/\Sigma \qquad (5.7)$$

Clearly this reduces to the case of a potential field outside the prominence sheet when $c = 0$.

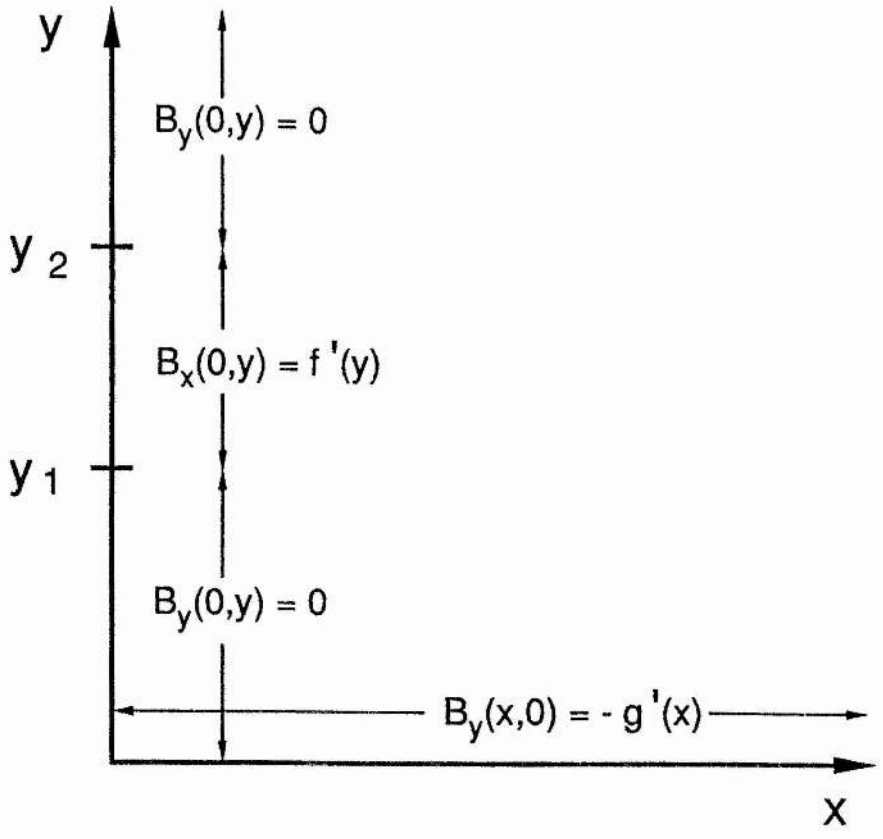

Fig. 5.1 The conditions imposed on the boundaries of the quarter plane Q. The prominence lies between the two horizontal bars on the y-axis.

We now consider a boundary-value problem (see Figure 5.1) in which we are given (from observed values in principle) the normal magnetic field components along the photosphere

$$B_y(x,0) = -\partial_x A(x,0) = -g'(x) \qquad \text{on P} \qquad (5.8)$$

and across the prominence

$$B_x(0,y) = \partial_y A(0,y) = f'(y) \qquad \text{on } \Sigma \qquad (5.9)$$

where the prime (') represents the derivative of a function with respect to its dependent variable. We will also assume from now on that g(x) is a continuous even function and that the prominence sheet lies in the plane $\{x = 0\}$ on $\Sigma = \{x = 0,\ 0 \le y_1 \le y \le y_2,\ -\infty < z < \infty\}$ giving $\Gamma = \{x = 0,\ 0 \le y_1 \le y \le y_2\}$. As a consequence, A(x,y) satisfies

$$A(-x,y) = A(x,y) \qquad \text{in D} \qquad (5.10)$$

which yields the relation as $x \to 0$

$$B_y(0,y) = 0 \qquad \text{on T} \qquad (5.11)$$

where $T = \{x = 0,\ 0 \le y < y_1 \ \cup\ y > y_2,\ -\infty < z < \infty\}$. Note that because of equation (5.11)

$$g'(0) = 0 \qquad (5.12)$$

Since the field is invariant in z and symmetric in Ω about $\{x = 0\}$, A(x,y) satisfies the following mixed boundary-value problem

$$\nabla^2 A + 2c^2 = 0 \quad \text{in } Q \qquad (5.13a)$$

$$\partial_x A(0,y) = 0 \quad \text{on } \{0 \le y < y_1\} \cup \{y_2 < y \le \infty\} \qquad (5.13b)$$

$$\partial_y A(0,y) = f'(y) \quad \text{on } \{y_1 \le y \le y_2\} \qquad (5.13c)$$

$$A(x,0) = g(x) \quad \text{on } \{0 \le x < \infty\} \qquad (5.13d)$$

in the quarter plane $Q = \{0 < x < \infty, 0 < y < \infty, z = 0\}$. The boundary conditions given by equations (5.8), (5.9) and (5.11) have been expressed in terms of A(x,y) and its partial derivatives using equation (2.25).

5.4.2 Solution of the boundary-value problem

We will now outline the solution of the above problem that will enable us to obtain A everywhere in Q. Firstly let us define A(x,y) to be the sum of two further scalar flux functions so that

$$A(x,y) = A_p(x,y) + A_0(x,y) \qquad (5.14)$$

where $A_0(x,y)$ is a particular solution of equation (5.13a) given by

$$A_0(x,y) = -c^2 (x^2 + y^2) / 2 \qquad (5.15)$$

which is independent of the imposed boundary conditions and A_p is the analytic (or potential) function solution of the boundary-value problem

$$\nabla^2 A_p = 0 \quad \text{in } Q \qquad (5.16a)$$

$$\partial_x A_p(0,y) = 0 \quad \text{on } \{0 \le y < y_1\} \cup \{y_2 < y \le \infty\} \qquad (5.16b)$$

$$\partial_y A_p(0,y) = f'(y) + c^2 y \quad \text{on } \{y_1 \le y \le y_2\} \qquad (5.16c)$$

$$A_p(x,0) = g(x) + c^2 x^2 / 2 \quad \text{on } \{0 \le x < \infty\} \qquad (5.16d)$$

The equations (5.16a) to (5.16d) may be reformulated as a mixed boundary-value problem in the quarter complex plane $Q_c = \{Re[\eta] > 0, Im[\eta] > 0\}$ (where $\eta = x + iy$) for the potential field $B_p(\eta)$ where

$$B_p(\eta) = B_{px}(\eta) - iB_{py}(\eta) = \partial_y A_p + i\,\partial_x A_p \qquad (5.17)$$

The problem then reduces to that of finding the holomorphic function B_p whose real or imaginary part satisfies the following mixed boundary conditions

$$Im\,[B_p(iy)] = 0 \quad \text{on } \{0 \le y < y_1\} \cup \{y_2 < y \le \infty\} \qquad (5.18a)$$

$$Re\,[B_p(iy)] = f'(y) + c^2 y \quad \text{on } \{y_1 \le y \le y_2\} \qquad (5.18b)$$

$$Im\,[B_p(x)] = g'(x) + c^2 x \quad \text{on } \{0 \le x < \infty\} \qquad (5.18c)$$

and from equation (5.14) the nonpotential field B associated with the flux function A is given by

$$B(\eta,\bar{\eta}) = B_p(\eta) - i c^2 \bar{\eta} \qquad (5.19)$$

where $\bar{\eta}$ denotes the complex conjugate of η.

We shall use a similar technique to find the solution for $B_p(\eta)$ to that used in previous papers concerning the equilibria of current sheets in potential fields (e.g. Demoulin et. al.,1989; Aly et. al.,1989; Amari and Aly, 1990b,c). The procedure is outlined below.

Using the conformal mapping $\xi = \eta^2$, where $\xi = X + iY$, we transform the quarter complex plane Q_c onto the upper-half complex plane $\Omega_c = \{-\infty < Re[\xi] < \infty,\ Im[\xi] > 0\}$ and reformulate equations (5.18a) to (5.18c) as the mixed boundary-value problem to determine in Ω_c the holomorphic function L_p defined by

$$L_p(\xi) = i\, B_p(\sqrt{\xi}) \tag{5.20}$$

whose real or imaginary part is given on the real axis by

$$Re\,[L_p(X)] = -\,g'(\sqrt{X}) - c^2\sqrt{X} \quad \text{on } \{0 \le X < \infty\} \tag{5.21a}$$

$$Re\,[L_p(X)] = 0 \quad \text{on } \{-y_1^2 < X \le 0\} \tag{5.21b}$$

$$Im\,[L_p(X)] = f'(\sqrt{-X}) + c^2\sqrt{-X} \quad \text{on } \{-y_2^2 \le X \le -y_1^2\} \tag{5.21c}$$

$$Re\,[L_p(X)] = 0 \quad \text{on } \{-\infty < X < -y_2^2\} \tag{5.21d}$$

Setting

$$h'(t) = g'(t) + c^2 t \tag{5.22}$$

the general solution for L_p which is bounded at infinity and also at $\xi = -y_2^2$ but not necessarily at $\xi = -y_1^2$ is given by the Keldysh-Sedov formula (Muskhelishvili, 1953) as

$$L_p(\xi) = \frac{1}{i\pi}\frac{(\xi+y_2^2)^{1/2}}{(\xi+y_1^2)^{1/2}}\left(\int_0^{\infty}\frac{-h'(\sqrt{t})}{t-\xi}\frac{(t+y_1^2)^{1/2}}{(t+y_2^2)^{1/2}}\,dt\right. \tag{5.23}$$

$$\left. + i\int_{-y_2^2}^{-y_1^2}\frac{f'(\sqrt{-t})+c^2\sqrt{-t}}{t-\xi}\frac{(t+y_1^2)^{1/2}}{(t+y_2^2)^{1/2}}\,dt\right) + (\alpha+i\beta)\frac{(\xi+y_2^2)^{1/2}}{(\xi+y_1^2)^{1/2}}$$

where α and β are two real constants and $h'(t)$ is such that the integral exists, requiring that

$$h'(t)\, t^r \to 0 \text{ as } t \to \infty, \text{ where } r > 0 \tag{5.24}$$

Transforming back into the quarter complex plane Q_c by applying the inverse conformal mapping $\eta = \sqrt{\xi}$, and using equations (5.19) and (5.17) to rewrite the expression in terms of $B(\eta,\bar{\eta})$, we obtain (after a change of variable in both integrals) the result

$$B(\eta,\bar{\eta}) = B_x - iB_y = -\,i\,c^2\bar{\eta} + \frac{2}{\pi}\frac{(\eta^2+y_2^2)^{1/2}}{(\eta^2+y_1^2)^{1/2}}\left(\frac{(\beta-i\alpha)\pi}{2}\right. \tag{5.25}$$

$$+\int_0^{\infty} \frac{t\,h'(t)}{t^2-\eta^2}\,\frac{(t^2+y_1^2)^{1/2}}{(y_2^2+t^2)^{1/2}}\,dt \;-\; \int_{y_1}^{y_2} \frac{t(f'(t)+c^2t)}{t^2+\eta^2}\,\frac{(t^2-y_1^2)^{1/2}}{(y_2^2-t^2)^{1/2}}\,dt\Bigg)$$

The field components are then given by equation (5.25) as

$$B_x = \mathrm{Re}[B] = -c^2y + \frac{2}{\pi}R_s\left(I_1-I_3+\frac{\beta\pi}{2}\right) - \frac{4}{\pi}I_s\left(I_2+I_4-\frac{\alpha\pi}{4}\right) \quad (5.26)$$

$$B_y = -\mathrm{Im}[B] = c^2x - \frac{4}{\pi}R_s\left(I_2+I_4-\frac{\alpha\pi}{4}\right) - \frac{2}{\pi}I_s\left(I_1-I_3+\frac{\beta\pi}{2}\right) \quad (5.27)$$

where

$$R_s = \mathrm{Re}\left(\frac{(\eta^2+y_2^2)^{1/2}}{(\eta^2+y_1^2)^{1/2}}\right) \quad (5.28)$$

$$I_s = \mathrm{Im}\left(\frac{(\eta^2+y_2^2)^{1/2}}{(\eta^2+y_1^2)^{1/2}}\right) \quad (5.29)$$

$$I_1 = \int_0^{\infty} \frac{t\,h'(t)\,(t^2+y_1^2)^{1/2}\,(t^2-x^2+y^2)}{((t^2-x^2+y^2)^2+4x^2y^2)\,(y_2^2+t^2)^{1/2}}\,dt \quad (5.30)$$

$$I_2 = \int_0^{\infty} \frac{t\,h'(t)\,(t^2+y_1^2)^{1/2}\,x\,y}{((t^2-x^2+y^2)^2+4x^2y^2)\,(y_2^2+t^2)^{1/2}}\,dt \quad (5.31)$$

$$I_3 = \int_{y_1}^{y_2} \frac{t\,(f'(t)+c^2t)\,(t^2-y_1^2)^{1/2}\,(t^2+x^2-y^2)}{((t^2+x^2-y^2)^2+4x^2y^2)\,(y_2^2-t^2)^{1/2}}\,dt \quad (5.32)$$

$$I_4 = \int_{y_1}^{y_2} \frac{t\,(f'(t)+c^2t)\,(t^2-y_1^2)^{1/2}\,x\,y}{((t^2+x^2-y^2)^2+4x^2y^2)\,(y_2^2-t^2)^{1/2}}\,dt \quad (5.33)$$

Practice in the manipulation of these integral expressions may be obtained by checking that as $x \to 0^+$ or as $y \to 0^+$, the boundary conditions imposed along the prominence or on the photosphere, respectively, are indeed recovered. This calculation is detailed in Appendix A.

5.4.3 Constraints on the arbitrary functions and parameters

Clearly from equation (5.25) the field is bounded at $\eta = iy_2$ (the top of the prominence sheet) and does not in general tend to zero at infinity. In order to ensure that the field is bounded at the other

extremity of the sheet, given by $\eta = iy_1$, we impose the following two constraints which must be satisfied by the forms of the arbitrary functions and the choice of parameter values.

$$\int_0^{\infty} \frac{t\, h'(t)\, dt}{(t^2+y_2^2)^{1/2}(t^2+y_1^2)^{1/2}} = \int_{y_1}^{y_2} \frac{t\,(f'(t)+c^2t)\, dt}{(y_2^2-t^2)^{1/2}(t^2-y_1^2)^{1/2}} - \frac{\beta\pi}{2} \qquad (5.34)$$

$$\alpha = 0 \qquad (5.35)$$

As stated above we may recover the case of a potential field outside the prominence simply by setting the parameter $c = 0$ and see that equation (5.25) is then the unique solution of the mixed boundary-value problem given by equations (5.18a) to (5.18c) bounded at $\eta = iy_2$ and tending towards zero at infinity. It can then be verified that the constraints given by equations (5.34) and (5.35) simplify to those found in the potential models (see Aly et al., 1989). One may also check that equation (5.34) is the generalised constraint found by Amari and Aly (1990c) for the equilibrium of a "force-free" current sheet in an external potential field vanishing at infinity in which $f'(y) = 0$ and the right-hand side of equation (5.34) vanishes.

Rather than calculate the value of β which satisfies the constraint once the arbitrary functions and parameters have been chosen, we may rewrite equation (5.25) in a form in which β is replaced by an integral representation given by equation (5.34) to obtain

$$B(\eta,\bar{\eta}) = B_x - iB_y = -ic^2\bar{\eta} + \frac{2}{\pi}\frac{(\eta^2+y_2^2)^{1/2}}{(\eta^2+y_1^2)^{1/2}} X \qquad (5.36)$$

$$\left(\int_0^{\infty} \frac{t\, h'(t)(\eta^2+y_1^2)\, dt}{(t^2-\eta^2)(t^2+y_1^2)^{1/2}(t^2+y_2^2)^{1/2}} + \int_{y_1}^{y_2} \frac{t(f'(t)+c^2t)(\eta^2+y_1^2)\, dt}{(y_2^2-t^2)^{1/2}(t^2-y_1^2)^{1/2}(t^2+\eta^2)} \right)$$

This will automatically ensure that the field is bounded at the lower end-point of the prominence sheet. Correspondingly the field components become

$$B_x(x,y) = -c^2y + \frac{2}{\pi}R_s\left(I_5+I_6\right) - \frac{4}{\pi}I_s\left(I_2+I_4\right) \qquad (5.37)$$

$$B_y(x,y) = c^2x - \frac{4}{\pi}R_s\left(I_2+I_4\right) - \frac{2}{\pi}I_s\left(I_5+I_6\right) \qquad (5.38)$$

where

$$I_5 = \int_0^{\infty} \frac{t\,h'(t)\,(t^2(x^2-y^2+y_1^2)+y_1^2(y^2-x^2)-(x^2+y^2)^2)}{(t^2+y_1^2)^{1/2}\,(t^2+y_2^2)^{1/2}\,((t^2-x^2+y^2)^2+4x^2y^2)}\,dt \quad (5.39)$$

$$I_6 = \int_{y_1}^{y_2} \frac{t\,(f'(t)+c^2t)\,(t^2(x^2-y^2+y_1^2)+y_1^2(x^2-y^2)+(x^2+y^2)^2)}{(y_2^2-t^2)^{1/2}\,(t^2-y_1^2)^{1/2}\,((t^2+x^2-y^2)^2+4x^2y^2)}\,dt \quad (5.40)$$

Note that along the y-axis these reduce to

$$B_x(0,y) = -c^2y + \frac{2}{\pi}\frac{(|y^2-y_2^2|)^{1/2}}{(|y^2-y_1^2|)^{1/2}}\,X \quad (5.41)$$

$$\left(\int_0^{\infty}\frac{t\,h'(t)\,(y_1^2-y^2)\,dt}{(t^2+y_1^2)^{1/2}(t^2+y_2^2)^{1/2}(t^2+y^2)} + \int_{y_1}^{y_2}\frac{t(f'(t)+c^2t)(y_1^2-y^2)\,dt}{(t^2-y_1^2)^{1/2}(y_2^2-t^2)^{1/2}(t^2-y^2)}\right)$$

$$B_y(0,y) = 0 \quad (5.42)$$

for $0 \le y < y_1$ and $y > y_2$ and to

$$B_x(0,y) = f'(y) \quad (5.43)$$

$$B_y(0^+,y) = -\frac{2}{\pi}(y^2-y_1^2)\frac{(|y^2-y_2^2|)^{1/2}}{(|y^2-y_1^2|)^{1/2}}\,X \quad (5.44)$$

$$\left(\int_0^{\infty}\frac{t\,h'(t)\,dt}{(t^2+y_1^2)^{1/2}(t^2+y_2^2)^{1/2}(t^2+y^2)} + \int_{y_1}^{y_2}\frac{t\,(f'(t)+c^2t)\,dt}{(t^2-y_1^2)^{1/2}(y_2^2-t^2)^{1/2}(t^2-y^2)}\right)$$

for $y_1 \le y \le y_2$. h'(t) is such that all the integrals in equations (5.23) to (5.44) exist, and this is true provided that equation (5.24) is satisfied.

5.4.4 Topology of the field

So far we have assumed nothing about the topology of the field configuration. However, it is clear that in order to produce a prominence model which is of a particular type of bipolar configuration we must simultaneously choose the functions f'(y) and g'(x) to satisfy the following conditions.

a) For a normal (N-type) configuration

$xg'(x) < 0\ (> 0)$ on $\{-\infty < x < \infty\}/\{0\}$

and $f'(y) < 0\ (> 0)$ on $\{y_1 < y < y_2\}$ (5.45)

b) For an inverse (I-type) configuration

$xg'(x) < 0\ (> 0)$ on $\{-\infty < x < \infty\}/\{0\}$

and $f'(y) > 0\ (< 0)$ on $\{y_1 < y < y_2\}$ (5.46)

We are now in a position to understand why the equivalent model describing the case of a potential field outside the prominence (Demoulin et. al., 1989) failed to produce any inverse configurations in which the field vanishes at infinity and is nonsingular in Ω. If we set $c = 0$ and $\beta = 0$ we see that $h'(x) = g'(x)$ from equation (5.22) and since from equation (5.46) $g'(x)$ is of opposite sign to $f'(y)$, the constraint given by equation (5.34) is impossible to satisfy (the two sides being of opposite sign).

We now consider the form of the underlying photospheric field. From equations (5.22) and (5.24) we see that

$$h'(x) \to 0, \quad g'(x) \to -c^2 x \quad \text{as} \quad x \to \infty \tag{5.47}$$

If we are to consider a purely bipolar photospheric field (which we will assume is the case from now on) then we must choose

$$xg'(x) < 0 \qquad \text{on } \{-\infty < x < \infty\}/\{0\} \tag{5.48}$$

From equations (5.45) and (5.46) it follows that an N-type configuration is obtained if $f'(y) < 0$ and that an I-type configuration is obtained if $f'(y) > 0$.

Now let us consider the direction of the purely horizontal field above the prominence sheet, i.e. along the y-axis. We will show that there exists some y^* such that

$$B_x(0,y) < 0 \qquad y \geq y^* \geq y_2 \tag{5.49}$$

Indeed, we see from equation (5.41) that

$$B_x(0,y) \leq -c^2 y + 2(I_7 + I_8(y))/\pi = G(y) \tag{5.50}$$

where

$$I_7 = \int_0^{\infty} \frac{t\,|h'(t)|\,dt}{(t^2+y_1^2)^{1/2}(t^2+y_2^2)^{1/2}} \tag{5.51}$$

$$I_8(y) = \int_{y_1}^{y_2} \frac{t(|f'(t)+c^2 t|)(y^2-y_1^2)\,dt}{(t^2-y_1^2)^{1/2}(y_2^2-t^2)^{1/2}(y^2-t^2)} \tag{5.52}$$

$G(y)$ is a monotonically decreasing function of y from $G(y_2)$ (which may be positive or negative) to $G(\infty) = -\infty$ and hence there will certainly exist some y^* such that equation (5.49) is satisfied. Note that $G(y_2) < 0$ implies that $y^* = y_2$ whereas $G(y_2) > 0$ implies that $y^* > y_2$.

This result is not surprising in light of the fact that the overall field is (from equation (5.14)) essentially the superposition of a potential field B_p and a particular integral field B_0, the field lines of

which are concentric circular arcs with centres located at the origin along which the field is directed anti-clockwise (i.e. in the negative x-direction as they cross the y-axis) and increasing in strength with distance from the origin. Of course the above properties of B_0 imply that simply altering the sign of f'(y) and g'(x) simultaneously does not result in the same field line projection in Q with the field oppositely directed. Rather this field results from viewing the field along the negative as opposed to the positive z-axis.

5.4.5 Necessary conditions for equilibrium

Of course, once we have selected the arbitrary functions f'(y) and g'(x) along with the values of c, y_1 and y_2, we still have to ensure that the configuration is in equilibrium between the combined vertical action of the gravitational and Lorentz forces. As we noted in section 5.3, the Lorentz force must be in the positive y-direction everywhere along the vertical extent of the sheet in order for there to be such an equilibrium. Thus along the sheet we must have

$$B_x(0,y)\, B_y(0^+,y) \geq 0 \qquad \text{on } \{y_1 \leq y \leq y_2\} \tag{5.53}$$

or

$$f'(y)\, B_y(0^+,y) \geq 0 \qquad \text{on } \{y_1 \leq y \leq y_2\} \tag{5.54}$$

In order to consider the possibility of equilibrium we examine the vertical field component along the prominence which is given by equation (5.44). First consider the case $f'(y) \geq 0$ in $[y_1,y_2]$ which, since $xg'(x) < 0$ as required by equation (5.48), will yield an I-type configuration. From equation (5.54) we clearly require that $B_y(0^+,y) \geq 0$ in $[y_1,y_2]$. Let us evaluate the sign of $B_y(0^+,y_i)$ for $i = 1,2$. For $i = 2$, since the second integral in equation (5.44) is negative we see that there is no sign restriction on the first integral for equation (5.54) to be satisfied. For $i = 1$, however, since the second integral is positive we see that the first integral must be negative for an equilibrium to exist and this can only be true if $h'(x) < 0$ (and hence $g'(x) < -c^2 x$ from equation (5.22)) on at least some subinterval of $[0,\infty)$. This condition does not violate the earlier condition given for a bipolar field (equation (5.48)) which simply requires that $g'(x) < 0$ in $[0,\infty)$.

Now consider the case $f'(y) \leq 0$ in $[y_1,y_2]$ which, by virtue of equation (5.48), will yield an N-type configuration. The equilibrium condition is now satisfied by $B_y(0^+,y) \leq 0$ in $[y_1,y_2]$. From a similar argument to the one detailed above we now see that if $f'(y) < -c^2y$ in

$[y_1,y_2]$ then for i = 1 the first integral must be positive and if $f'(y) > -c^2y$ in $[y_1,y_2]$ then for i = 2 the first integral must again be positive. This is only possible if $h'(x) > 0$ (and hence $g'(x) > -c^2x$) on at least some subinterval of $[0,\infty)$. Again this condition does not violate the condition for a bipolar field provided $g'(x) < 0$ in $[0,\infty)$. Note that if $f'(y) + c^2y$ changes sign in $[y_1,y_2]$ conditions for equilibrium are not at all obvious.

Of course these results only show that equilibrium might be possible in I-type or N-type configurations, respectively, given the above restrictions on g'(x) and f'(y). It will be demonstrated in section 5.5 that equilibrium configurations of both types are indeed possible with particular choices of f'(y) and g'(x). In summary, we have the following necessary conditions for constructing an equilibrium configuration of a given type with a purely bipolar photospheric field.

a) N-type

$f'(y) \leq 0$ in $[y_1,y_2]$ $\qquad$ $g'(x) < 0$ in $(0,\infty)$

If $f'(y) + c^2y$ is of constant sign in $[y_1,y_2]$, then $g'(x) > -c^2x$ on at least some subinterval of $(0,\infty)$.

b) I-type

$f'(y) \geq 0$ in $[y_1,y_2]$ $\qquad$ $g'(x) < 0$ in $(0,\infty)$

$g'(x) < -c^2x$ on at least some subinterval of $(0,\infty)$ if $f'(y) + c^2y$ is of constant sign.

5.4.6 Prominence mass

Once a configuration is obtained which satisfies the equilibrium condition described by equation (5.54), there exists at each point on the sheet a unique mass density m(y) given by equation (5.4) for which the gravitational and Lorentz forces are exactly balanced. Using equation (5.44) we may write this as

$$m(y) = \frac{4f'(y)}{\mu\pi g_c}\frac{(y_2^2-y^2)^{1/2}}{(y^2-y_1^2)^{1/2}} X \qquad (5.55)$$

$$\left(\int_0^{\infty} \frac{t\, h'(t)\, (y_1^2-y^2)\, dt}{(t^2+y_1^2)^{1/2}(t^2+y_2^2)^{1/2}(t^2+y^2)} + \int_{y_1}^{y_2} \frac{t(f'(t)+c^2t)(y_1^2-y^2)\, dt}{(t^2-y_1^2)^{1/2}(y_2^2-t^2)^{1/2}(t^2-y^2)} \right)$$

and the total mass per unit length of the prominence is then given by equation (5.5) as

$$M = \int_{y_1}^{y_2} m(y)\, dy \qquad (5.56)$$

Note that the mass density may not be imposed in this formulation but rather is a result of the calculations.

5.4.7 The longitudinal component of the magnetic field

Recall that the longitudinal component of the magnetic field is given by

$$B_z(A) = \pm 2c\sqrt{A(x,y)} \qquad (5.7)$$

where $A \geq 0$ for $B_z(A)$ physically to exist (i.e. $B_z(A) \in \Re$) . Note that along the photosphere we have imposed that

$$A(x,0) = g(x) \qquad \text{on } \{-\infty < x < \infty\} \qquad (5.13d)$$

and we have seen that for a bipolar field

$$xg'(x) < 0 \qquad \text{on } \{-\infty < x < \infty\}/\{0\} \qquad (5.48)$$

along with

$$g'(0) = 0 \qquad (5.12)$$

$$g'(x) \to -c^2x \quad \text{as} \quad x \to \infty \qquad (5.47)$$

From equations (5.47) and (5.46), g(x) is obviously a monotonically decreasing function of x in $[0,\infty)$ with no finite lower bound. Thus it is clear that beyond some value of $x = x_0$ say, g(x) and hence A(x,0) will certainly become negative. Since A(x,y) is constant along field lines, the particular one along which A(x,y) = 0 (so that there is no longitudinal field as seen from equation (5.6)) then represents the boundary of the region in Q within which A > 0 and our model is physically acceptable. Note that if any of the field lines intersecting the photosphere are to be included in this region, g(0) must be positive. Adding an arbitrary positive constant to g(x) in no way affects g'(x) (= $-B_y(x,0)$, which is essentially what we impose) or indeed the projection of the field lines in Q but will extend the region within which the model is valid (since x_0 is increased) and increase the shear at any particular point. It is worth noting that the physics of the model, which depends only on A, is unaffected by the choice of the sign of $B_z(A)$. For a given A, the two possible signs result in two fields; one being the reflection about $\{x = 0\}$ of the other.

5.5 Application of the method for a particular choice of boundary conditions

In this section we demonstrate the construction of magnetic field configurations for particular forms of the arbitrary functions f'(y) and g'(x) and particular values of the parameters c, y_1 and y_2. The procedure is to select f'(y) to be of the sign required for the chosen type of configuration (negative or positive for N-type or I-type respectively), then select g'(x) that satisfies the conditions described in section 5.4.5. Values must also be given to c, y_1 and y_2. From equations (5.37) and (5.38) the field components in Q can now be calculated everywhere and they automatically satisfy the constraints given by equations (5.34) and (5.35) which ensure that the field is bounded at the endpoints of the sheet Γ. The field line projections in Q may then be plotted by the method described below. Finally we must check that the equilibrium condition given by equation (5.54) is satisfied everywhere along the sheet to ensure that we have constructed a physically valid model in which support of the entire sheet against gravitational forces is possible.

5.5.1 Method used to obtain plots of the magnetic field

Since A(x,y) is constant along field lines the easiest method of plotting field lines is to produce a contour plot in Q of equally spaced values of A(x,y). Unfortunately, we do not have an explicit expression for A(x,y) and so must resort to a numerical approach.

Along the photosphere, since we have imposed $B_y(x,0)$ we obviously know (to within a constant) A(x,0) from equation (5.13d). For a particular point (x_p,y_p) in Q we can find $A(x_p,y_p)$ from

$$A(x_p,y_p) = A(x_p,0) + \int_0^{y_p} dA \qquad (5.57)$$

which from equation (2.25) becomes

$$A(x_p,y_p) = A(x_p,0) + \int_0^{y_p} B_x(x_p,y)\, dy \qquad (5.58)$$

Thus for each value of x_p we can calculate from equation (5.37) $B_x(x_p,y)$ at several values of y and so evaluate numerically the integral in equation (5.58) to obtain $A(x_p,y_p)$ for various values of y_p. This enables us to obtain values of A on a grid of points in Q and hence produce a

contour plot.

5.5.2 A particular choice of boundary conditions

We now construct particular configurations of the magnetic field for a simple form of the imposed normal field components. The most straightforward choice for the field across the prominence is

$$B_x(0,y) = f'(y) = a \qquad \text{on } \{y_1 \le y \le y_2\} \tag{5.59}$$

where a is a real constant, positive or negative for an I-type or N-type model, respectively.

For the vertical field along the photosphere we choose

$$B_y(x,0) = -g'(x) = bx/(x^2 + d^2) + c^2x \qquad \text{on } \{-\infty < x < \infty\} \tag{5.60}$$

where b and d are real constants. Note that $g'(x) \to -c^2x$ as $x \to \infty$, as required by equation (5.47), is nowhere singular and satisfies the conditions required for a bipolar field given by equation (5.47) and (5.48) provided

$$b \ge -c^2d^2 \tag{5.61}$$

Values of y_1 and y_2 are then selected and from equation (5.54) we see that to ensure equilibrium the condition simply becomes

$$B_y(0^+,y) \le 0 \qquad \text{on } \{y_1 \le y \le y_2\} \tag{5.62}$$

for an N-type configuration

$$B_y(0^+,y) \ge 0 \qquad \text{on } \{y_1 \le y \le y_2\} \tag{5.63}$$

for an I-type configuration where $B_y(0^+,y)$ is obtained from equation (5.44).

Examples of both types of configuration are seen in Figures 5.2 and 5.3 along with the corresponding variation of $B_y(0^+,y)$ along the prominence sheet in order to verify that the above condition holds. Note that for both types of model the field strength increases without bound as we move to infinite distances from the sheet but that in the localised area about the sheet (and in particular at the extreme points) the field is everywhere finite. We may construct models in which the prominence is either attached to the photosphere ($y_1 = 0$) or is detached ($y_1 > 0$). The O-type neutral point above the sheet in the case of the I-type model is to be expected from the arguments in section 5.4.4 concerning the direction of $B_x(0,y)$. Note especially that for the first time we have been able to produce an I-type model in equilibrium everywhere in which the field is locally finite with closed field lines above the prominence and an X-type neutral point below. This is particularly important since the majority of mature quiescent

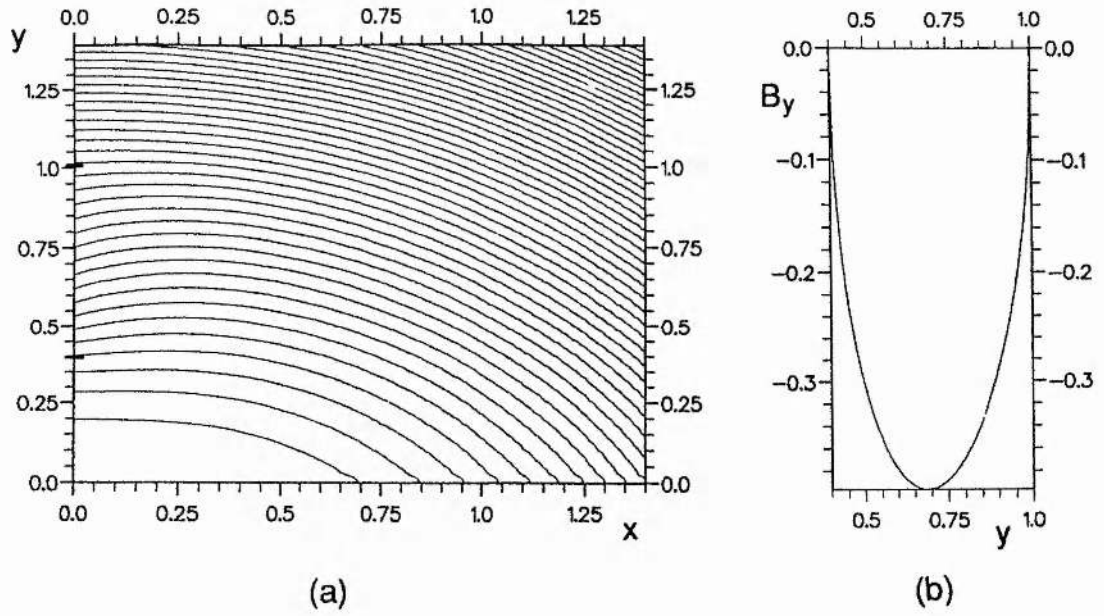

Fig. 5.2 (a) The projection in the x-y plane of the field lines for a normal configuration constructed using the particular functional form of the boundary conditions detailed in section 5.5. $y_1 = 0.4$, $y_2 = 1.0$, $a = -1.0$, $b = -1.0$, $c^2 = 1.0$, $d^2 = 1.0$. (b) The vertical field component $B_y(0^+,y)$ plotted as a function of height along the vertical extent of the prominence sheet.

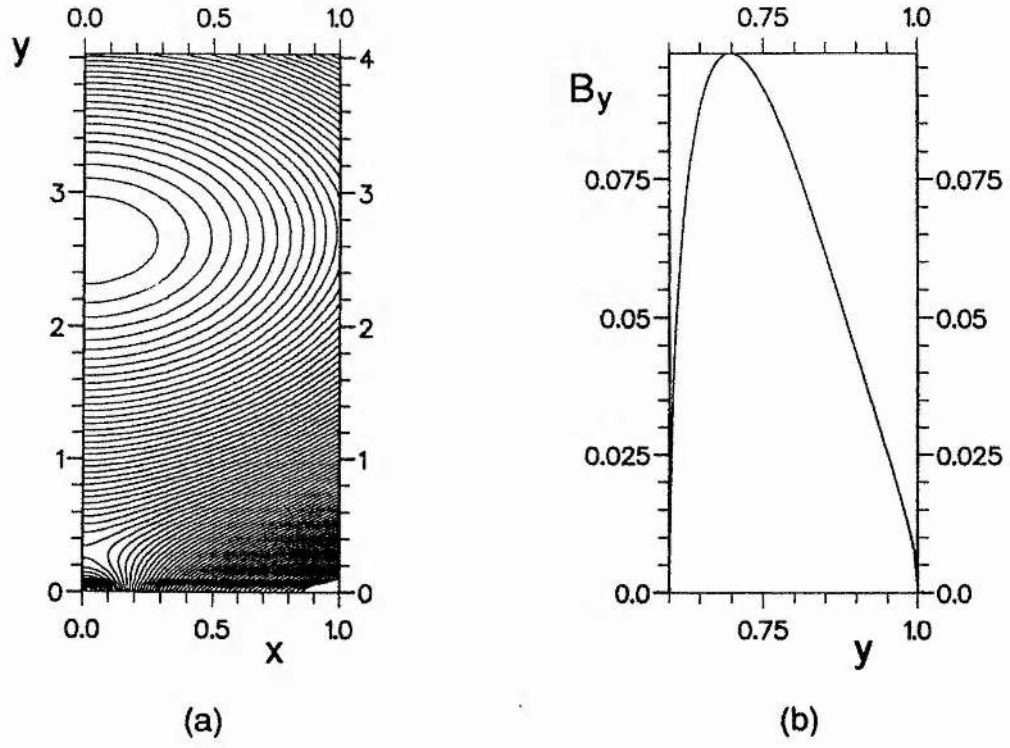

Fig. 5.3 (a) The projection in the x-y plane of the field lines for an inverse configuration. $y_1 = 0.6$, $y_2 = 1.0$, $a = 1.0$, $b = 1.1$, $c^2 = 1.0$, $d^2 = 0.01$. (b) The vertical field component $B_y(0^+,y)$ plotted as a function of height along the vertical extent of the prominence sheet.

prominences are known observationally to be of I-type.

The mass density per unit length of the prominence m(y) which will be supported by the field is given by equation (5.4) as

$$m(y) = 2\,|a|\,|B_y(0^+,y)| \,/\, \mu\, g_c \qquad (5.64)$$

In this simple case we see that m(y) is directly proportional to $B_y(0^+,y)$ and the shapes of the two graphs against y will be identical. The total prominence mass per unit length M may be obtained by numerically integrating equation (5.64) to get

$$M = \frac{2|a|}{\mu g_c} \int_{y_1}^{y_2} |B_y(0^+,y)|\, dy \qquad (5.65)$$

5.6 Extension to the case of a quadrupolar photospheric field

Recall that the solution of the boundary-value problem specified by equations (5.13a) to (5.13d) results in a field B(x,y) (described by equations (5.25) to (5.44)) whose properties were developed in sections 5.4.4 to 5.4.7 under the assumption that the underlying photospheric field is of a purely bipolar topology. We may extend our model to incorporate a quadrupolar photospheric field simply by replacing equation (5.48) with

$$g'(x) > 0 \qquad \text{on } \{0 < x < x_c\} \qquad (5.66)$$

$$g'(x) < 0 \qquad \text{on } \{x_c < x < \infty\} \qquad (5.67)$$

where

$$g'(x_c) = 0 \qquad (5.68)$$

to avoid discontinuity of the vertical field component at $x = x_c$. We must of course retain the conditions described by equations (5.12) and (5.47) to ensure that the field is continuous at $x = 0$ and that the integral representation of the field is meaningful.

Obviously the deduction concerning the sign of the horizontal field component above the prominence sheet remains valid since this was independent of the form of h'(x) and so $B_x(0,y) < 0$ for $y > y_c$ say, where $y_c \geq y_2$. However, the conditions for equilibrium become a little more uncertain, though it may be seen from equation (5.66) that $h'(x) > 0$ at least for $0 < x < x_c$ and so this may well decrease the possibility of equilibrium if $f'(y) \geq 0$ in $[y_1,y_2]$ and increase this possibility if $f'(y) \leq 0$ in $[y_1,y_2]$.

Regarding the shear of the field and the region in the x-y plane in which the model is physically valid, we see now that g(x) is a

monotonically increasing function of x in $[0,x_c]$ and a monotonically decreasing function of x with no lower bound in $[x_c,\infty)$ and hence $A(x,0)$ will again become negative beyond some value of $x = x_0$ where $A(x_0,0) = 0$. Assuming $g(0) \geq 0$, the field line passing through $(x_0,0)$ again bounds the region in Q within which the model is valid.

Returning to our particular choice in section 5.5 for the form of the boundary conditions, we see that a quadrupolar photospheric field may be imposed simply by replacing equation (5.61) with the condition

$$b < -c^2d^2 \tag{5.69}$$

As before, once values of y_1 and y_2 are selected, the configuration must be checked to ensure that equilibrium has been achieved along the sheet by confirming that equation (5.62) or (5.63) holds.

An example of such an equilibrium configuration is shown in Figure 5.4.

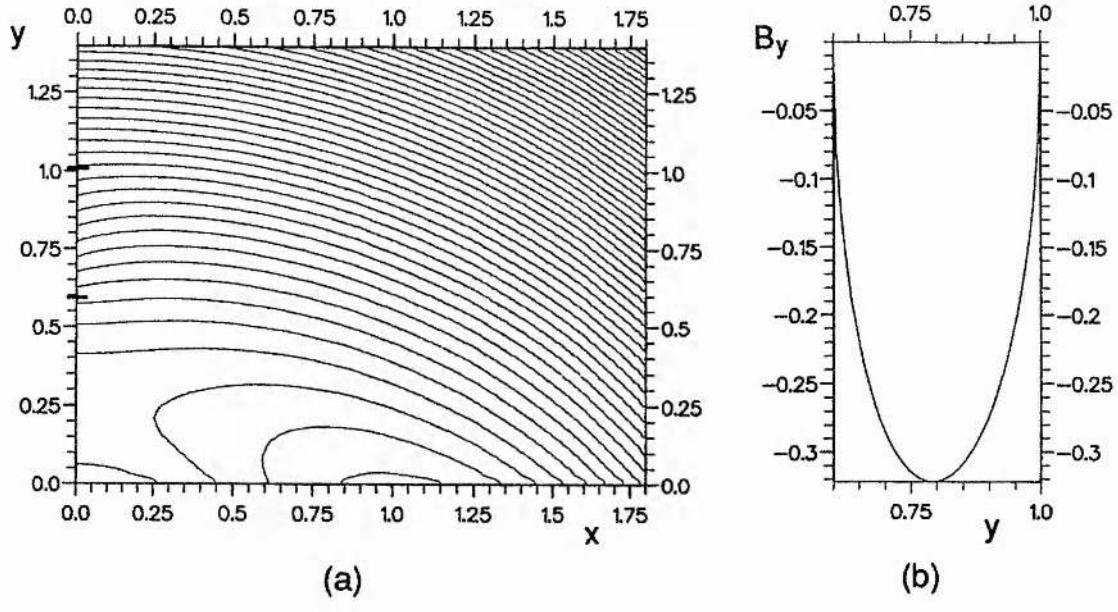

Fig. 5.4 (a) The projection in the x-y plane of the field lines for a particular quadrupolar configuration. $y_1 = 0.6$, $y_2 = 1.0$, $a = -1.0$, $b = -2.0$, $c^2 = 1.0$, $d^2 = 1.0$. (b) The corresponding distribution of the vertical field component $B_y(0^+,y)$ along the prominence sheet.

5.7 Discussion

We have developed a method for constructing symmetrical, z-invariant and locally bounded magnetic field configurations in which a finite, vertical sheet of mass and current (modelling a prominence) is

in static equilibrium between the combined forces of a uniform gravitational field and a constant-current force-free field. The method requires the more or less arbitrary specification of the normal magnetic field components along the photosphere and across the prominence and these may to some extent be chosen to be in agreement with observational data. Furthermore the relative strength of the longitudinal field component must be given.

We have demonstrated for simple boundary conditions that equilibrium can be achieved for both N-type and I-type configurations and in particular have constructed a locally bounded I-type configuration in which closed field lines exist above the prominence and an X-type neutral point below. Such a configuration has not previously been possible in the models described in section 2.5 which consider potential or linear force-free fields outside the current sheet.

In our model it is not possible to select completely arbitrarily the forms of the imposed field components and automatically ensure that an equilibrium configuration results. Rather, we must check that we have achieved an equilibrium configuration after we have chosen f'(y) and g'(x). The necessary conditions found in section 5.4.5 do however provide useful guide-lines for choosing these functions.

In selecting as boundary conditions the normal field components along the photosphere and across the prominence we are in no way necessarily imitating the physical processes which govern the formation of a prominence. The details of these processes are not well understood, but it is these that determine such properties as the prominence mass density, height, current distribution, etc. The mathematical analysis of the model could therefore be generalised by selecting an alternative boundary condition to the normal field across the prominence while keeping all the other assumptions unchanged. One may wish to impose for example the current density distribution along the prominence (see chapter 6) or the mass density distribution by unit of flux. It seems reasonable to keep as a boundary condition the normal field along the photosphere since from the principals of line-tying this field is predominantly determined by motions within the photosphere rather than physical processes within the corona.

At first sight, two apparent problems with our model are a) the divergence of the field strength at large distances from the

prominence sheet and b) the loss of a physical meaning for $B_z(A)$ when $A < 0$. It may be possible to overcome both problems if the constant-current field is "cut-off" at some field line (for which $A = A_c \geq 0$) and either a potential field or an open field with flows is assumed to exist in the region beyond this field line. The later possibility may be relevant for explaining the helmet streamers which are frequently observed above quiescent prominences. Either action would result in a free boundary-value problem in which the unknown shape of the bounding field line ($A = A_c$) would need to be determined, in general numerically, by magnetic pressure balance. In the case of purely circular field lines the azimuthal component of the potential field is simply inversely proportional to the radial distance from the helical axis and so it may be that analytical progress is possible for almost circular field lines by a perturbation expansion.

Appendix A

Recovery of the boundary conditions

In order to regain the boundary conditions which we have imposed along the prominence or photosphere we examine the field (given by equation (5.25) with $\alpha = 0$ (see equation (5.35))) in the limits as x or $y \to 0^+$ respectively.

Firstly consider the case in which $x \to 0^+$ for $y_1 \leq y \leq y_2$. Equation (5.25) becomes

$$B(0^+,y) = -c^2 y - \frac{2i}{\pi} \frac{(y_2^2-y^2)^{1/2}}{(y^2-y_1^2)^{1/2}} \lim_{x\to 0^+} \left(I_1 - I_3 + 2i(I_2+I_4) + \frac{\beta\pi}{2} \right) \quad (A1)$$

where I_1 to I_4 are defined in section 5.4.2.

Neither I_1 nor I_2 is singular as $x \to 0^+$ at any point in their range of integration and so they simply become

$$I_1 = \int_0^\infty \frac{t\, h'(t)\, (t^2+y_1^2)^{1/2}\, dt}{(t^2+y^2)^{1/2}\, (t^2+y_2^2)^{1/2}}, \qquad I_2 = 0$$

As $x \to 0^+$, the integrand of I_3 is seen to be singular at $t^2 = y^2$ but for $t^2 \neq y^2$ the integrand is finite and (in general) nonzero and the integral is given by the Cauchy principal value as

$$I_3 = \lim_{\varepsilon\to 0^+}\left(\int_{y_1}^{y-\varepsilon}\frac{t(f'(t)+c^2t)(t^2-y_1^2)^{1/2}\,dt}{(t^2-y^2)(y_2^2-t^2)^{1/2}} + \int_{y+\varepsilon}^{y_2}\frac{t(f'(t)+c^2t)(t^2-y_1^2)^{1/2}\,dt}{(t^2-y^2)(y_2^2-t^2)^{1/2}}\right)$$

The fourth integral also has a singular integrand at $t^2 = y^2$ as $x \to 0^+$ but elsewhere in the integration range the integrand is zero. Thus the integral may be expressed in terms of a Dirac δ-function as

$$I_4 = \int_{y_1}^{y_2}\frac{t(f'(t)+c^2t)(t^2-y_1^2)^{1/2}\delta(t^2-y^2)\,dt}{(y_2^2-t^2)^{1/2}} = \frac{i\pi}{2}\frac{(f'(y)+c^2y)(y^2-y_1^2)^{1/2}}{(y_2^2-y^2)^{1/2}}$$

After some elementary algebra equation (A1) then yields the field components

$$B_x(0^+,y) = \mathrm{Re}[B(0^+,y)] = f'(y) \qquad (A2)$$

$$B_y(0^+,y) = -\mathrm{Im}[B(0^+,y)] = \frac{2}{\pi}\frac{(y_2^2-y^2)^{1/2}}{(y^2-y_1^2)^{1/2}}\left(I_1-I_3+\frac{\beta\pi}{2}\right) \qquad (A3)$$

where I_1 to I_4 take the values calculated above. Note that in equation (A2) we have succeeded in recovering the boundary condition imposed across the prominence sheet.

Similarly if we consider the limit as $y \to 0^+$, equation (5.25) becomes

$$B(x,0^+) = -ic^2x - \frac{2}{\pi}\frac{(y_2^2+x^2)^{1/2}}{(x^2+y_1^2)^{1/2}}\lim_{y\to 0^+}\left(I_1-I_3+2i(I_2+I_4)+\frac{\beta\pi}{2}\right) \qquad (A4)$$

Here I_1 is given by the Cauchy principal value and I_2 may be expressed in terms of a δ-function while I_3 and I_4 are easily reduced to give (after some algebra) the field components

$$B_x(x,0^+) = \frac{2}{\pi}\frac{(y_2^2+x^2)^{1/2}}{(x^2+y_1^2)^{1/2}}\left(I_1-I_3+\frac{\beta\pi}{2}\right) \qquad (A5)$$

$$B_y(x,0^+) = -g'(x) \qquad (A6)$$

and we see that equation (A6) is simply the imposed photospheric boundary condition.

6 PROMINENCE SHEETS SUPPORTED BY CONSTANT-CURRENT FORCE-FREE FIELDS. II - IMPOSITION OF NORMAL PHOTOSPHERIC FIELD COMPONENT AND PROMINENCE SURFACE CURRENT

6.1 Chapter summary

In this chapter we continue our investigation into the magnetohydrostatic equilibrium of a sheet of mass and current in a constant-current force-free field. Section 6.2 outlines the differences in the approach taken in this chapter compared with that of chapter 5. In section 6.3 we describe the coordinate system used and the assumptions made in setting up the model. In section 6.4 we formulate the boundary-value problem, solve it and discuss the properties of this solution, particularly with regard to the field topology and the possibility of equilibrium solutions. The use of the method is demonstrated in section 6.5 in which examples of both N-type and I-type models are generated for particular forms of the boundary conditions. In section 6.6 we discuss the particular case in which the current sheet reduces to a current filament. Finally section 6.7 contains a discussion of the results arising from this model.

6.2 Introduction

In chapter 5 we described a particular method of generating longitudinally invariant magnetohydrostatic equilibria in which a finite, vertical sheet of mass and current (representing a prominence sheet) is supported against gravity by an external constant-current force-free field. The model was developed under the assumption that the values of the normal magnetic field component along the photosphere and across the prominence were given as functions of position. This allowed us to construct a mixed boundary-value problem in the first quadrant which when solved enabled us to determine the coronal field everywhere. This corresponds to the so-called "BVP3" described in Aly et al. (1989), already considered in the case of a potential coronal field by Anzer (1972) and Demoulin et al. (1989). It was shown in chapter 5 that in general, arbitrary choices for these two field components would not result in a bounded field or an equilibrium configuration, although necessary (and, in the case of boundedness,

sufficient) conditions on the two components were derived for the field to satisfy these properties. It was demonstrated that for a particular simple functional form of the imposed field components satisfying these conditions, we could indeed generate configurations of both N-type and I-type. The field was bounded everywhere locally and the prominence sheet was in equilibrium along its entire length. Although the choice of the functional forms of the two imposed field components is not determined by applying any physical principle, they may to some degree be chosen to be in agreement with observational data.

In this present chapter we wish to develop the model in a somewhat different manner. We keep all the assumptions described in chapter 5 and retain as a boundary condition the normal magnetic field along the photosphere. Along the prominence sheet, however, we now wish to impose instead the surface current density. This allows us to construct a different boundary-value problem (corresponding to the so-called "BVP1" in Aly et al. (1989)) which will again enable us to determine the magnetic field everywhere. This form of the boundary conditions has been considered previously by Anzer (1985) and Amari and Aly (1990a) in the case of potential and linear force-free coronal fields, respectively. The work is extended in this chapter by the solution of BVP1 in which a constant-current force-free field lies outside the prominence sheet.

6.3 Mathematical description of the model

We adopt the cartesian coordinate system (x,y,z) in which the corona occupies the half-space $D = \{-\infty < x < \infty, 0 < y < \infty, -\infty < z < \infty\}$ lying above the photosphere $P = \{-\infty < x < \infty, y = 0, -\infty < z < \infty\}$. The magnitudes of all physical quantities are assumed to be invariant under translations parallel to the z-axis and thus we need only consider the model in the upper half x-y plane perpendicular to the prominence axis which we take without loss of generality to be that passing through the origin denoted by $\Omega = \{-\infty < x < \infty, 0 < y < \infty, z = 0\}$.

Since prominences are seen to be globally stationary for periods of several days, it is assumed that the coronal magnetic field is essentially time-invariant and hence the system is governed by the magnetohydrostatic equations (see section 2.2)

$$\mathbf{j} \times \mathbf{B} + \rho \mathbf{g}_c - \nabla p = \mathbf{0} \qquad (2.21)$$

$$\mathbf{j} = \nabla \times \mathbf{B} / \mu \qquad (2.5)$$

$$\nabla . \mathbf{B} = 0 \qquad (2.2)$$

where gravity is assumed to be uniform and to act in the negative y-direction so that

$$\mathbf{g_c} = - g_c \mathbf{e_y} \qquad g_c > 0 \qquad (6.1)$$

In our model we are interested only in the global structure of the magnetic field supporting the prominence and hence we consider all the plasma to be cold and condensed into an infinitesimally thin current sheet Σ whose intersection with Ω is the line segment Γ. Thus the plasma density takes the functional form

$$\rho(x,y) = m(x,y)\, \delta(\Gamma) \qquad (6.2)$$

where m is the surface mass density per unit length on Σ and $\delta(\Gamma)$ is the Dirac measure located on Γ. Outside Σ, we assume that the magnetic field is force-free.

Since **B** is independent of z we can express the field components in terms of a scalar flux function A(x,y) as (see section 2.3)

$$\mathbf{B} = \left(\frac{\partial A}{\partial y}(x,y), - \frac{\partial A}{\partial x}(x,y), B_z(x,y) \right) \qquad (2.25)$$

immediately satisfying equation (2.2). Following Amari and Aly (1990a), the component form of equation (2.21) (in which **B** and **j** are written in terms of A by equations (2.5) and (2.25)) yields

$$B_z = B_z(A) \qquad (6.3)$$

$$\partial_x A \, (\nabla^2 A + B_z(A)\, B_z'(A)) = 0 \qquad (6.4)$$

$$\partial_y A \, (\nabla^2 A + B_z(A)\, B_z'(A)) + \mu\, m\, g_c\, \delta(\Gamma) = 0 \qquad (6.5)$$

where $B_z'(A) = dB_z(A)/dA$.

Let us define the quantity $X|_\Gamma = (X|_{\Gamma+} + X|_{\Gamma-})/2$ where $X|_{\Gamma\pm}$ are the limits of X as Γ is approached from its positive and negative sides, respectively. Equations (6.4) and (6.5) then yield two conditions which the magnetic field must satisfy, namely

$$\partial_y A|_\Gamma = B_x|_\Gamma \neq 0 \quad \text{for } m \neq 0 \qquad (6.6)$$

$$- \partial_x A|_\Gamma = B_y|_\Gamma = 0 \qquad (6.7)$$

By virtue of the above property of $B_x|_\Gamma$, equation (6.5) can be rewritten as

$$\nabla^2 A + B_z(A)\, B_z'(A) + \mu j_\Sigma\, \delta(\Gamma) = 0 \qquad (6.8)$$

where

$$j_\Sigma = \frac{m\, g_c}{B_x(x,y)|_\Gamma} \qquad (6.9)$$

is the surface current on Σ flowing in the z-direction. Equation (6.8), along with the boundary condition

$$A(x,0) = g(x) \qquad \text{on } \{-\infty < x < \infty\} \qquad (6.10)$$

then defines a boundary-value problem which determines A(x,y) in Ω once $B_z(A)$, j_Σ and Γ have been prescribed. Note that equation (6.10) is equivalent to specifying the normal field component along the photosphere as

$$B_y(0,y) = -dg(x)/dx = -g'(x) \qquad \text{on } \{-\infty < x < \infty\} \qquad (6.11)$$

For a physically acceptable model, we will assume that g(x) and g'(x) are both continuous functions.

Once A(x,y) has been computed, m can be calculated from equation (6.9). Note that in the present formulation this quantity is a result of the calculations and cannot be prescribed. Of course, our model is only physically meaningful if m is a positive quantity, requiring that

$$j_\Sigma \, B_x|_\Gamma \geq 0 \qquad (6.12)$$

The total mass per unit length of the prominence sheet is clearly given by

$$M = \int_\Gamma m \, ds \qquad (6.13)$$

It should be noted that an arbitrary prominence sheet Γ will not, in general, satisfy the horizontal equilibrium condition expressed by equation (6.7). If it does not, the position of such a sheet must subsequently be adjusted by some complex iterative method until equilibrium is achieved. Such complications can be avoided by considering a magnetic field configuration which has the property that

$$A(-x,y) = A(x,y) \qquad (6.14)$$

and in which Γ is situated on the y-axis so that

$$\Gamma = \{x = 0, \, 0 \leq y_1 \leq y \leq y_2\} \qquad (6.15)$$

since equation (6.7) is then satisfied automatically. In this chapter we will assume that Γ is indeed given by equation (6.15) and we will ensure that our fields comply with the condition given by equation (6.14) by insisting that the imposed photospheric flux is symmetric about the origin i.e.

$$g(-x) = g(x) \qquad (6.16)$$

Note that this in turn implies that

$$g'(-x) = -g'(x) \qquad (6.17)$$

As a result of equation (6.14) we further see that

$$g'(0) = 0 \qquad (6.18)$$

Because of the symmetry we have imposed on the model, we need only illustrate the projection of the system in the first quadrant of Ω as sketched in Figure 6.1.

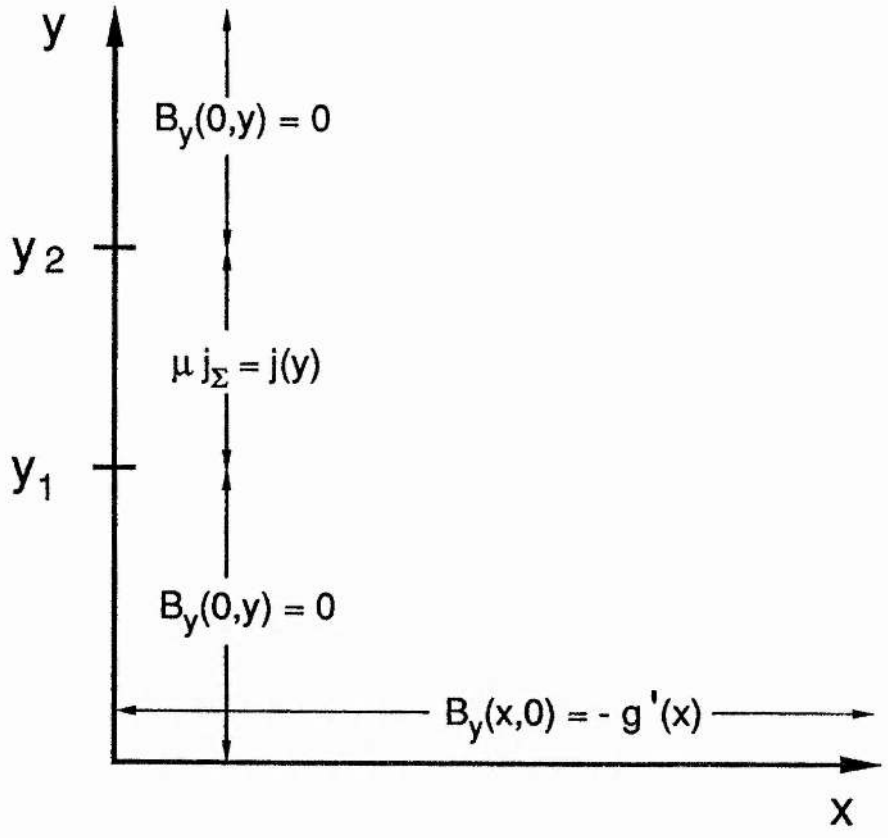

Fig. 6.1 The conditions imposed on the boundaries of the first quadrant of the x-y plane. y is measured vertically and the prominence sheet stretches between y_1 and y_2.

We can now devise a method which will enable us to construct z-invariant magnetic field configurations containing a current sheet. Firstly, we compute A(x,y) everywhere in Ω having specified $B_z(A)$, g(x) satisfying equations (6.16) and (6.18), j_Σ and Γ satisfying equation (6.15). If the resulting magnetic field satisfies equation (6.12), we can determine the unique mass density on Σ from equation (6.9) and the total mass from equation (6.13). If equation (6.12) is not satisfied, however, the model is incompatible with the support of a prominence sheet in a magnetic field since the sheet is not then in magnetohydrostatic equilibrium.

6.4 Interaction of a current sheet with a constant-current force-free field

6.4.1 Solution of the boundary-value problem

We now specify the functional form of the coronal field to be of the constant-current force-free type and correspondingly we set

$$B_z(A) = \pm 2\,c\,\sqrt{A(x,y)} \qquad (6.19)$$

where $c \geq 0$ is a real constant and $A(x,y) \geq 0$ for the above functional form of $B_z(A)$ to be physically meaningful. Equation (6.8) then becomes

$$\nabla^2 A(x,y) + 2\,c^2 + \mu j_\Sigma\,\delta(\Gamma) = 0 \qquad \text{in } \Omega \qquad (6.20)$$

where Γ is given by equation (6.15). This expression reduces to the case of a potential coronal field when $c = 0$.

We further specify

$$\mu j_\Sigma = j(y) = \varepsilon\, I\, j_0(y) \qquad \text{on } \{y_1 \leq y \leq y_2\} \qquad (6.21)$$

where $\varepsilon = \pm 1$ and $I > 0$ is a real constant such that

$$\int_{y_1}^{y_2} j(y)\,dy = \varepsilon\, I \qquad (6.22)$$

Clearly I/μ gives the total amount of current along the sheet and ε indicates the direction of this current. For the sake of simplicity we are deliberately restricting our choice of the functional form of $j(y)$ to be of constant sign in $[y_1,y_2]$ (see Aly et al. (1989) for an argument concerning the case where $j(y)$ is allowed to change sign with a potential field outside the current sheet).

Equations (6.20), (6.10)and (6.21) define a boundary-value problem in Ω for $A(x,y)$ which we may solve by considering the decomposition of $A(x,y)$ into two further scalar flux functions, namely

$$A(x,y) = A_0(x,y) + A_p(x,y) \qquad (6.23)$$

where $A_0(x,y)$ is a particular solution of

$$\nabla^2 A_0(x,y) + 2\,c^2 = 0 \qquad (6.24)$$

given by

$$A_0(x,y) = -c^2\,(x^2 + y^2)\,/\,2 \qquad (6.25)$$

which is independent of the boundary conditions and $A_p(x,y)$ is the solution of the boundary-value problem

$$\nabla^2 A_p + j(y)\,\delta(\Gamma) = 0 \qquad \text{in } \Omega \qquad (6.26)$$

$$A_p(x,0) = h(x) \qquad \text{on } \{-\infty < x < \infty\} \qquad (6.27)$$

where

$$h(x) = g(x) + c^2\,x^2\,/\,2 \qquad (6.28)$$

Note that $h(x)$ is an even function and $h'(x) = dh(x)/dx$ is an odd function.

Equations (6.26) and (6.27) can be solved using Green's theorem

$$A_p = \int_{y_1}^{y_2} G(x,y;0,y')\, j(y')\, \delta(\Gamma)\, dy' \qquad (6.29)$$

$$+ \int_{-\infty}^{\infty} \frac{\partial G}{\partial y'}(x,y;x',0)\, h(x')\, dx'$$

where G is the Green's function of the Laplace equation in Ω with homogenous boundary conditions, namely

$$G(x,y;x',y') = \frac{1}{4\pi} \ln \frac{(x-x')^2+(y+y')^2}{(x-x')^2+(y-y')^2} \qquad (6.30)$$

and so the solution of the boundary-value problem defined by equations (6.26) and (6.27) gives $A_p(x,y)$. After combining this with $A_0(x,y)$ from equation (6.25), we finally obtain

$$A(x,y) = -\frac{c^2}{2}(x^2+y^2) + \frac{1}{\pi}\int_{-\infty}^{\infty} \frac{y\, h(x')}{(x-x')^2+y^2}\, dx' \qquad (6.31)$$

$$+ \frac{1}{4\pi}\int_{y_1}^{y_2} j(y') \ln \frac{x^2+(y+y')^2}{x^2+(y-y')^2}\, dy'$$

The magnetic field components are given by equation (2.25) as

$$B_x(x,y) = -c^2 y + \frac{1}{\pi}\int_{-\infty}^{\infty} \frac{[(x-x')^2-y^2]\, h(x')}{[(x-x')^2+y^2]^2}\, dx' \qquad (6.32)$$

$$+ \frac{1}{\pi}\int_{y_1}^{y_2} \frac{j(y')\, y'\, [x^2-(y^2-y'^2)]}{[x^2+(y+y')^2][x^2+(y-y')^2]}\, dy'$$

$$B_y(x,y) = c^2 x + \frac{2}{\pi}\int_{-\infty}^{\infty} \frac{y\, h(x')\, (x-x')}{[(x-x')^2+y^2]^2}\, dx' \qquad (6.33)$$

$$+ \frac{1}{\pi}\int_{y_1}^{y_2} \frac{j(y')\, x\, y\, y'}{[x^2+(y+y')^2][x^2+(y-y')^2]}\, dy'$$

and $B_z(x,y)$ from equations (6.19) and (6.31). Thus, if we are given the functional form of h(x) and j(y), we are able to determine the value of

$A(x,y)$ and the field components everywhere in Ω.

Note that for the field to be bounded at the extreme ends of the prominence sheet we require that $j(y_1) = j(y_2) = 0$ and in this particular case $j(y)$ must satisfy

$$j(y) \approx \xi(y)(y_2-y)^{\alpha} \ (\alpha>0) \text{ near } y = y_2 \text{ where } \xi(y_2) \neq 0 \qquad (6.34)$$

$$j(y) \approx \eta(y)(y-y_1)^{\beta} \ (\beta>0) \text{ near } y = y_1 \text{ where } \eta(y_1) \neq 0 \qquad (6.35)$$

For the existence of the first integral in equation (6.31) we must have

$$h(x) \rightarrow C_1 |x|^r \text{ as } x \rightarrow \pm\infty, \text{ where } r < 1 \qquad (6.36)$$

From equation (6.28) we then see that

$$g(x) \rightarrow - c^2 x^2 / 2 + C_1 |x|^r \quad \text{as } x \rightarrow \pm\infty \qquad (6.37)$$

This constraint immediately implies that

$$B_y(x,0) = -g'(x) \rightarrow c^2 x \quad \text{as } x \rightarrow \pm\infty \qquad (6.38)$$

and thus, for a purely bipolar photospheric field, which we will assume is the case from now on, we must have

$$x\, g'(x) < 0 \equiv x\, B_y(x,0) > 0 \qquad \text{on } \{-\infty < x < \infty\}/\{0\} \qquad (6.39)$$

i.e. the vertical field component along the photosphere is upward in the first quadrant of Ω and downward in the second quadrant.

6.4.2 Conditions for the equilibrium of a configuration

As yet, we have said nothing about selecting the functional forms of $j(y)$ and $h(x)$ in order to produce a configuration in which equilibrium is achieved along the entire vertical extent of the sheet. For this to occur we require the Lorentz force to be directed upwards everywhere on Γ so that we satisfy from equations (6.12) and (6.21)

$$\varepsilon\, B_x(0,y) > 0 \qquad \text{on } \{y_1 \leq y \leq y_2\} \qquad (6.40)$$

Note that equations (6.39) and (6.40) imply that for any current sheet which is indeed in equilibrium, $\varepsilon = +1$ corresponds to an I-type configuration and $\varepsilon = -1$ corresponds to an N-type configuration. Also note that, had we allowed the function $j(y)$ to change sign at one or more points in $[y_1,y_2]$ then $B_x(0,y)$ would also have had to change sign at the same points for the equilibrium condition (equation (6.12)) to be satisfied.

From equation (6.32) we obtain $B_x(0,y)$ in terms of $j(y)$ and $h(x)$ as

$$B_x(0,y) = - c^2 y + \frac{1}{\pi} \int_{-\infty}^{\infty} \frac{(x'^2-y^2)\, h(x')}{(x'^2+y^2)^2}\, dx' \qquad (6.41)$$

$$+\frac{1}{\pi}\int_{y_1}^{y_2}\frac{j(y')\,y'\,(y'^2-y^2)}{(y+y')^2(y-y')^2}\,dy'$$

The first integral may be simplified by an integration by parts and the second is given in $[y_1,y_2]$ by the Cauchy Principal Value so we may write

$$B_x(0,y) = -c^2y + [\,H(y) + \varepsilon\, I\, J(y,y_1,y_2)\,]/\pi \qquad (6.42)$$

where

$$H(y) = 2\int_0^{\infty}\frac{x'\,h'(x')}{x'^2+y^2}\,dx' \qquad (6.43)$$

$$J(y,y_1,y_2) = \begin{cases} \lim_{\zeta\to 0}\left(\int_{y_1}^{y-\zeta}\frac{-y'\,j_0(y')}{y^2-y'^2}\,dy' + \int_{y+\zeta}^{y_2}\frac{-y'\,j_0(y')}{y^2-y'^2}\,dy'\right) & \text{in } [y_1,y_2] \\ \int_{y_1}^{y_2}\frac{-y'\,j_0(y')}{y^2-y'^2}\,dy' & \text{in } (0,y_1)\cup(y_2,\infty) \end{cases} \qquad (6.44)$$

Note that

$$J(y_1,y_1,y_2) \geq 0 \quad \text{and} \quad J(y_2,y_1,y_2) \leq 0 \qquad (6.45)$$

Before proceeding further with the case of a constant-current field outside the prominence, it is worth considering some properties of the model in which the coronal field is potential. Our model reduces to this case in the limit $c = 0$ which implies, from equation (6.28), that $h(x) = g(x)$. From equation (6.42) we then obtain

$$B_x(0,y) = [\,H(y) + \varepsilon\, I\, J(y,y_1,y_2)\,]/\pi \qquad (6.46)$$

Since $B_y(x,0) = -g'(x)$ does not have to tend to a definite nonzero value at large values of x (unlike the case when $c \neq 0$; see equation (6.38)) but only has to vanish, we can construct purely bipolar configurations for either

$$x\,g'(x) < 0 \qquad \text{on } \{-\infty < x < \infty\}/\{0\} \qquad (6.47)$$

or

$$x\,g'(x) > 0 \qquad \text{on } \{-\infty < x < \infty\}/\{0\} \qquad (6.48)$$

The projection of the field in Ω produced by taking one sign of $x\,g'(x)$ and ε will just be the reflection about $x = 0$ of the field produced by the opposite signs of both $x\,g'(x)$ and ε.

Let us consider the horizontal field component at the upper extreme of the prominence sheet for $c = 0$. From equation (6.46) we

obtain

$$B_x(0,y_2) = [\, H(y_2) + \varepsilon I\, J(y_2,y_1,y_2)\,] / \pi \qquad (6.49)$$

Assume that $x\, g'(x) < 0$ (alternatively, > 0). It is readily seen from equation (6.49) that for $\varepsilon = +1$ (-1), $B_x(0,y_2) < 0$ (> 0), whereas the equilibrium condition given by equation (6.40) requires that $B_x(0,y_2) \geq 0$ (≤ 0). Thus, as a necessary condition for equilibrium to be attained at the top of the prominence sheet when $c = 0$, we must have

$$x\, g'(x) < 0\ (> 0) \text{ and } \varepsilon = -1\ (+1) \qquad (6.50)$$

Both of these cases result in an N-type configuration so we see that for a potential field outside the prominence, no I-type equilibrium configurations exist.

Let us return now to the case for which $c \neq 0$. From now on we make the restriction that $h'(x)$ be of constant sign in $0 < x < \infty$. This will ensure that $|H(y)|$ is a monotonically decreasing function of y, allowing us to proceed with the following analysis. We will consider in turn both I-type and N-type models in order to determine under what conditions we may expect to produce an equilibrium configuration.

6.4.2.1 Inverse-type configurations

Consider first the case $\varepsilon = +1$ which, as stated above, corresponds to an I-type configuration if the equilibrium condition given by equation (6.40) is satisfied.

6.4.2.1.1 Existence of a maximum value of y_2 (a necessary condition for equilibrium)

For an equilibrium configuration we must in particular satisfy

$$B_x(0,y_2;I) = -c^2 y_2 + [\, H(y_2) + I\, J(y_2,y_1,y_2)\,] / \pi \geq 0 \qquad (6.51)$$

Immediately we see that, since the first and third terms are negative, we must have $H(y_2)$ (and hence $h'(x)$ in $(0,\infty)$) positive. Since $B_x(0,y_2;I)$ is a monotonically decreasing function of I, we see that $B_x(0,y_2;I) < B_x(0,y_2;0)$, so a necessary condition for the inequality in equation (6.51) to be satisfied is that $B_x(0,y_2;0) > 0$. Because $dB_x(0,y_2;0)/dy_2 < 0$ with no finite lower bound, there clearly exists some y_{2max} such that this necessary condition holds only if $y_2 < y_{2max}$ and hence equilibrium may be possible depending on the value of I. y_{2max} is given by the (in general) implicit equation

$$\pi c^2 y_{2max} = H(y_{2max}) \qquad (6.52)$$

It is interesting to note that the introduction of any non-zero value of c allows the possibility of an I-type equilibrium configuration

(impossible in the potential case with c = 0 as demonstrated above). Furthermore, since we also require that h'(x) > 0, we see that an O-type neutral point with closed field lines above the photosphere must exist when the field is free from any current sheet for prominence support to be possible when the sheet is added.

6.4.2.1.2 Existence of a maximum value of I (a necessary condition, a sufficient condition and a necessary and sufficient condition for equilibrium)

Given h'(x) > 0 and y_2 satisfying the above conditions, we see from equation (6.51) that $B_x(0,y_2;I)$ is a monotonically decreasing function of I. Thus there exists an upper bound on $I = I_{c2}$, say, such that $B_x(0,y_2;I_{c2}) = 0$ and the inequality in equation (6.51) is only satisfied for $I < I_{c2}$. I_{c2} is given explicitly by

$$I_{c2}(c,y_1,y_2) = \frac{\pi c^2 y_2 - H(y_2)}{J(y_2,y_1,y_2)} \qquad (6.53)$$

Note that since $B_x(0,y_2;I) < B_x(0,y_1;I)$ for all I (consider equation (6.42)), equilibrium is certainly achieved at $(0,y_1)$ if it is achieved at $(0,y_2)$. $I < I_{c2}$ is a necessary condition for equilibrium.

Of course in general, equilibrium will be lost at some point on the sheet other than y_2 for a smaller value of I than I_{c2}. This is dependent on the precise form of the function $J(y,y_1,y_2)$ in $[y_1,y_2]$ which is not in general a monotonically decreasing function of y. In order to guarantee that equilibrium is obtained along the whole of the sheet, we can choose $I < I_{c1}$, where I_{c1} is defined as the maximum current such that $B_x(0,y_2;I_{c1}) \geq 0$ and $dB_x(0,y;I_{c1})/dy \leq 0$ in $[y_1,y_2]$. Note that for the first of these inequalities to be satisfied, $I_{c1} \leq I_{c2}$. Unfortunately, finding the value of I_{c1} is a task which must be tackled numerically for each particular case. We see that $I < I_{c1} \leq I_{c2}$ is a sufficient condition for equilibrium to occur along the entire sheet.

Lastly, let us denote by I_c the largest value of I for which equilibrium is lost (i.e. $B_x(0,y)$ vanishes) at only one point on the sheet $(0,y_c)$, say. This implies that

$$B_x(0,y_c;I_c) = 0 \qquad (6.54)$$

which in turn implies that $I_{c1} \leq I_c \leq I_{c2}$. Since this is (by the definitions of I_c and y_c) the only point for which $B_x(0,y)$ vanishes in $[y_1,y_2]$ and since $B_x(0,y)$ and its first derivative with respect to y are continuous functions of y in $[y_1,y_2]$, $y = y_c$ must be a turning point of $B_x(0,y)$. Thus y_c and I_c will also satisfy

$$dB_x(0,y;I_c)/dy \mid_{y=yc} = 0 \qquad (6.55)$$

giving two equations in these two unknowns (c.f. Amari and Aly, 1990a). Unfortunately, equations (6.54) and (6.55) are not (in general) tractable analytically and would have to be solved numerically for any given values of the parameters c, y_1 and y_2 and the functions j(y) and h(x). Note that $I < I_c$ is a necessary and sufficient condition for equilibrium.

6.4.2.2 Normal-type configurations

We now consider the case $\varepsilon = -1$ which will yield an N-type configuration if the equilibrium equation

$$B_x(0,y;I) = -c^2 y + [\, H(y) - I\, J(y,y_1,y_2) \,]/\pi \leq 0 \text{ in } [y_1,y_2] \qquad (6.56)$$

is satisfied.

6.4.2.2.1 Existence of a minimum y_2 (a necessary condition for equilibrium)

If h'(x) is positive for $x > 0$ then since $B_x(0,y_2;I)$ is a monotonically increasing function of I, we have $B_x(0,y_2;I) > B_x(0,y_2;0)$ and so a necessary condition for equation (6.56) to be satisfied is that $B_x(0,y_2;0) < 0$. Because $dB_x(0,y_2;0)/dy_2 < 0$ with no lower bound and $B_x(0,0;0) > 0$, we see that there exists some y_{2min} such that this condition can only be fulfilled for $y_2 > y_{2min}$. Clearly y_{2min} is given implicitly by

$$\pi c^2 y_{2min} = H(y_{2min}) \qquad (6.57)$$

Physically, $(0,y_{2min})$ is the location of an O-type neutral point in the field in the absence of any current sheet. Note that, unlike the I-type case, we are unable to state that equilibrium exists at $(0,y_1)$ if it exists at $(0,y_2)$ because $B_x(0,y_1;I)$ is not necessarily smaller than $B_x(0,y_2;I)$. Thus $y_2 > y_{2min}$ is a necessary condition for equilibrium if h'(x) is positive in $(0,\infty)$.

If h'(x) is negative in this range there are no such restrictions on y_2.

6.4.2.2.2 Existence of a maximum value of I (a necessary condition, a sufficient condition and a necessary and sufficient condition for equilibrium)

Values of I_{c2}, I_c and I_{c1} may be obtained as in the case of an inverse-type configuration to give necessary, sufficient and necessary and sufficient conditions for equilibrium, respectively. This is left as an exercise for the reader.

6.4.3 Existence of a maximum of the total mass M

6.4.3.1 Inverse-type configurations

Consider the prominence sheet to be of finite length $y_2 - y_1$ (nonzero since we are not interested here in the case of a current filament). We will show that for a given value of y_1 and y_2 there exists an upper bound on M. We know that there exists a maximum current $I_c \leq I_{c2}$ for which equilibrium can exist along the entire length of the sheet. Let us denote by J_{max} the maximum value of $J(y,y_1,y_2)$ in $[y_1,y_2]$. This must be finite from our restrictions on j(y). We can then see that at every point on the sheet in an equilibrium configuration we certainly satisfy

$$B_x(0,y) < - c^2 y_1 + [H(y_1) + I_{c2} J_{max}] / \pi = B_{xmax} \qquad (6.58)$$

Let us further denote

$$j_{max} = I_{c2} j_{0max} \qquad (6.59)$$

where j_{0max} is the maximum of j_0 in $[y_1,y_2]$. Then we see from equation (6.9) that at every point along the sheet

$$m < j_{max} B_{xmax} / \mu g_c$$

and so

$$M < \int_{y_1}^{y_2} \frac{j_{max} B_{xmax}}{\mu g_c} dy = \frac{j_{max} B_{xmax} (y_2-y_1)}{\mu g_c} \qquad (6.60)$$

$$= M_{max}(\varepsilon=+1,c,y_1,y_2)$$

We now show that for any given value of $y_2 - y_1$ there exists an upper bound on M_{max}. Since $J(y,y_1,y_2)$ is bounded for all nonzero $y_2 - y_1$ we can find (in general by numerical methods) finite values for J^* and J_i where, for $0 < y_2 < y_{2max}$, J^* is the maximum value of $J(y,y_1,y_2)$ in $[y_1,y_2]$ and J_i is the minimum value of $|J(y_2,y_1,y_2)|$. Then we can see from equation (6.58) that for any choice of y_1

$$B_{xmax} < H(0) + I^*_{c2} J^* = B^*_{xmax} \qquad (6.61)$$

where, from equation (6.53),

$$I_{c2} < H(0)/J_i = I^*_{c2} \qquad (6.62)$$

and so

$$B^*_{xmax} = H(0) (1 + J^*/J_i) \qquad (6.63)$$

(Recall from section 6.4.2.1.1 that for equilibrium, h'(x) and hence H(z) must be positive). Let us further define

$$j^*_{max} = I^*_{c2} j^*_{0max} \qquad (6.64)$$

where, for $0 < y_2 < y_{2max}$, j^*_{0max} is the maximum of $j_0(y)$ in $[y_1,y_2]$. Then we have an upper bound on $M_{max} = M^*_{max}$, say, for a given normal field

distribution on the photosphere and form of the surface current along the prominence which is given by

$$M^*_{max}(\varepsilon=+1,c,y_2-y_1) = j^*_{max}\, B^*_{xmax}\, y_{2max} / \mu\, g_c \qquad (6.65)$$

6.4.3.2 Normal-type configurations

We know that there exists a maximum value of $I = I_c \leq I_{c2}$ for which equilibrium is attainable at every point on the sheet. Thus we know that in an equilibrium configuration we certainly have in $[y_1,y_2]$

$$|B_x(0,y)| < |-c^2 y_2 + [\, H(y_2) - I_{c2}J_{max}\,]/\pi| = B_{xmax} \quad \text{if } h'(y) > 0 \qquad (6.66)$$

$$|B_x(0,y)| < |-c^2 y_2 + [\, H(y_1) - I_{c2}J_{max}\,]/\pi| = B_{xmax} \quad \text{if } h'(y) < 0 \qquad (6.67)$$

As for the I-type case we can determine M_{max}, given by equation (6.60) with B_{xmax} given by the above expression, as an upper bound on the total prominence mass per unit length.

We cannot calculate a finite upper bound on M_{max} as we did in the I-type case since here we have no finite upper limit on the value of y_2. In fact by adjustment of the parameters y_1 and y_2 any finite mass may be supported. This is not surprising since, as we will show in section 6.4.4, at a large height above the origin, the transverse field in the absence of a current sheet is in the negative direction (as required in this case for equilibrium) and increases in magnitude with height. Thus we may well expect that it is possible to introduce a larger finite amount of mass (equivalent to a larger current I) at an increased height since this will disturb the background field less than at a lower height. Since there is no theoretical limit in this model to the height at which the mass may be placed we expect no upper bound on the amount of mass the field can support.

6.4.4 Topology of the field

Consider the sign of the horizontal field component along the y-axis. We will show that there exists some y^* such that

$$B_x(0,y) < 0 \qquad y \geq y^* \geq y_2 \qquad (6.68)$$

From equation (6.32) we see that above and below the prominence sheet (i.e. for $0 \leq y \leq y_1$ and $y \geq y_2$)

$$B_x(0,y) = -c^2 y + \frac{1}{\pi}\int_{-\infty}^{\infty} \frac{(x'^2-y^2)\, h(x')}{(x'^2+y^2)^2}\, dx' + \frac{1}{\pi}\int_{y_1}^{y_2} \frac{y'\, j(y')\, (y'^2-y^2)}{(y+y')^2(y-y')^2}\, dy' \qquad (6.69)$$

Thus we see that for $y \geq y_2$

$$B_x(0,y) \leq -c^2 y + \frac{1}{\pi}\left(|H(y)| + \int_{y_1}^{y_2} \frac{y'\,|j(y')|}{y^2-y'^2}\,dy'\right) = G(y) \quad (6.70)$$

Note that G(y) is a monotonically decreasing function of y from $G(y_2)$ (which may be positive or negative) to $G(\infty) = -\infty$ and hence there certainly exists some y^* such that equation (6.68) is satisfied. Note that $G(y_2) < 0$ implies $y^* = y_2$ whereas $G(y_2) \geq 0$ implies $y^* \geq y_2$.

The above result on the sign of $B_x(0,y)$ is to be expected, since at large distances from the origin equation (6.31) reduces to

$$A(x,y) \approx -c^2 (x^2 + y^2) / 2 \quad (6.71)$$

which is just the particular solution $A_0(x,y)$ in equation (6.25). The magnitude of the field corresponding to this flux function is an increasing function of the distance from the origin and the field lines consist of concentric circles about the origin along which the field is directed anti-clockwise (i.e. in the negative x-direction when crossing the y-axis).

6.4.5 The longitudinal component of the magnetic field

Recall that the longitudinal component of the magnetic field is given by

$$B_z(A) = \pm 2c\sqrt{A(x,y)} \quad (6.19)$$

where $A(x,y) > 0$ for $B_z(A)$ to have a physical meaning (i.e. $B_z(A) \in \Re$). In our development of the model we have imposed

$$A(x,0) = g(x) \quad \text{on } \{-\infty < x < \infty\} \quad (6.10)$$

to be an even function about $x = 0$ and have found that

$$g'(x) \to -c^2 x / 2 \text{ as } x \to \pm\infty \quad (6.38)$$

$$x\,g'(x) < 0 \quad \text{on } \{-\infty < x < \infty\}/\{0\} \quad (6.39)$$

$$g'(0) = 0 \quad (6.18)$$

for the field to be bounded locally, the photospheric field to be bipolar and the vertical field to be continuous at the origin, respectively. Let us assume that $A(0,0) > 0$. From equations (6.38) and (6.39), g(x) (and hence A(x,0)) is a monotonically decreasing function of x in $(0,\infty)$ with no finite lower bound and thus A(x,0) will certainly be negative for $|x| \geq x_0$, say, where $A(x_0,0) = A(-x_0,0) = 0$. Since A(x,y) is constant along field lines, the field line passing through $(x_0,0)$ and $(-x_0,0)$ forms a boundary to a region in Ω, within which $A(x,y) > 0$ and the model is physical. The addition of an arbitrary positive constant to g(x) will

extend the region of validity for the model (since x_0 will then increase) and increase the shear at any point but will not alter the projection of the field lines in Ω. Note that the physics of the model (dependent on A(x,y) only) is unaffected by the choice of the sign of $B_z(A)$ in equation (6.19).

6.4.6 Relationship between the present formulation and that of Chapter 5

Recall that in chapter 5 we imposed not the surface current $j_\Sigma(y)$ along the prominence but the normal magnetic field $B_x(0,y) = f'(y)$ across the prominence sheet. Equation (6.42) can thus be interpreted as a linear Fredholm integral equation of the first kind for j(y) given f'(y). This can be seen by writing equation (6.42) as

$$F(y) = \int_{y_1}^{y_2} K(y,y')\, j(y')\, dy' \qquad (6.72)$$

where

$$F(y) = \pi f'(y) + \pi c^2 y - H(y) \qquad (6.73)$$

$$K(y,y') = \frac{-y'}{(y^2 - y'^2)} \qquad (6.74)$$

Similarly, if we set x = 0, equation (6.31) can be thought of as just such an equation for j(y) given f(y) (= A(0,y)). Here the corresponding functions F(y) and K(y,y') are

$$F(y) = 4\pi \left(f(y) + \frac{c^2 y^2}{2} - \frac{1}{\pi} \int_{-\infty}^{\infty} \frac{y\, h(x')}{x'^2 + y^2}\, dx' \right) \qquad (6.75)$$

$$K(y,y') = \ln \left(\frac{y+y'}{y-y'} \right)^2 \qquad (6.76)$$

Having then determined j(y) from either of the equations, A(x,y) may then be deduced from equation (6.31).

6.5 Application of the method for a particular chioce of boundary conditions

In this section we will demonstrate the construction of both N-type and I-type models for particular functional forms of g(x) and j(y) and values of c, y_1, y_2.

6.5.1 Method of constructing equilibrium configurations

We first select the functional form of the even function g(x) such that it satisfies equations (6.38), (6.39) and (6.18). Once a value of c is chosen, we may deduce from either equation (6.52) or (6.57) the location of any neutral point in the absence of a current sheet and hence obtain a maximum or minimum value of y_2, depending on the configuration type. We can then select a position for the prominence (by chosing y_1 and y_2) such that equilibrium will certainly be possible for a small enough net current I.

The non-negative function $j_0(y)$ is then chosen to satisfy equations (6.34) and (6.35) and ε is selected to be ± 1 according to the type of configuration being sought.

We must now check that for the value of I that is chosen, $B_x(0,y)$ satisfies equation (6.40) and hence gives an equilibrium solution. The prominence mass density per unit length can then be calculated at any point in $[y_1,y_2]$ using equation (6.9) and the total mass per unit length from equation (6.13).

Once it is confirmed that the solution is indeed an equilibrium one, we may use equation (6.31) to calculate A(x,y) on a grid of points in Ω. A contour map of A(x,y) may then be produced with contours at equally spaced values of A(x,y) which is equivalent to a plot of the field line projections in Ω.

6.5.2 A particular choice of boundary conditions

We will now work through the method outlined above with particular simple forms of g(x) and j(y). Other forms which satisfy the conditions stated above may, of course, be used but without observational evidence to prefer any other form we will select one that enables us to demonstrate the method in a relatively straightforward manner.

For the distribution of the photospheric flux we select

$$g(x) = \begin{cases} (a - c^2)x^2/2 & |x| \le 1 \\ a(0.5 + \ln|x|) - c^2x^2/2 & |x| \ge 1 \end{cases} \qquad (6.77)$$

where a is an arbitrary real constant. Note that equation (6.37) is satisfied by the above choice and that any arbitrary constant may be added to g(x) in order to increase the region of validity of the model (see section 6.3.5). The above form of g(x) gives

$$h(x) = \begin{cases} ax^2/2 & |x| \le 1 \\ a(0.5 + \ln|x|) & |x| \ge 1 \end{cases} \qquad (6.78)$$

$$g'(x) = \begin{cases} (a-c^2)x & |x| \le 1 \\ (a-c^2x^2)/x & |x| \ge 1 \end{cases} \qquad (6.79)$$

$$h'(x) = \begin{cases} ax & |x| \le 1 \\ a/x & |x| \ge 1 \end{cases} \qquad (6.80)$$

which enables us to obtain H(y) analytically from equation (6.43) as

$$H(y) = 2a\left(1 - \frac{y^2+1}{y}\tan^{-1}\frac{1}{y} + \frac{\pi}{2y}\right) \qquad (6.81)$$

$|H(y)|$ is clearly a monotonically decreasing function of y with a maximum value of 4a at $y = 0$ and vanishing as $y \to \infty$. The sign of H(y) is just that of a and so we must have (see section 6.4.2.1) $a > 0$ for an I-type configuration. Equation (6.39) is satisfied provided that $a < c^2$.

Selecting values for a and c we may next deduce the location of any neutral point in the background field (i.e. in the absence of a current sheet) by seeking a solution for $y > 0$ of

$$B_x(0,y)|_{I=0} = -c^2 y + H(y)/\pi = 0 \qquad (6.82)$$

It is clear that one such solution will exist if $a > 0$ but not if $a \le 0$. The height of this neutral point then gives the minimum height for the upper end point of the prominence in an N-type model or the maximum height for this point in an I-type model. Thus we can choose values of y_1 and y_2 for which an equilibrium solution is certainly possible for small enough values of I.

For our form of j(y) we will take that chosen by Anzer (1985) and Amari and Aly (1990a), namely

$$j(y) = \varepsilon I j_0(y) = \varepsilon I \frac{6}{(y_2-y_1)^3}(y_2-y)(y-y_1) \qquad (6.83)$$

which satisfies the conditions described in section 6.4.1. We can then obtain the following expressions from equation (6.44)

$$J(y,y_1,y_2) = \frac{-3}{(y_2-y_1)^3} X \qquad (6.84)$$

$$\left(y_1^2-y_2^2 + (y-y_1)(y-y_2)\ln\frac{|y_2-y|}{|y-y_1|} + (y+y_1)(y+y_2)\ln\frac{y_2+y}{y+y_1}\right)$$

for $y \neq y_1, y_2$

$$J(y_1,y_1,y_2) = \frac{-6}{(y_2-y_1)^3}\left(\frac{y_1^2-y_2^2}{2} + y_1(y_1+y_2)\ln\frac{y_1+y_2}{2y_1}\right) \qquad (6.85)$$

$$J(y_2,y_1,y_2) = \frac{-6}{(y_2-y_1)^3}\left(\frac{y_1^2-y_2^2}{2} - y_2(y_1+y_2)\ln\frac{y_1+y_2}{2y_2}\right) \qquad (6.86)$$

and we see that equation (6.45) is indeed satisfied. It is a tedious exercise to confirm the following properties of $J(y,y_1,y_2)$. As y increases, $J(y,y_1,y_2)$ first decreases from its negative value at $y = y_1$ to

a minimum value, whereupon it increases, passing through a single simple zero to reach a maximum positive value before decreasing to a positive value at $y = y_2$. Typical plots of $J(y,y_1,y_2)$ for particular y_1 and y_2 may be seen in Figures 6.3(c), 6.3(g) and 6.3(k).

In Figure 6.2 we plot 2 typical background fields in the absence of a current sheet (I = 0), one with an O-type neutral point

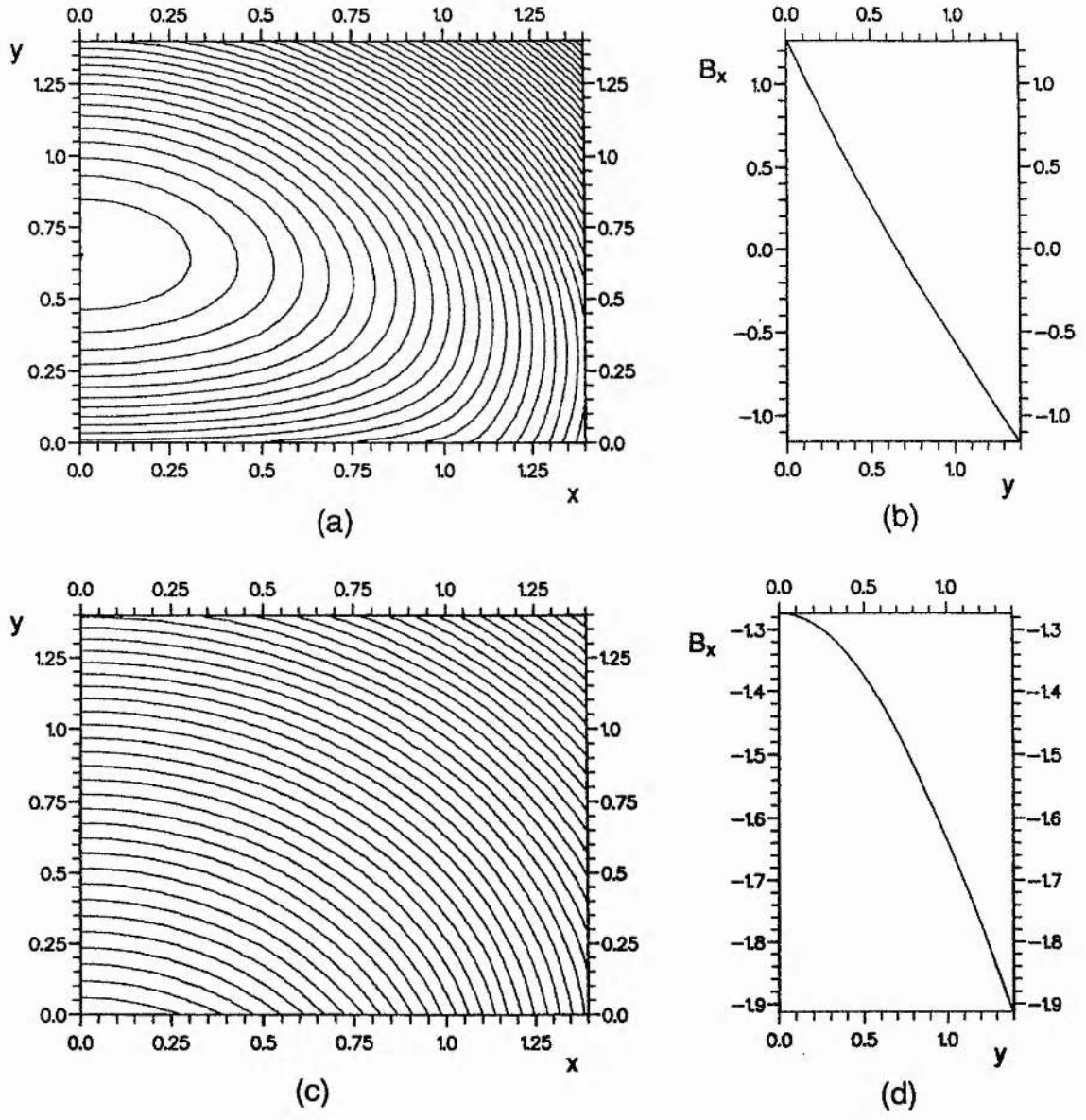

Fig. 6.2 Two particular configurations generated using the particular boundary conditions described in section 6.5. No current sheet is present on the y-axis (i.e. I = 0.0). (a) The projection in the x-y plane of the field lines obtained by taking a = 1.0 and c^2 = 1.2. The configuration contains an O-type neutral point located on the y-axis. (b) The corresponding form of the horizontal field on the y-axis, $B_x(0,y)$, plotted as a function of y. (c) The field lines for a = -1.0 and c^2 = 1.0. The configuration does not contain an O-type neutral point. (d) The form of $B_x(0,y)$ for a = -1.0 and c^2 = 1.0.

lying on the vertical axis (Figure 6.2(a)) in which h'(x) > 0 and one without (Figure 6.2(c)) in which h'(x) < 0. The corresponding transverse field components across the y-axis are shown in Figures 6.2(b) and 6.2(d), respectively. Note that in both cases, $B_x(0,y)$ is a monotonically decreasing function of y.

In Figure 6.3 we introduce a current sheet at an appropriate position along the vertical axis by selecting y_1, y_2 and a value of I

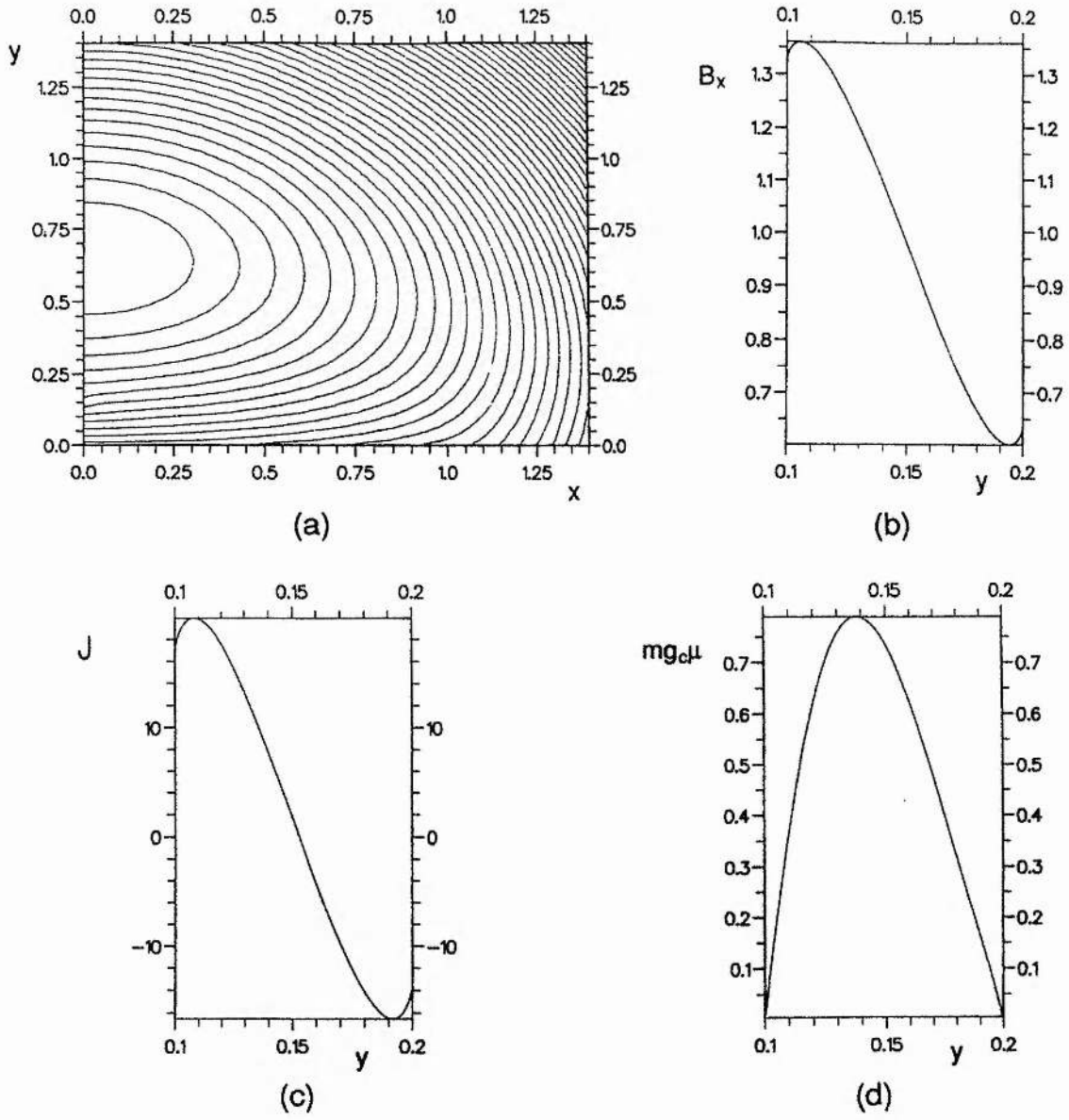

Fig. 6.3 (a) The projection in the x-y plane of the field lines for an I-type configuration generated from the photospheric boundary condition of Fig. 6.2(a) Here $y_1 = 0.1$, $y_2 = 0.2$, $I = 0.05$ and $\varepsilon = +1$. (b) The corresponding form of $B_x(0,y)$ plotted as a function of y between y_1 and y_2. (c) The corresponding form of $J(y,y_1,y_2)$ plotted as a function of y between y_1 and y_2. (d) The corresponding form of $mg_{c\mu}$ plotted as a function of y between y_1 and y_2.

small enough to prevent a large distortion of the background field. Figure 6.3(a) shows an I-type model ($\varepsilon = +1$) generated from the background field in Figure 6.2(a). Note that no I-type model can be produced starting from the background field in Figure 6.2(c). Figure 6.3(b) shows the corresponding transverse field component across the prominence sheet as a function of y. Note that it is of the correct sign for all y in $[y_1, y_2]$ for the configuration to be in equilibrium. In Figure

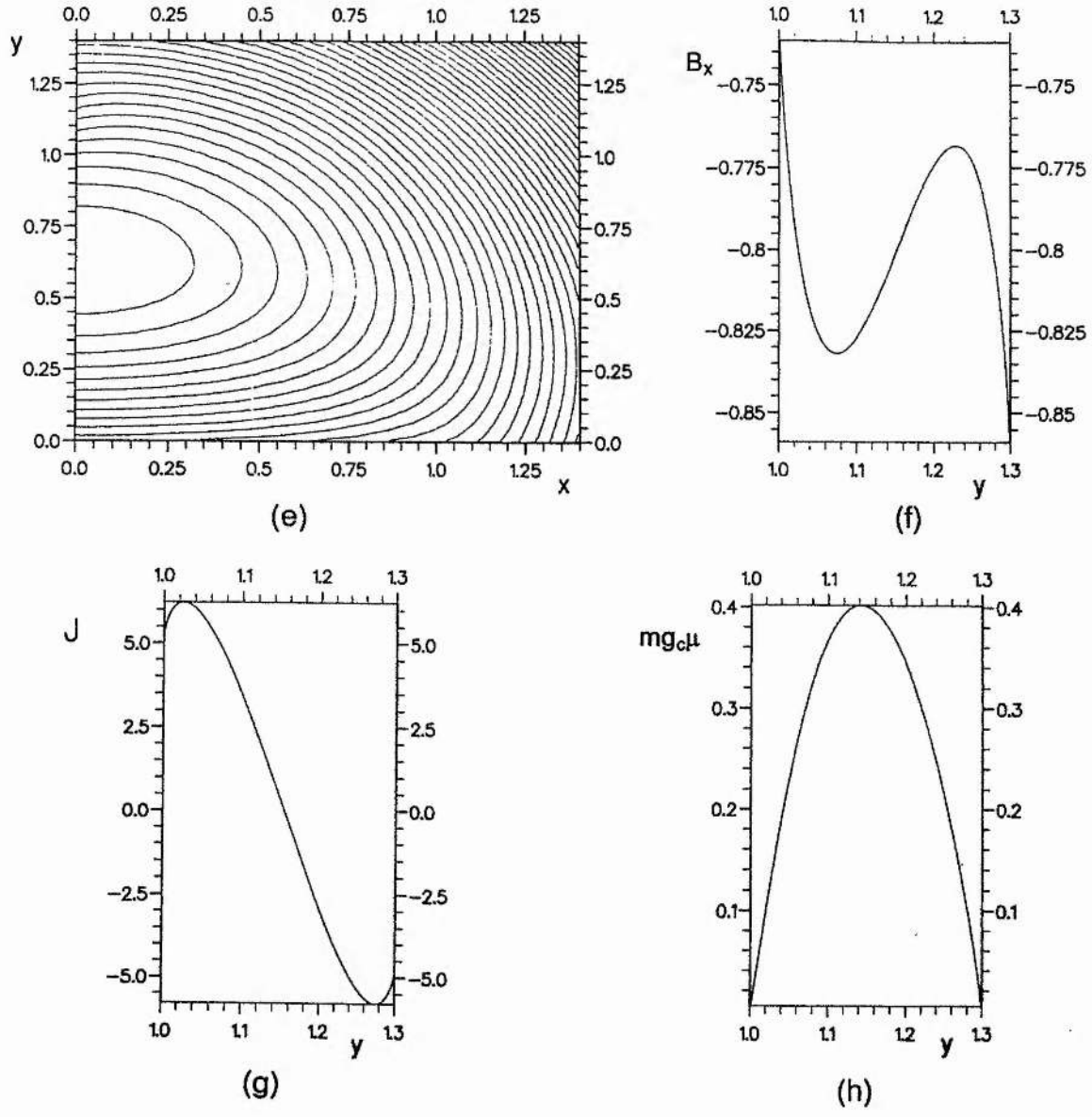

Fig. 6.3 (e) The projection in the x-y plane of the field lines for an N-type configuration generated from the photospheric boundary condition of Fig. 6.2(a) Here $y_1 = 1.0$, $y_2 = 1.3$, $I = 0.1$ and $\varepsilon = -1$. (f) The corresponding form of $B_x(0,y)$ plotted as a function of y between y_1 and y_2. (g) The corresponding form of $J(y,y_1,y_2)$ plotted as a function of y between y_1 and y_2. (h) The corresponding form of $mg_{c\mu}$ plotted as a function of y between y_1 and y_2.

6.3(c) we show the form of $J(y,y_1,y_2)$ as a function of y for the particular values of y_1 and y_2 used. Figure 6.3(d) shows the mass density as a function of y between y_1 and y_2. It is, of course, non-negative at every point in $[y_1,y_2]$ as required for a physical model.

Figures 6.3(e) and 6.3(i) show N-type models (ε = -1) generated from the background fields in Figures 6.2(a) and 6.2(c), respectively. Figures 6.3(f) and 6.3(j) show the corresponding

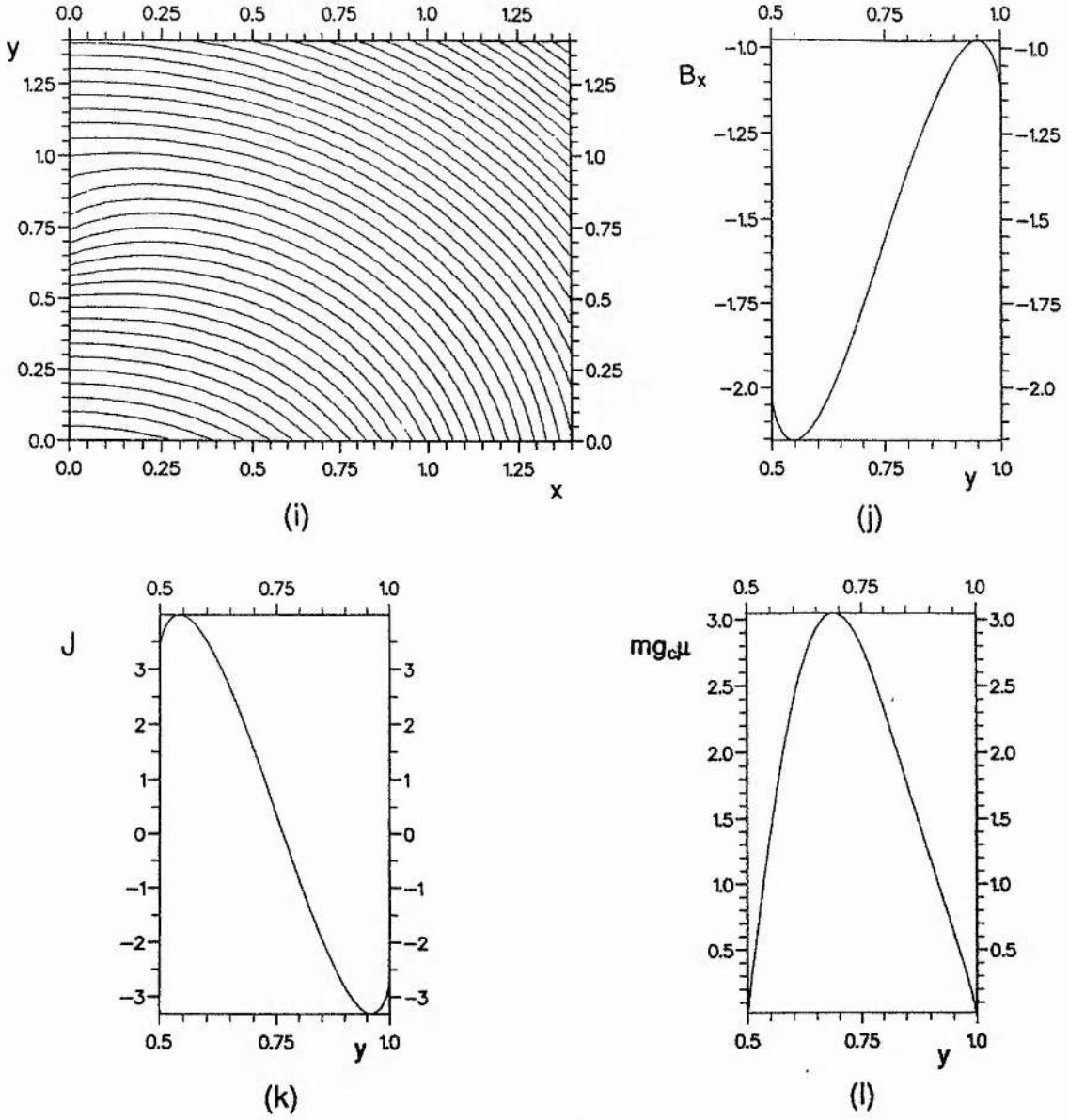

Fig. 6.3 (i) The projection in the x-y plane of the field lines for an N-type configuration generated from the photospheric boundary condition of Fig. 6.2(c) Here y_1 = 0.5, y_2 = 1.0, I = 0.6 and ε = -1. (j) The corresponding form of $B_x(0,y)$ plotted as a function of y between y_1 and y_2. (k) The corresponding form of $J(y,y_1,y_2)$ plotted as a function of y between y_1 and y_2. (l) The corresponding form of $mg_{c\mu}$ plotted as a function of y between y_1 and y_2.

transverse field component across the prominence sheet and we see that in both cases it is of the correct sign for all y in $[y_1,y_2]$ for the configuration to be in equilibrium. In Figures 6.3(g) and 6.3(k) we show the forms of $J(y,y_1,y_2)$ as a function of y for the particular values of y_1 and y_2 used. Figures 6.3(h) and 6.3(l) show the mass densities as a function of y for each of the models and we see that they are non-negative at every point in $[y_1,y_2]$ as required for a physically acceptable model.

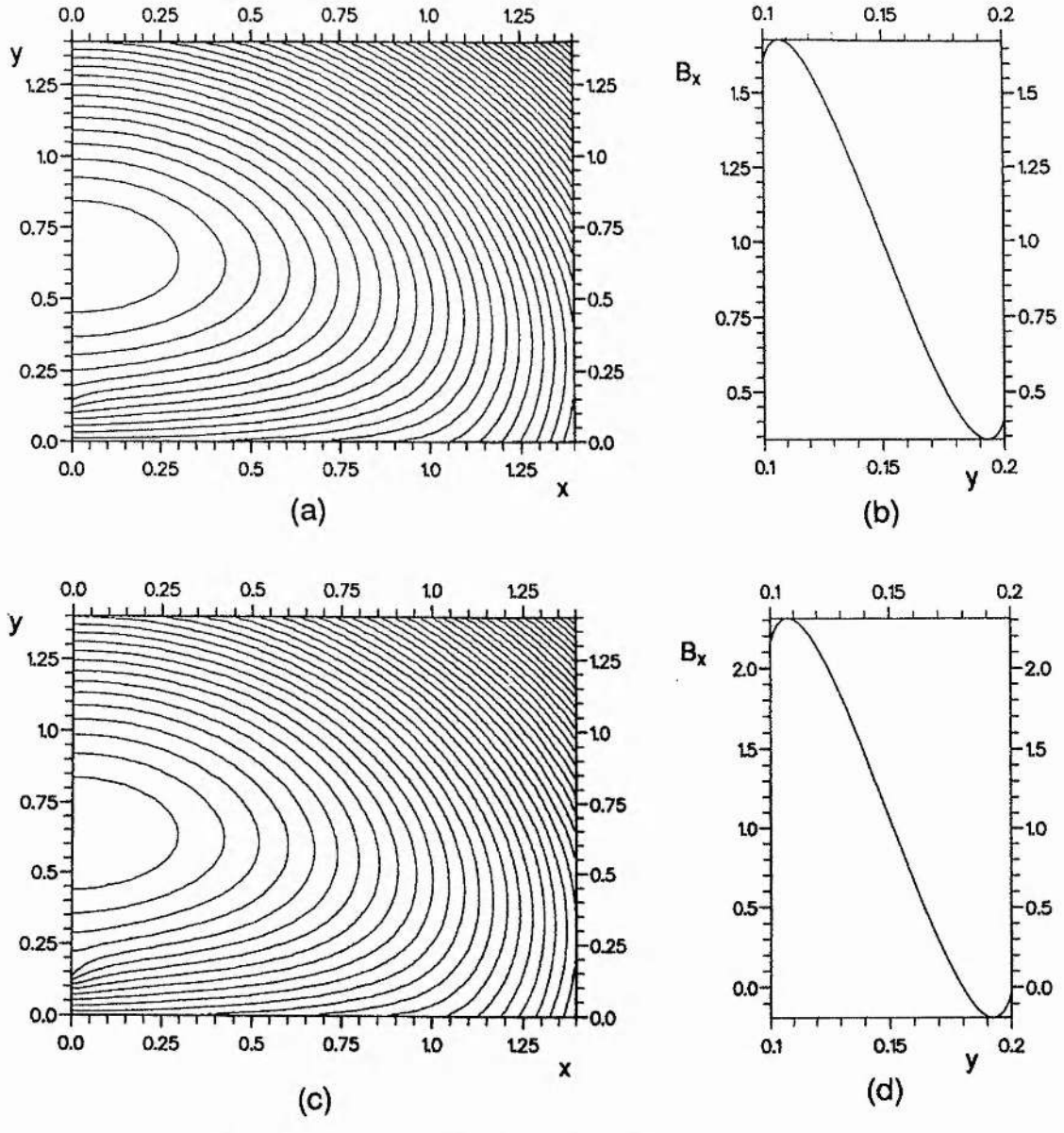

Fig. 6.4 The evolution of the configuration pictured in Fig. 6.3(a) is demonstrated as the strength of the current along the prominence sheet is increased. (a) The projection of the field lines in the x-y plane for I = 0.1. (b) The corresponding distribution of the transverse field component. (c) and (d) As (a) and (b) but with I = 0.2.

Now let us see what happens to the two equilibrium configurations shown in Figures 6.3(a) and 6.3(i) as we increase the current I but keep all other parameters fixed. Figures 6.2(a), 6.3(a), 6.4(a) and 6.4(c) show the evolution of the I-type model as I is increased from zero, with corresponding plots of $B_x(0,y)$ in Figures 6.2(b), 6.3(b), 6.4(b) and 6.4(d). By the time I reaches the value in Figure 6.4(c) the sheet has lost equilibrium near the upper end since $B_x(0,y)$ is no longer positive everywhere in $[y_1,y_2]$ and so the model is physically

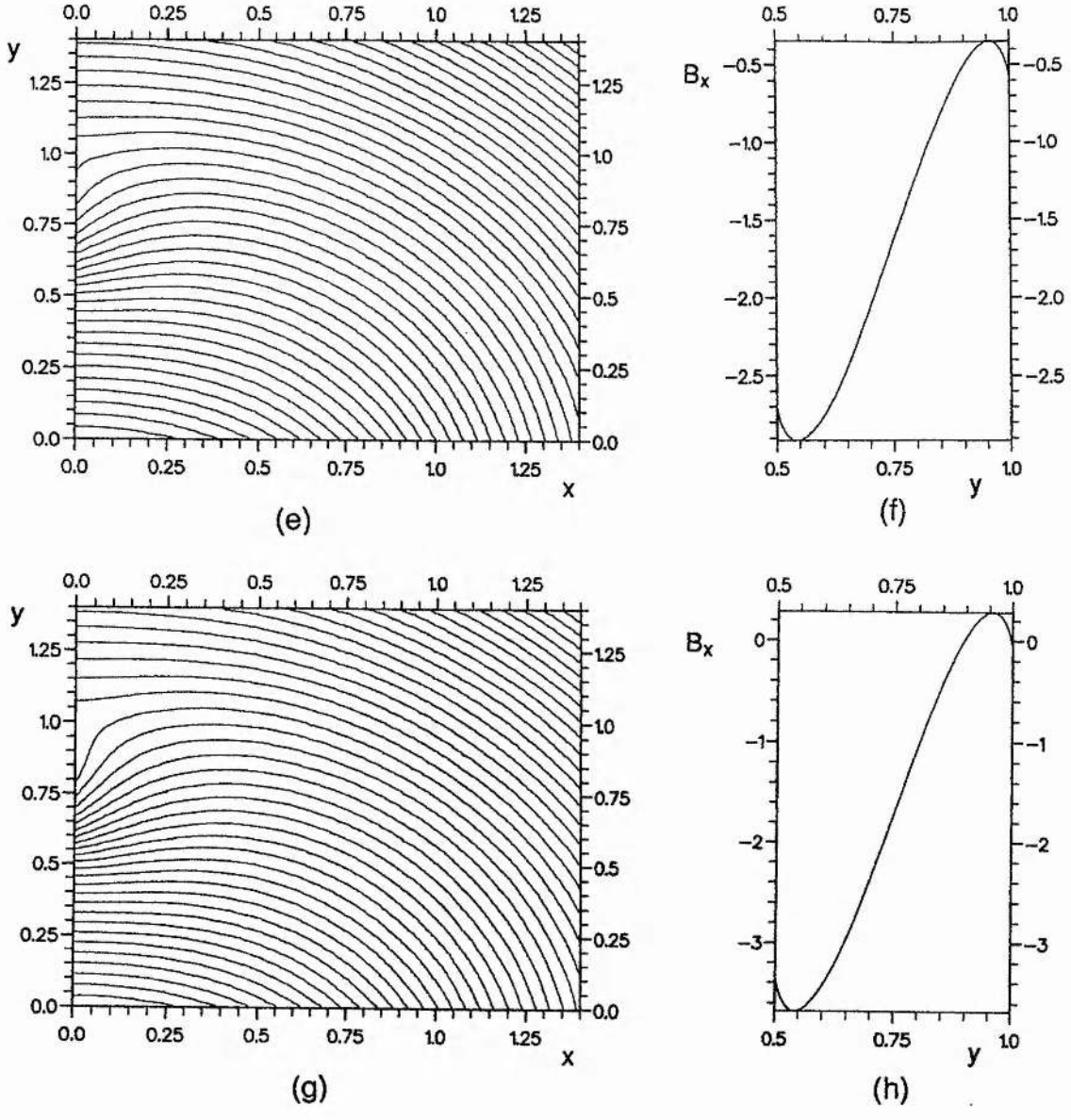

Fig. 6.4 The evolution of the configuration pictured in Fig. 6.3(i) is demonstrated as the strength of the current along the prominence sheet is increased. (e) The projection of the field lines in the x-y plane for I = 1.2. (f) The corresponding distribution of the transverse field component. (g) and (h) As (e) and (f) but with I = 1.8.

unacceptable for so large a value of I (see section 6.4.2.1.2 for a discussion on the existence of a critical current I_c beyond which non-equilibrium occurs somewhere on the sheet). The evolution of the N-type model as I is increased is shown in Figures 6.2(c), 6.3(i), 6.4(e) and 6.4(g) with corresponding forms of $B_x(0,y)$ plotted in Figures 6.2(d), 6.3(j), 6.4(f) and 6.4(h). The model ceases to have any physical meaning for some value of I less than that used to generate the configuration in Figure 6.4(g).

6.6 Reduction to the case of a current filament

In the previous sections we have assumed that the prominence is represented by a current sheet of finite length $y_2 - y_1$. Let us now briefly consider the case in which the prominence is represented by a current filament of strength I and mass per unit length m, lying parallel to the z-axis and intersecting Ω at $(0,y_1)$. This is equivalent to letting $y_2 \rightarrow y_1$ in our current sheet analysis.

Assuming that the photospheric boundary condition remains given by equation (6.10), our problem becomes that of determining A(x,y) everywhere in Ω from the following boundary-value problem

$$\nabla^2 A(x,y) + 2\,c^2 + \varepsilon\,\mu\,I\,\delta(x)\,\delta(y-y_1) = 0 \quad \text{in } \Omega \qquad (6.87)$$

$$A(x,0) = g(x) \quad \text{on } \{-\infty < x < \infty\} \qquad (6.10)$$

where ε (= ± 1) gives the direction of the current along the filament. We assume that g(x) again satisfies equations (6.16) and (6.18) so ensuring that the filament is in horizontal equilibrium.

Proceeding in the manner of section 6.4.1, it is easily seen that the solution to this boundary-value problem obtained using Green's theorem is

$$A(x,y) = -\frac{c^2}{2}(x^2+y^2) + \frac{1}{\pi}\int_{-\infty}^{\infty} \frac{y\,h(x')}{(x-x')^2+y^2}\,dx' + \frac{\varepsilon\mu I}{4\pi}\ln\frac{x^2+(y+y_1)^2}{x^2+(y-y_1)^2} \qquad (6.88)$$

where h(x) is given by equation (6.28) and h'(x) is assumed to be of constant sign in $(-\infty,\infty)$. In order to ensure the existence of the integral in equation (6.88), h(x) must again satisfy equation (6.36). The field components are given by equation (2.25) as

$$B_x(x,y) = -c^2 y + \frac{1}{\pi}\int_{-\infty}^{\infty} \frac{[(x-x')^2-y^2]\, h(x')}{[(x-x')^2+y^2]^2}\, dx' \qquad (6.89)$$

$$+ \frac{\varepsilon\mu I}{\pi} \frac{y_1\,[x^2-(y^2-y_1^2)]}{[x^2+(y+y_1)^2][x^2+(y-y_1)^2]}$$

$$B_y(x,y) = c^2 x + \frac{2}{\pi}\int_{-\infty}^{\infty} \frac{y\, h(x')\,(x-x')}{[(x-x')^2+y^2]^2}\, dx' \qquad (6.90)$$

$$+ \frac{\varepsilon\mu I}{\pi} \frac{x\, y\, y_1}{[x^2+(y+y_1)^2][x^2+(y-y_1)^2]}$$

Of course, for the filament to be in vertical equilibrium, there must be a balance between the magnetic and gravitational forces acting on it and so we must satisfy

$$\varepsilon I B_x(0,y_1) = m g_c \qquad (6.91)$$

where $B_x(0,y_1)$ (obtained by putting $y = y_1$ in equation (6.89) and letting $x \rightarrow 0$) comprises the background horizontal field component in the absence of any current filament plus the repulsion force between the filament and the oppositely directed image filament located below the photosphere at $(0,-y_1)$ (Kuperus and Raadu, 1974; Amari and Aly, 1989). In the following discussion we assume that y_1 is fixed by observation, I is a free parameter and m is to be determined from equation (6.91). Of course, for a physical model we require that m is positive and so an equilibrium solution must obviously satisfy

$$\varepsilon I B_x(0,y_1) = \varepsilon I\,(-c^2 y_1 + H(y_1)/\pi) + \mu I^2/4\pi y_1 = E(I) > 0 \qquad (6.92)$$

It is clear that

$$E(0) = 0 \qquad (6.93)$$

and that

$$dE(I)/dI = E'(I) = -\varepsilon c^2 y_1 + \varepsilon H(y_1)/\pi + \mu I/2\pi y_1^2 \qquad (6.94)$$

is a linearly increasing function of I, regardless of the choice of sign of ε or $H(y_1)$. Note also that

$$E'(0) = \varepsilon B_x(0,y_1)|_{I=0} \qquad (6.95)$$

Let us consider the following three cases in which the possible forms of the graphs of E'(I) and E(I) are sketched in Figure 6.5.

6.6.1 H(y) < 0 and ε = -1

In this case, $E'(I) > 0$ and hence equation (6.93) implies that $E(I) > 0$ for all $I > 0$. Thus the inequality in equation (6.92) will always be satisfied and so for any non-zero I we are able to support some mass

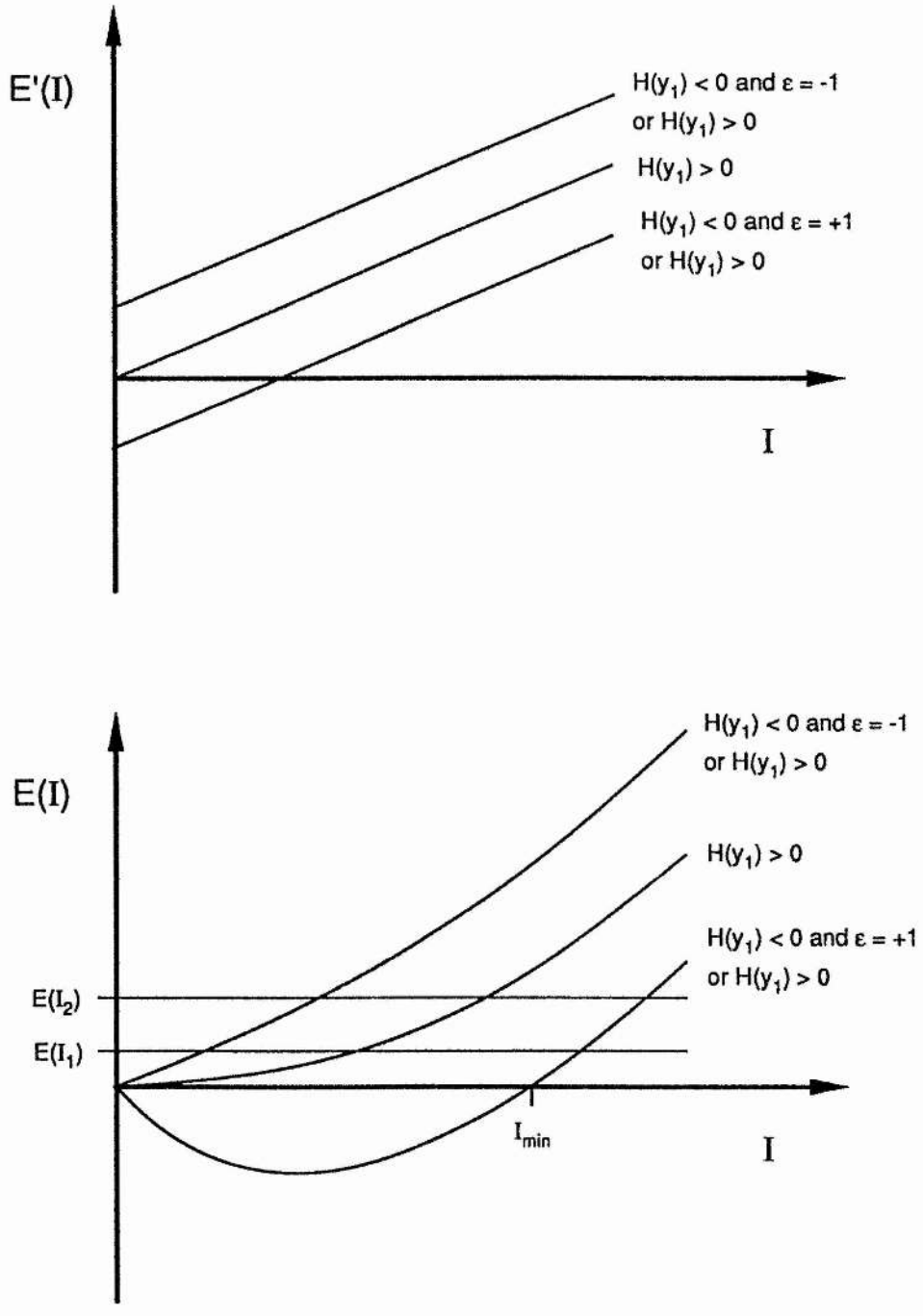

Fig. 6.5 Sketch graphs of the possible forms of the function E'(I) and the corresponding forms of the function E(I). The two horizontal lines show the solution of $E(I_i) = mg_c$ for i = 1,2.

m determined by equation (6.91).

6.6.2 H(y) < 0 and $\varepsilon = +1$

We see that in this case, $E'(0) < 0$. Since $E'(I)$ is a linearly increasing function of I it is clear that the inequality in equation (6.92) will only be satisfied for $I > I_{min}$ where I_{min} is given explicitly by the non-zero solution to $E(0) = 0$, namely

$$I_{min} = 4y_1(\pi c^2 y_1 - H(y_1))/\mu \qquad (6.96)$$

6.6.3 H(y) > 0

For this case we can see that the sign of $E'(0)$ is not uniquely determined by the choice of sign of ε but depends also on the sign of the background magnetic field as indicated by equation (6.95). If $E'(0) \geq 0$ then the equilibrium condition is automatically satisfied for all $I > 0$. However, if $E'(0) < 0$ there exists a value of I_{min} such that the equilibrium condition is only satisfied for $I > I_{min}$. If $\varepsilon = +1$, I_{min} is given by equation (6.96) and if $\varepsilon = -1$

$$I_{min} = 4y_1(H(y_1) - \pi c^2 y_1)/\mu \qquad (6.97)$$

Figure 6.5 shows the solutions of $E(I_i)$ where $i = 1,2$ (which, if positive, equal mg_c from equation (6.91)) for $I_1 < I_2$. It is clear from the figure that in all of the three cases described above, an increase in the filament current I will result in a corresponding increase in the filament mass per unit length m.

6.7 Discussion

We have presented a second method of constructing longitudinally invariant magnetic field configurations in which a symmetric, finite, vertical current sheet is in magnetohydrostatic equilibrium between the combined forces exerted by a background constant-current force-free field and a uniform gravitational field. In the present formulation we have imposed both the normal magnetic field component along the photosphere and the current density along the prominence sheet as functions of position. We have found both necessary and sufficient conditions on these functions for the local magnetic field to be bounded everywhere and for the resultant configuration to be in equilibrium.

The method has been used to generate both N-type and I-type

configurations by selecting a convenient form for the imposed functions. We have examined the evolution of these configurations as the strength of the current (and hence the mass) is increased while all other parameters are held fixed. It has been shown that in general the sheet loses equilibrium near its upper extremity as I is increased beyond a certain value. A form of j(y) which falls off more rapidly as y approaches y_2 would allow a larger value of I to be reached before equilibrium is lost. Alternatively, equilibrium may be regained by bodily moving the prominence downwards or upwards in an I-type or N-type configuration, respectively. It is not suggested, however, that any of these scenarios occur during the evolution of a real prominence, since quantities such as the longitudinal extent, mass density, height, etc. are governed by the physical processes occurring in the vicinity of the prominence.

Two apparent problems with our model are a) the divergence of the field at large distances from the prominence and b) the loss of a physical meaning for $B_z(A)$ when $A < 0$. These may be avoided by "cutting-off" the constant-current field at some field line for which $A \geq 0$. The consequences of such an action are discussed in section 5.7.

7 CONCLUSION

In chapters 3 to 6 we have developed 4 methods for obtaining models of the global magnetic field in the neighbourhood of a quiescent solar prominence. In each case we have in mind the idea of relatively dense prominence plasma being supported in a magnetic field line dip where the associated magnetic tension force balances the gravitational force acting on the prominence mass. We have shown that such an equilibrium is possible in our models and that the magnetic fields generated by them conform to either one of the two observed topologies, namely N- or I-type.

The Twisted Flux Tube and reconnection models described in chapters 3 and 4, respectively, have in common the idea that the magnetic field is helical in nature allowing the support of dense prominence plasma in the low points of the windings but they differ in the physical process by which the helical structure is created. Such models conveniently explain the strong longitudinal field component in the neighbourhood of a prominence as well as the helical appearance frequently observed in erupting prominences. However, it should be born in mind that when viewed side on, a longitudinally sheared field in which the vertical component changes sign across a prominence sheet may give rise to the illusion of a helical structure. Further observations are required in order to determine the precise topology of the global magnetic field throughout the region surrounding the prominence and how it changes during the prominence lifetime. If these should confirm the importance of a helical magnetic field in prominence formation and support then theoreticians must consider further physical processes which could result in such fields.

In both of these models we assume that the field is invariant along the longitudinal prominence axis in order to facilitate the analysis. However, many prominences exhibit a great deal of non-uniformity along this axis. Such irregularity might result partly form an uneven distribution of twist along each particular field line or across the radius of the tube. A further problem with this assumption is that all prominences are, of course, finite in length, a feature ignored by virtually all existing analytical models.

One of the problems with the formalism we have used in constructing the equilibria in our Twisted Flux Tube model is that we

consider the tube in isolation from the photosphere and impose B_z as a function of A. This distribution is not readily determined from observations and it would be preferable to relate the twist on each field line within the tube to observed photospheric flows at the footpoints where the field lines are anchored. Such a model is considered by Dahlburg et al. (1991) who examine the effect twisting photospheric motions have on an initial current-free arcade using a 3-dimensional numerical MHD code. They find that the resulting rapid expansion of the field suppresses the formation of field line dips suitable for prominence support. However, this may simply be due to a lack of resolution in the code. Furthermore, Priest et al. (1989) showed the existence of a critical twist that must be surpassed for a dip to be produced and it is possible that this twist was not achieved in the numerical simulations.

An advantage of the formalism of the reconnection model is that the environment surrounding the prominence plays an important role in the model. In particular, the evolution of the model relates directly to the photospheric motions in the locality of the polarity inversion line and the reconnection process which forms the helical field lines can only occur if converging motions are present. However, the loss of a degree of freedom due to the restriction of cylindrical symmetry (necessary to enable analytical progress) means that we are unable to impose the footpoint velocity in this model. Instead this distribution becomes a result of the mathematical analysis. This represents a severe constraint on the model, the only recourse being to allow for azimuthal variation of the field which necessarily requires numerical solution of the equilibrium equation.

In both the numerical analysis of van Ballegooijen and Martens (1989) and the analytical extension presented in chapter 4, no allowance is made for the deformation of the helix produced by prominence material collecting in the helical windings. An obvious extension to the model would be the inclusion of prominence material represented by a current sheet containing mass lying between the polarity inversion line and the helical axis. However, in order to retain the idea of an evolving process it would be necessary to impose the distribution of the prominence mass, normal magnetic field component or surface current as a function of both position and time. A further improvement would be to allow the reconnection process to take place

in a finite region rather than solely along the polarity inversion line. Such complications necessarily disallow the assumption of cylindrical symmetry and these ideas could only be incorporated using numerical techniques.

It should be pointed out that the irregular structure of many prominences along the longitudinal axis could partly be explained in the reconnection model by a non-uniform reconnection rate along the polarity inversion line.

The boundary-value problem approach of chapters 5 and 6 has in its favour the fact that the distribution of the normal magnetic field components along the photosphere and across the prominence (or the prominence surface current or mass) may be chosen to approximate observed distributions. Once more, however, we must assume that we know the functional form of $B_z(A)$ in order to make analytical progress and so far only very simple forms have been considered due to the difficulties involved in solving equation (2.27) when it is nonlinear.

A further problem with this type of model is that no attempt is made to explain how the field evolves to the state generated by the choice of a particular set of boundary conditions. Rather, it represents a snap shot of the prominence at a particular moment in time. In order to overcome this criticism it has been suggested that a sequence of equilibrium solutions to the simplified magnetohydrostatic equilibrium equation

$$\nabla^2 A + \frac{d}{dA}\left(\frac{B_z^2(A)}{2}\right) = \nabla^2 A + \lambda^2 f(A) = 0 \qquad (2.27)$$

could be considered as a quasi-static evolution as λ^2 (and hence B_z) increases from zero. In general it is found that no neighbouring equilibrium exists beyond some critical value of λ^2 and it is conjectured that the field then evolves dynamically. However, Klimchuck and Sturrock (1989) have followed Priest and Milne (1980) and Priest (1981) in demonstrating that this concept does not have any physical meaning since such a sequence does not in general "lose equilibrium" when it is redefined in terms of the corresponding photospheric boundary conditions and so is not a valid method of following an evolution.

It may instead be possible to use the boundary-value problem formulation to generate a particular prominence field using observed boundary conditions and see how such a field evolves due to subsequent

photospheric motions using a numerical MHD code or the iterative method described by Wolfson (1989). Even so the issue of the initial prominence formation is ignored by this approach.

A further extension to this type of model would be to attempt the formulation and solution of the boundary-value problem in which it is assumed that the distribution of the prominence mass density is given.

One obvious deficiency in all current sheet models is the inherent assumption that the prominence is well represented by a sheet that is infinitesimally thin. The temperature and pressure within the sheet are necessarily zero and it is assumed that the density of the surrounding coronal plasma is vanishingly small. In common with virtually all previous authors, we have glossed over this problem by stating that we are interested only in the global magnetic field outside the prominence and on these length scales the prominence width is relatively negligible. In reality, however, prominences do have an appreciable thickness and there is a transition between the coronal field and the prominence internal structure. As a first step towards incorporating a finite, vertical prominence sheet with a non-zero width in an analytical model of the global field, Hood and Anzer (1990) have produced a two temperature N-type configuration in which they take given prominence conditions and are able to match the internal field smoothly onto an external linear force-free coronal field with physically acceptable properties.

Furthermore, Hood (1991) has suggested a method by which the current sheet in an existing analytical equilibrium may be expanded to some finite thickness and the internal properties of the prominence plasma may be deduced. The field profile within the prominence region may be chosen to match onto the known external field and the magnetohydrostatic equilibrium equation (2.21) used to determine the distribution of the prominence density, pressure and temperature as functions of position. Although it is preferable to impose these variables in constructing a prominence model, it would nonetheless be interesting to study the distributions that would be predicted by some of the existing current sheet models. In particular the solutions presented in chapter 3 for the field components in the Twisted Flux Tube model have a particularly simple form and could readily be subjected to this type of analysis.

Particularly challenging for theoreticians is the relaxation of the condition that the field surrounding the prominence is invariant in one direction. This could allow the modelling of structures along the prominence, either on a large-scale such as the prominence feet or on a small-scale such as the fibril structure. For example, Demoulin et al. (1989) have modelled the prominence feet using an analytical 3-dimensional linear force-free field which is periodic in the longitudinal direction. Also, Priest et al. (1991) and Hood et al. (1991) have presented models for the fibril structure but at present very few models exist for either of these phenomena.

It is interesting to note that very few analytical models to date attempt to explain how the field topology could change from N- to I-type in the course of the prominence evolution as suggested by the observations outlined in section 2.3. The Twisted Flux Tube model is particularly encouraging in this respect in that during the early stages of the evolution, the twist could be of either sense but over a long period of time Coriolis forces act to produce an I-type configuration. It is to be hoped that future prominence models will incorporate more of the time-dependent characteristics of prominences.

Many of the extensions suggested here necessarily require the use of numerical analysis. As computer efficiency improves and increasingly robust MHD codes are written there is obviously an ever-widening variety of applications for which these codes may be used in the study of prominences. Even so, it is necessary to remember the important role played by analytical solutions to the MHD equations which, although often applicable only in highly idealised situations, demonstrate the basic principles behind a model without fear of numerical error, undesirable effects due to imposed boundary conditions or numerical diffusion of the magnetic field. In addition, a useful check for numerical codes is their ability to reproduce known analytical solutions.

We should be aware that the wide variety in the appearance of prominences and the fact that there are two different topologies for the global magnetic field mean that it is quite possible for more than one process to exist by which prominences are formed and subsequently evolve. Until observations indicate otherwise, it is the theorist's task to investigate whatever possibilities are open to him. It is only through increasingly improving our knowledge of prominences with better

observations and more sophisticated models that we can ever hope to unravel the many remaining mysteries behind the existence of these fascinating objects.

8 REFERENCES

Aly J. J., Amari T. and Columbi S. 1989, in *Solar Plasma Phenomena.*, ed. M. A. Dubois, F. Baly-Dubau and D. Gresillon (Paris : l'Ecole Polytechnique), p.181.

Amari T. and Aly J. J., 1989 *Astron. Astrophys.* **208**, 261.

Amari T. and Aly J. J., 1990a *Astron. Astrophys.* **231**, 213.

Amari T. and Aly J. J., 1990b *Astron. Astrophys.* **227**, 628.

Amari T. and Aly J. J., 1990c preprint.

Amari T., Demoulin P., Browning P., Hood A. W. and Priest E. R., 1991 *Astron. Astrophys.* **241**, 604.

Anzer U., 1972 *Solar Phys.* **24**, 324.

Anzer U., 1985 in *Measurements of Solar Vector Magnetic Fields.* ed. M. J. Hagyard (NASA CP-2374), p.101.

Anzer U., 1988 in *The Dynamics and Structure of Quiescent Solar Prominences.* ed. E. R. Priest, p.143.

Anzer U. and Priest E. R., 1985 *Solar Phys.* **95**, 263.

Athay G., Querfeld C. W., Smartt R. N.,Landi Degl'Innocenti E. and Bommier V., 1983, *Solar Phys.* **89**, 3.

Babcock H. W. and Babcock H. D., 1955 *Astrophys. J.* **121**, 349.

Birn J., Goldstein H. and Schindler K., 1978 *Solar Phys.* **57**, 81.

Dahlburg R. B., Antiochos S. K. and Zang T. A., 1991 *Astrophys. J.* in press.

Demoulin P., Malherbe J. M., and Priest E. R., 1989 *Astron. Astrophys.* **211**, 428.

Demoulin P. and Priest E. R., 1988 *Astron. Astrophys.* **206**, 336.

Demoulin P., Priest E. R. and Anzer U., 1989 *Astron. Astrophys.* **221**, 326.

Hermans L. M. and Martin S. F.,1986 in *Coronal and Prominence Plasmas.* ed. A. I. Poland (NASA CP-2442), p.369.

Hood A. W., 1991 private communication.

Hood A. W. and Anzer U., 1990 *Solar Phys.* **126**, 117.

Hood A. W., Priest E. R. and Anzer U., 1991 submitted to *Solar Phys.*

Kim I. S., 1990 in *Dynamics of Quiescent Prominences.* ed. V. Ruzdjak and E. Tandberg-Hanssen (IAU CP-117), p.49.

Kippenhahn R. and Schluter A., 1957*Zs. Astrophys.* **43**, 36.

Klimchuck J. A. and Sturrock P. A., 1989 *Astrophys. J.* **345**, 1034.

Kuperus M. and Raadu M. A., 1974 *Astron. Astrophys.* **31**, 189.

Kuperus M. and Van Tend W., 1981 *Solar. Phys.* **71**, 125.

Leroy J. L., 1988 in *The Dynamics and Structure of Quiescent Solar Prominences.* ed. E. R. Priest, p.77.

Leroy J. L., Bommier V., Sahal-Brechot S., 1983 *Solar. Phys.* **83**, 135.

Malherbe J. M., and Priest E. R., 1983 *Astron. Astrophys.* **123**, 80.

Martin S. F.,1986 in *Coronal and Prominence Plasmas.* ed. A. I. Poland (NASA CP-2442), p.73.

Martin S. F., 1990 in *Dynamics of Quiescent Prominences.* ed. V. Ruzdjak and E. Tandberg-Hanssen (IAU CP-117), p.1.

Martin S. F., Livi S. H. B., and Wang J., 1985 *Australian J. Phys.*, **38**, 929.

Muskhelishvili N. I., 1953 *Singular Integral Equations.*, (Groningen : Noordhoff), p. 279.

Priest E. R., 1981 in *Solar Flare Magnetohydrodynamics.* ed. E. R. Priest (New York : Gordon and Breach), p139

Priest E. R., 1988 *The Dynamics and Structure of Quiescent Solar Prominences.* (Dordrect : Reidel)

Priest E. R., 1990 in *Dynamics of Quiescent Prominences.* ed. V. Ruzdjak and E. Tandberg-Hanssen (IAU CP-117), p.150.

Priest E. R., Hood A. W. and Anzer U., 1989 *Astrophys. J.* **344**, 1010.

Priest E. R., Hood A. W. and Anzer U., 1991 *Solar Phys.* **132**, 199.

Priest E. R. and Milne A. M., 1980 *Solar Phys.* **65**, 315.

Schmieder., 1990 in *Dynamics of Quiescent Prominences*. ed. V. Ruzdjak and E. Tandberg-Hanssen (IAU CP-117), p.85.

Tandberg-Hanssen E. and Anzer U., 1970 *Solar Phys.* **15**, 158.

Van Ballegooijen A. A. and Martens P. C. H., 1989 *Astrophys. J.* **343**, 971.

Van Tend W. and Kuperus M., 1978 *Solar Phys.* **59**, 115.

Wolfson R., 1989 *Astrophys. J.* **344**, 471.